DESIGN AND CHARACTERIZATION OF NANOWIRE ARRAY AS THERMAL INTERFACE MATERIAL FOR ELECTRONICS PACKAGING

A Thesis

by

JUEI-CHUN CHIANG

Submitted to the Office of Graduate Studies of
Texas A&M University
in partial fulfillment of the requirements for the degree of

MASTER OF SCIENCE

December 2008

Major Subject: Mechanical Engineering

DESIGN AND CHARACTERIZATION OF NANOWIRE ARRAY AS THERMAL INTERFACE MATERIAL FOR ELECTRONICS PACKAGING

A Thesis

by

JUEI-CHUN CHIANG

Submitted to the Office of Graduate Studies of
Texas A&M University
in partial fulfillment of the requirements for the degree of

MASTER OF SCIENCE

Approved by:

Chair of Committee,	Sheng-Jen ("Tony") Hsieh
Committee Members,	Jun Kameoka
	Steve Suh
Head of Department,	Dennis O'Neal

December 2008

Major Subject: Mechanical Engineering

ABSTRACT

Design and Characterization of Nanowire Array as Thermal Interface Material for Electronics Packaging. (December 2008)

Juei-Chun Chiang, B.S., National Taiwan University

Chair of Advisory Committee: Dr. Sheng-Jen ("Tony") Hsieh

To allow electronic devices to operate within allowable temperatures, heat sinks and fans are employed to cool down computer chips. However, cooling performance is limited by air gaps between the computer chip and the heat sink, due to the fact that air is a poor heat conductor. To alleviate this problem, thermal interface material (TIM) is often applied between mating substrates to fill air gaps. Carbon nanotube (CNT) based TIM has been reported to have excellent thermal impedance; however, because it is non biodegradable, its potential impact on the environment is a concern.

In this thesis research, two types of TIMs were designed, synthesized, and characterized. The first type, *Designed TIM 1*, consisted of anodic aluminum oxide (AAO) templates with nanochannels (pore size=80nm) embedded with copper nanowires by electrodeposition. This type of nanostructure was expected to have low thermal impedance because the forest-like structure of copper nanowires can bridge two mating surfaces and efficiently transport heat one dimensionally from one substrate to the other.

The second type, *Designed TIM 2*, was fabricated by sandwiching *Designed TIM 1* with commercially available thermal grease to further reduce thermal impedance. It

was expected that the copper nanowire structures would secure the thermal grease in place, thus preventing grease pump-out under contact pressure, which is a common problem associated with the usage of thermal grease.

The morphologies of the two designed TIMs were studied using scanning electron microscopy (SEM), and their thermal properties were determined using ASTM D5470-06, the standard method for testing thermal transmission properties of thermally conductive materials. Experiments were conducted to evaluate the proposed TIMs, as well as commercially available TIMs, under different temperature and pressure settings.

Experimental results suggest that the thermal impedance of TIMs can be reduced by increasing contact pressure or reducing thickness. *Designed TIM 2* yielded 0.255℃-cm^2/W, which is lower than thermal grease and other available TIMs at the operating temperature of 50 to 60℃. Considering the application limitations and safety issues of thermal grease, phase change material, and CNT-based TIMs, our designed TIMs are safe and promising for future applications.

DEDICATION

This thesis is dedicated to my parents who have supported me all the way since the beginning of my studies.

Also, this thesis is dedicated to my girl friend, Jasmine Lin, and my adorable puppy, Cookie, who have been a great source of inspiration and motivation.

Finally, this thesis is dedicated to all of my good friends who have always encouraged me and shared my feelings.

ACKNOWLEDGEMENTS

First and foremost, I would like to thank my advisor, Dr. Sheng-Jen ("Tony") Hsieh, who dedicated time and patience to teach me how to be a successful researcher.

I would also like to thank my committee members, Dr. Steve Suh and Dr. Jun Kameoka for providing me advice throughout the course of this research.

Next, I would like to thank Dr. Chien-Chon Chen, who taught me lots of knowledge in the field of nanotechnology and helped me build the experimental fixture and fabricate specimens.

Thanks also go to my girl friend, Jasmine Lin, and my sweet puppy, Cookie, for making my time in Texas a great experience. I also want to extend my gratitude to Charles Chen, Albert Wan, Alison Hsieh, Jason Liu, Erwin Hsu, and Justin Yang for supporting and helping me at Texas A&M University.

Finally, thanks to my mother and father for their encouragement and unconditional love.

NOMENCLATURE

AAO	anodic aluminum oxide
ANOVA	analysis of variance
AC	alternating current
CBD	chemical bath deposition
CNT	carbon nanotube
CPU	central processing unit
DC	direct current
DF	degree of freedom
H_0	null hypothesis
H_A	alternative hypothesis
h	convection heat transfer coefficient ($W/m^2/K$)
IC	integrated circuits
K	thermal conductivity (W/m-K)
MWNT	multi-walled carbon nanotube
PCM	phase change material
PCT	phase change temperature
PED	pulsed electrodeposition
PEG	polyethylene glycol
Q	heat flow (W)
RR	rejection region

$R_{contact}$	thermal contact resistance (℃-cm^2/W)
$R_{material}$	inherent thermal resistance (℃-cm^2/W)
SEM	scanning electron microscope
SWNT	single-walled carbon nanotube
TS	test statistic
T_s	surface temperature (℃)
T_∞	fluid temperature (℃)
TIM	thermal interface material

Greek Symbols

α	significance level
ε	emissivity (dimensionless)
θ	Thermal impedance (℃-cm^2/W)

TABLE OF CONTENTS

Page

LIST OF FIGURES

FIGURE Page

FIGURE Page

FIGURE Page

LIST OF TABLES

TABLE Page

TABLE Page

1. INTRODUCTION

1.1 The importance of thermal management for electronics

The rapidly increasing power consumption as well as the decreasing die-size of integrated circuits (IC) necessitates more research on the improvement of electronics' thermal management [1]. The main reason is that the further enhancement of central processing unit (CPU) performance, functionality, reliability, and miniaturization has been restricted by the overheating of CPUs [2-4]. Currently, a multichip module may have as many as a few hundred chips on a single substrate [3]. Therefore, the high power density, which leads to the expense of high power demand and the resultant excessive heat generation [5], is a major problem to be solved.

Both the reliability and life expectancy of electronic devices are inversely related to the component temperatures [6]. The reduction in the operating temperature corresponds to an exponential increase in both the reliability and life expectancy of a typical silicon semiconductor electronic device [7-10]. Basically, the life expectancy roughly doubles for every 10℃ reduction in temperature for silicon and other electronic devices [11].

Of all the electronic devices, smaller ones are more susceptible to Joule heating, a direct result of the relevant temperature between its elevated operating temperature and the ambient temperature, due to its higher current densities. It is believed that Joule heating will result in poor performance and short lifetime of electronics [12]. Since the

---

This thesis follows the style of Microelectronics Journal.

size of electronic devices is decreasing, Joule heating may be a serious issue to be considered.

It has been reported that heat dissipation from a 3.73 GHz Intel Pentium IV processor may reach as much as 115 W [13]. The heat that needs to be dissipated away per unit area of a single chip will increase dramatically over the next few decades. The computer chip temperature will be significantly high if such highly-dense power is trapped in it. It is imperative that we gain direct control over this issue.

In order to cope with this problem, heat sinks along with cooling fans are employed to cool down computer chips. Heat sinks built geometrically with large exposed surface area can be used to enhance thermal convection; while fans mounted above heat sinks can be used to increase the convection heat transfer coefficient (forced convection).

1.2 The need for developing thermal interface materials (TIMs)

A heat sink resting on the top of a computer chip can be used to dissipate excessive generated heat. However, its cooling performance is limited by the conformability between the computer chip and the heat sink. In other words, one of the primary obstacles to the thermal management of electronic devices operating at high powers is the quality of the physical contact between the computer chip and the heat sink [14]. For example, the actual physical contact area of a computer chip with nominal cross-sectional area of 1 cm^2 may be as small as 0.01 cm^2 due to the non-flatness and roughness of mating surfaces. Therefore, the physical contact between heat sink and

computer chip is a dominating factor in thermal management. To alleviate this critical problem, it is urgent to improve the conformability of the two mating substrates.

To enhance the number of physical contacts at the computer chip-heat sink interface, we need to apply a thermal interface material (TIM) between them. The main purpose for the application of a TIM is to effectively dissipate heat from an electronic device to a heat sink by filling air gaps formed at the interface. The path of heat removal from a computer chip to the environment involves thermal conduction across the interface of the computer chip, through a TIM, into a heat sink, and then thermal convection into the surrounding ambient [1].

In sum, in order to manage the electronic devices operating below the maximum allowable operation temperature, we need to make use a heat sink/ fan assembly and an effective TIM to dissipate generated heat to the ambient air.

Currently, there are various types of commercial TIMs available. TIMs like thermal grease, phase change material, thermally-conductive adhesive tapes, thermally-conductive pads and thermally conductive elastomer insulators all have been widely used in response to a specific situation.

A common defect of all the commercially available TIMs is the low maximum operating temperature. Of all the TIMs, the maximum operating temperature is 200℃ [15]. Considering the increasing high power density of new electronics, the limitation of the maximum operating temperature needs to be further increased.

In this thesis research, we designed and proposed two types of TIMs (*Designed TIM 1* and *Designed TIM 2*). The *Designed TIM* 1 is composed of copper nanowire

arrays (diameter=80nm) fabricated by anodic aluminum oxide (AAO) templates. Since this type of TIM is composed of metal (copper nanowires) and ceramics (Al_2O_3, AAO), its resistance to high temperature is expected. Next, free-standing copper nanowires may provide massive one dimensional ballistic transportation of heat with less resistance. Therefore, it is expected that heat will only be transported uni-directionally from CPU to heat sink, and no lateral heat spreading will take place. According to SEM images, our designed TIM can have as many as ~4×10^{11} nanowires per square centimeter (pore size=15nm).

To cope with the possibly remained air-filled voids between copper nanowire arrays and mating surfaces, the *Designed TIM* 2 was proposed. We sandwiched the *Designed TIM* 1 structure by applying a thin layer of thermal grease on both sides of it to fill out air-filled voids, if any. Due to the high thermal performance and high thermal conductivity of thermal grease, low thermal impedance of this proposed sandwich structure is expected. The expected heat transfer mechanism is that the thermal grease applied on top-and bottom-side of copper nanowire arrays can literally fill all air voids at the interfaces and efficiently conduct heat into the copper nanowire arrays and heat sink, respectively.

In this thesis research, the *designed TIM 1* refers to the TIM composed of copper nanowire arrays; while the *designed TIM 2* refers to the TIM with the application of thermal grease on both sides of *designed TIM 1*.

1.3 Format of research

This thesis is divided into seven sections, as follows:

Section 1 describes the important role of TIM in thermal management of electronics and the need for improving it.

Section 2 summarizes and compares some commercially available TIMs. Previous research related to the application of nanotechnology to the improvement of thermal performance of TIMs is also reviewed. Next, the characteristics of AAO templates as well as some nanomaterials are reviewed. Finally, two types of copper nanowires based designed TIMs are briefly proposed.

Section 3 presents the objective of this research, and the details of proposed TIM designs. Next, the fabrication processes for both AAO templates and copper nanowire arrays are listed step-by-step. The fabricated specimens were analyzed with SEM images.

Section 4 focuses on the design of experiments. Experimental hypothesis, measure of performance, and the experimental procedures are carefully discussed.

Section 5 focuses on the experimental results. The result of each design of experiment was presented by experimental plots followed by statistical hypothesis testing. A summary of experimental results of this thesis research was given in the end.

Section 6 focuses on the validation of experimental results of designed TIMs' thermal properties by built mathematical models.

Section 7 summarizes this research and identifies future directions.

2. LITERATURE REVIEW

2.1 Current state of thermal interface materials design

Typically, a heat sink/fan assembly is mounted on a computer chip to facilitate heat dissipation. However, due to the roughness and non-flatness of mating surfaces of computer chip and heat sink, the interface will be filled with air gaps. Air, which has low thermal conductivity (K=0.026 W/m-K) [1], is a poor heat conductor and will hinder the heat dissipation process (Figure 1(a)). In order to facilitate heat dissipation, it is necessary to apply an efficient TIM between mating surfaces to eliminate air gaps.

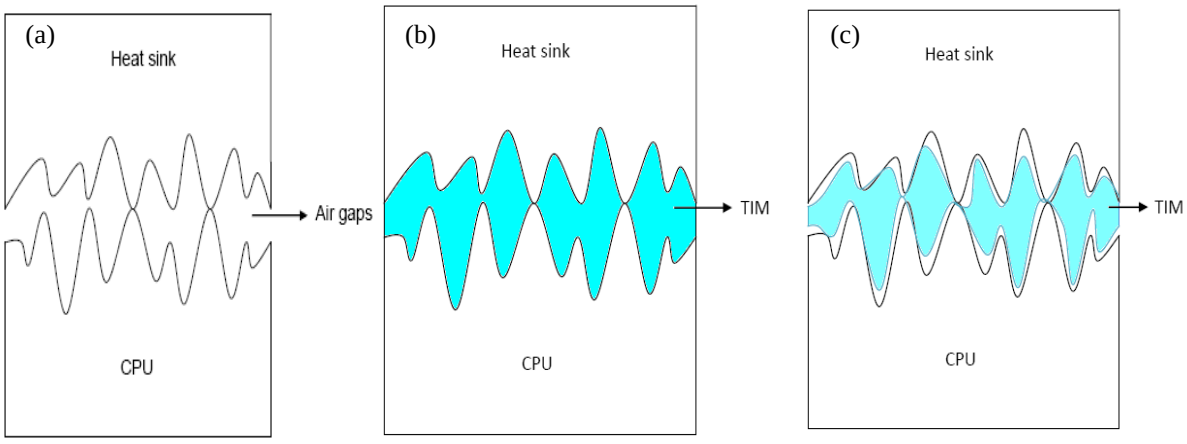

Figure 1 Schematic diagrams showing the physical contact between a CPU and a heat sink. (a) without a TIM, (b) Ideal physical contacts between a CPU and a heat sink with a TIM, (c) Actual physical contacts between a CPU and a heat sink with a TIM. Figure is not drawn to scale.

It is reported that as much as 99% of the mating interface surface area will be separated by air gaps resulting from the superimposing of microroughness on a

macroscopic non-planar in the form of a combination of concaves, convexes, and waves [1]. Even though the number of contact points between two mating substrates like the CPU and the heat sink can be increased by applying more contact pressure on either one side or both sides of the mating interface, the load constraints on CPU make it impractical and unfeasible to do so. Therefore, the solution turns to a TIM that can efficiently bridge two mating substrates and remove those air gaps (Figure 1(b), 1(c)). The primary reason we want to replace air pockets with TIM is that air is a poor heat conductor. As a result, any materials having relatively higher thermal conductivities then that of the air and conform well to the mating surfaces are potential TIM candidates. According to Intel's roadmap, the contribution of TIM in a CPU is elevated from 12% to 26%, which correspond to Pentium III and Pentium IV, respectively. Therefore, TIM will play an increasingly significant role in thermal management for electronic devices [2].

It is clear from Figure 1 that even though we may choose a material with extremely high thermal conductivity, it is still a waste without having good thermal contacts between mating surfaces [2, 16]. As a result, thermal impedance is a more important factor in thermal management than thermal conductivity. In other words, a TIM with high thermal conductivity cannot guarantee good heat-dissipation capacity without low thermal impedance.

There are several selection criteria for an effective TIM. For example, high thermal conductivity, good conformation with mating substrates, low thickness, non-toxicity, reliability, and easy application [1, 4, 17-19].

Currently, there are a variety of TIMs developed to solve thermal problems of electronics. Popular TIMs like thermal grease, soft metals, phase change materials (PCMs), thermally conductive elastomers, thermally conductive compounds, and thermally conductive adhesive tapes have been widely used. The properties of these TIMs are listed in Table 1.

Table 1 Advantages and disadvantages of commercial TIMs [15].

TIM	Thermal impedance (℃-cm^2/W)	Thermal conductivity (W/m-K)	Advantages	Disadvantages
Thermal grease	0.07-0.13	0.8-3.0	-excellent conformability -low thermal impedance -high maximum operating temperature (200℃)	-messy and hard to apply -no electrical insulation -high phase change temperature needs to be met before optimal performance can be reached -pump-out under contact pressure
Phase change material (PCM)	0.13-2.26	0.7-1.0	-good conformability -grease-like behavior -easy installation -no pump-out	-limited choices of matrix materials -strong adhesive bonding may damage motherboards -high phase change temperature needs to be met before optimal performance can be reached -low maximum operating temperature (125℃)
Thermally conductive adhesive tapes	2.0-7.7	0.4-1.4	-eliminate the need for mechanical attachment -easily reworkable	-moderate thermal performance - low maximum operating temperature (150℃)
Thermally conductive elastomer insulators	2.1-4.1	0.4-1.5	-good dielectric strength -excellent mechanical strength --high maximum operating temperature (200℃)	-moderate thermal performance
Thermally conductive pads	1.93-9.1	1.5-6	-good conformability -easy installation	- low maximum operating temperature (150℃) -moderate thermal performance

Thermal grease is defined as a paste composed of silicone or hydrocarbon oil dispersed with thermally conductive fillers. The mechanism of how “optimal” thermal grease works is that the high thermal conductivity fillers will melt when the phase change temperature is met and the minimum bond line can be formed at the interface [1].

Due to its outstanding conformability at low contact pressure, it has the capability to fill the interstices and eliminate the interstitial air between two contact surfaces [20, 21]. Even though most of the thermal greases have relatively lower thermal conductivities than other kinds of TIMs, some high performance thermal greases may have better thermal conductivity values than other classes of TIMs [22].

However, the real application of thermal grease has some limitations. First, thermal grease is not manufacturing recommended as a result of it is messy and difficult to apply and remove. Second, the excess grease flowing out of joint under repeated thermal cycling due to the relative motion of the mating surfaces under thermal expansion and contractions needs to be removed to prevent contamination and possible electrical shorts. In other words, thermal grease may not provide electrical insulation between mating surfaces. Third, thermal grease may dry out with time, resulting in increased thermal resistance since the thermal grease degradation rate is a strong function of operating temperature and number of thermal cycles. Fourth, the thermal performance of thermal grease is highly related to the operating temperature [1,22]. For example, the commercial thermal grease we tested will only have optimal thermal performance until the operating temperature reaches above 62℃. Before that phase change temperature can be met, the thermal performance of thermal grease will be noticeably reduced.

Another commercial TIM is soft metals. This type of TIM may have higher thermal conductivity than other types of TIMs due to the nature of metals; however, unacceptably high contact pressure is required to conform itself with mating surfaces [1].

This is not practical since excess high clamping pressure can possibly damage electronics during packaging.

Phase change material (PCM), another type of TIM, is a mixture of suspended particles of high thermal conductivity and a base material. The characteristic of PCM is that the base material is solid at room temperature, but its viscosity diminishes and behaves like thermal grease once it has reached the phase change temperature (PCT) [1, 23]. PCMs have several advantages like low contact resistance, thermal grease-like behavior to fill air gaps and provide minimum thickness after reaching PCT, easy installation, and no pump out [1, 21, 22, 24]. However, PCMs still have some application limitations. First of all, most of the phase change materials have phase change temperatures around 50℃. The phase change temperature needs to be met before the thermal performance can be optimized. Second, there are only limited choices of materials that may be employed in the manufacturing of PCMs. Third, the maximum operating temperature of phase change materials is only around 125℃, the lowest among all commercially available TIMs. Fourth, PCMs have relatively lower thermal conductivity. Next, the strong adhesive bond formed by PCMs between the CPU and the heat sink may damage the motherboard and the CPU. Finally, moderate compressive pressure is required to bridge mating surfaces and causes the PCMs to flow, which might not be practical under certain circumstances [1, 22, 25].

Another kind of TIM is thermally conductive elastomers. Just like soft metals, unacceptably high contact pressure is required to fill interstitial voids between mating surfaces [1, 26], which limits its popularity and applications.

Thermally conductive adhesive tape, another commercially available TIM, is easy to install due to its double-sided adhesive characteristics. In other words, conventional mechanical fasteners are not required. However, due to its poor thermal performance, its application is limited [1, 26].

The last type of common TIM is thermally conductive compounds (TCCs), defined as elastomer paste filled with thermally conducive particles. The most noticeable characteristic of TCCs is that it can be easily applied in paste form and cured in-situ to conform to mating surfaces. Generally, the TCCs can only provide moderate thermal performance in comparison with other types of TIMs [1, 27].

2.2 Current state of using nanotechnology for TIMs design

A lot of research has been done on TIMs consist of high thermal conductivity fillers and matrixes [28, 30-38]. Both fillers and matrixes have their corresponding functionalities- Fillers may rapidly transfer heat while matrixes may either facilitate the installation of fillers or regulate the direction of fillers [28].

Carbon nanotubes (CNTs) were widely used as fillers to enhance thermal performance of TIMs [36-38] (Table 2). The most important reason is its high thermal conductivity in the axial direction [39-40].

Table 2 Performance of various kinds of TIMs from literatures.

	TIM	Thermal impedance (℃ – cm^2/W)	Thermal conductivity (W/m-K)
1	CNT/ Polymer composite[2]	0.265[1]	4.8
2	Phase change material (PCM) composed of aluminum mesh and the alkyl methyl silicone wax[28]	0.24	7.0
3	Low melting temperature alloy (LMTA) [28]	0.058	NP[2]
4	Silicon thermal grease filled with CNT[28]	0.027-0.077[3]	1.17-3.58
5	Carbon nanofiber /Cu composite[29]	0.25[4]	NP
6	Thermal grease (Silicon fluid with alumina powder filler) *ShinEtsu* [1]	0.101-0.387	2.89-4.5
7	Thermal grease *Berquist* [1]	0.226	7.5
8	Dry CNT arrays[30]	0.198[5]	NP
9	CNT array and a PCM[30]	0.052[6]	NP
10	Multiwalled Carbon Nanotubes (MWCNTs)[31]	0.111	NP
11	CNT/foil[24]	0.10	NP

[1] Obtained at 30psi
[2] Not published
[3] Obtained at 435psi
[4] Obtained at 60psi
[5] Obtained at 65psi
[6] Obtained at 50psi

The following researchers have studied and managed to enhance the thermal performance of TIMs with CNTs.

Quoc Ngo et al. proposed a carbon nanofiber/ copper composite as TIMs [29]. It was assumed that copper electrodeposited between carbon nanofibers can provide both mechanical stability of the whole matrix and enhance lateral heat spreading to neighboring nanofibers. The thermal impedance was reported as low as 0.25 ℃-cm^2/W.

T.M. Lee et al. proposed a CNT/ liquid crystal composite as TIMs. It was reported that the high order sequence of liquid crystal along with the high thermal conductivity of CNTs may generate the thermal impedance as low as 0.2465 ℃-cm^2/W [2].

Amama et al. fabricated multi-walled carbon nanotubes on silicon chips with the assist of dendrimer and claimed that the forest-like structures can effectively enhance heat flow between the chip and the heat sink. The reason is that nanotube forests

conform to the heat sink surface, which provides better contact between them. They reported the thermal interface resistance of multi-walled carbon nanotubes-based TIMs lower than 0.1 ℃-cm^2/W [41].

Anand Desai et al. conducted a numerical study of TIMs enhanced with CNTs [14]. Their major and surprising result was that there is no considerable difference in temperature drop for 10-50% of area occupied by nanotubes under the power input ranging between 10 and 1000 W, which means 10% of a silicon wafer surface occupied by carbon nanotubes may work almost equally effective as that of 50%. Anand Desai et al. also simulated one nanotube connecting a chip to a heat sink. Mathematical models were built to determine the steady state temperature distributions for the heat sink-nanotube-chip structure under different thermal conductivities, radii, and thicknesses [42].

J.J. Park et al. proposed a TIM that consisted of CNTs and a thermally conductive matrix with the thickness around 10 μm. The resultant thermal impedance was reported between 0.0265 and 0.0772 ℃-cm^2/W [28].

Xu et al. directly synthesized CNTs on silicon wafers and reported the thermal interface resistance around 0.198 ℃-cm^2/W [30]. They also tried to combine CNT arrays with traditional phase change materials. An even lower thermal interface resistance around 0.052 ℃-cm^2/W was produced. The authors claimed that nanotubes provide ballistic transport of both electrons and heat, and as much as three times of heat may be effectively transferred compared with traditional TIMs.

Baratunde A. Cola et al. designed a TIM comprised of a metal foil with CNTs synthesized on both of its surfaces [24]. It was proposed that this kind of composite will deform under moderate pressure and conform to mating surfaces. Thermal impedance as low as 0.1 ℃-cm^2/W was reported.

X.J. Hu et al. proposed a TIM consisting of silicon matrix, CNTs, and nickel spheres [36]. It was found that CNTs can effectively increase the overall effective thermal conductivity of the whole matrix with even small quantities. The authors claimed that the better compliance and wetting properties of CNTs make this kind of composite ideal as TIMs.

D.B. Cho et al. used CNTs-based thin film coating as a heat sink because of its large exposed surface area resulting from carbon nanotube's large aspect ratio and high thermal conductivity [33]. Therefore, it is evident that nanomaterials may be used as both TIMs and heat sinks.

However, even though the thermal conductivity of CNTs may be exceptionally high, they do have some serious defects limiting their future industrial applications. For example, the coagulating nature [43] and health-threatening possibilities [44-50] of CNTs hinder their future development in real industry.

2.3 Characteristics of anodic aluminum oxide (AAO)

Anodic aluminum oxide (AAO) has drawn much attention because its composing material, aluminum oxide (Al_2O_3) is one of the widely used oxide ceramic materials [51-52] and has many exciting characteristics even in terms of nanoscale. The large surface

area, high flexibility, high strength, low density, high melting point, high optical transparency, high refractive index, high dielectric constant, low permeability, low surface acidity, and good thermal/ chemical stability all make nanoscaled aluminum oxide promising in various applications [51-59].

AAO [60-65], which can also be termed anodic alumina nanoholds (AAN) [66], anodic alumina membrane (AAM) [67], porous alumina membrane (PAM) [56], nanoporous alumina membrane (NAM) [68], nanochannel alumina (NCA) [69], anodic porous alumina (APA) [70], anodic oxide film (AOF) [71], porous aluminum oxide (PAO)[72], and porous anodic alumina (PAA) [53], is a thin film with tunable uniform nanochannel/nanoporous structure formed by the anodization of high purity aluminum foil and can be served as a template in the fabrication of nanomaterials with controlled dimensions. It is believed that AAO template is an ideal template because of its tunable dimensions, good mechanical strength, and thermal stability [62].

AAO templates are fabricated by the anodization of aluminum, one of the most controllable self-assembly chemical processes. By manipulating experimental parameters like anodization bathing composition, anodization time, applied voltage, and bathing temperature, an AAO template with desired morphology regarding template thickness, pore size, and the number density of pores can be tailored. According to our experiments, pore size and template thickness is proportional to anodizing voltage and anodizing time, respectively.

In other words, the geometry of nanowire arrays fabricated by embedding nanochannels of AAO templates can be controlled by selecting AAO templates with

desired dimensions. With the employment of AAO templates, forest-like densely-packed identical nanostructures of the desired material can be synthesized within the cylindrical nanopores of a membrane having uniform diameters.

A lot of nanomaterials have been successfully fabricated by AAO templates. For example, CdS nanowires [73], carbon nanotubes (CNTs) [74-77], platinum (Pt) nanowires [75], gold (Au) nanowires [78], gold nanotubes [79], copper (Cu) nanowires [80], copper nanorods [80], nickel (Ni) nanowires [81], nickel nanotubes [79], cobalt (Co) nanowires [82], iron (Fe) nanowires [83], zinc (Zn) nanowires [84], and silver (Ag) nanowires [85] all have been successfully prepared by AAO templates.

Many methods can be applied to fabricate nanomaterials. For example, electrodeposition [63-65], sol-gel template [52], atomic layer deposition [53], chemical vapor deposition [86-87], chemical bath deposition (CBD) [88], and high-pressure injection method [62]. Among them, the electrodeposition technique, especially pulsed electrodeposition (PED), is of particular interest. With the help of AAO templates and pulsed electrodeposition, nanowires and nanotubes can be selectively fabricated. In addition, by tuning the electrodeposition time, temperature, pH value, and current density of the electrolyte, the length of nanowires can be precisely controlled. To achieve uniform growth front of metallic nanowires as the pulsed electrodeposition progresses, it is crucial that only a few monolayers of metal are deposited within each pulse cycle [89].

2.4 Thermal properties of nanomaterials

In this subsection, thermal properties of the most popular nanomaterials, CNTs, studied by former researchers were presented.

In 2000, Berber et al. made the usage of molecular dynamics simulations and derived the thermal conductivity value of a single-walled carbon nanotube (SWNT) to be 6,600 W/m-K (at room temperature) [42]. Later in 2002, Kim et al. reported the experimentally-derived thermal conductivity of a discrete multi-walled carbon nanotube (MWNT) to be 3000 W/m-K (at room temperature) in the axial direction [90]. In the same year, Hone et al. claimed the thermal conductivity of single-walled carbon nanotubes (SWNTs) to be in the range of 1750-5850 W/m-K [91-92]. The unusually high thermal conductivities may be the result of the incredibly high atomic bond strength present in CNTs. In contrast to their bulk states, phonon-phonon (umklapp) scattering is suppressed in CNTs because their size limits the allowed wave vectors in the dispersion relation [93]. However, small thermal conductivity values of discrete MWNTs were also reported. In 2002, Yang et al. reported the thermal conductivity value for discrete MWNTs to be 15 W/m-K [94]. Next, in 2004, Wang et al. reported the thermal conductivity value for discrete MWNTs to be 27 W/m-K [95]. In addition, the measured thermal conductivity of aligned bundles of SWNTs to be only 250 W/m-K at room temperature and only 2.3 W/m-K for a sintered sample [96]. It is argued that the wide variation of thermal conductivity values may be attributed to the inherently disordered nature of some carbon nanostructures grown by CVD processes [97]. Next, the several order of magnitude discrepancy of CNTs' thermal conductivity was clarified by the

utilization of molecular dynamics simulations [5]. In addition, it is reported that the thermal conductivity of CNTs increases with the length of nanotubes, and the value falls between 10 – 375 W/m-K [5].

A variety of approaches and assumptions have been proposed to account for the reduced thermal conductivity of nanoscaled materials [93]. For example, as the size of a structure decreases, the surface-to-volume ratio increases, thereby increasing the importance of surface effects such as boundary and interface scattering in relation to some volumetric effects. Therefore, heat transport in nanostructures can be much different than in bulk states.

Some major explanations are briefly specified here. The first one is the modification of the phonon dispersion relation and group velocity due to confinement effects [98-99]. The second one is the boundary scattering [100-101]. The last one is the quantized thermal conductance [102-103].

2.5 Proposed TIM designs

Two types of TIMs are designed, synthesized, and characterized in this thesis research. Basically, the anodization of aluminum foil and the technique of electrodeposition were utilized to fabricate our proposed designed TIMs.

In this research, we made use of the highly-ordered nanochannels of AAO templates formed by the anodization of aluminum films to prepare well-aligned copper nanowires. The copper nanowires, prepared by pulsed electrodeposition (PED, a common method used for gap-filling high-aspect ratio nanochannels), will be embedded

in AAO nanochannels with highly ordered and vertically aligned nanostructures. We can then selectively etch away partial AAO structure to expose copper nanowires on both sides by immersing AAO in the phosphoric acid (H_3PO_4) for a controlled period of time. The exposed length of copper nanowires can be determined by controlling the immersion time of AAO in the phosphoric acid. The copper nanowire arrays are expected to standing freely since the AAO is only partially dissolved, and the remaining AAO nanochannel structure will provide support to them laterally. It is expected that one-dimensional copper nanowires can provide low heat resistance path (Figure 2) for heat transportation. This type of TIM composed mainly of copper nanowires is termed *Designed TIM 1*.

Considering utilizing the thermal grease on both sides of *Designed TIM 1* to further fill air-filled voids existed between mating surfaces, another type of TIM was proposed. Basically, the *Designed TIM 2* is fabricated by applying a thin film of thermal grease on both sides of *Designed TIM 1*. Since thermal grease has the lowest thermal impedance value among commercial TIMs, it is expected that the application of thermal grease at interfaces may further enhance thermal performance of our *Designed TIM 1*. Next, it is also expected that the forest-like intrusive copper nanowires may "fix" thermal grease in place, instead of pumping-out under high contact pressure, which is a typical problem associated with the usage of thermal grease as TIM.

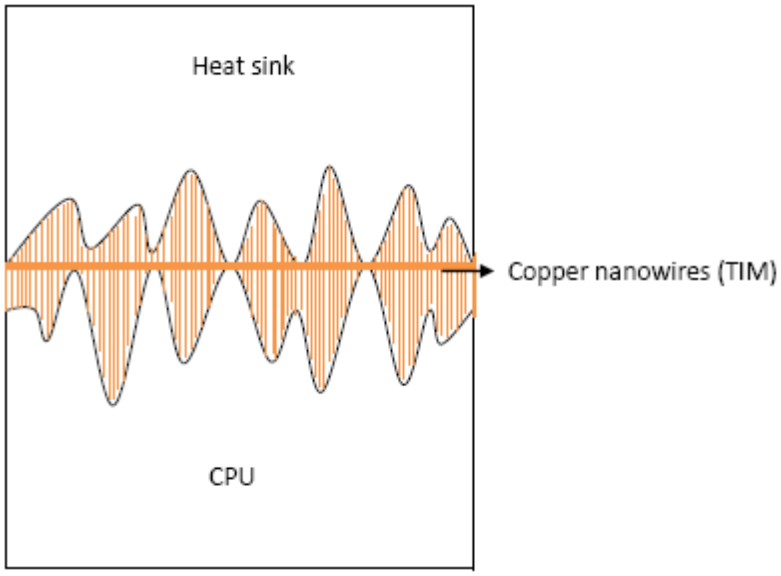

Figure 2 Schematic diagram showing the ideally physical contacts between a CPU and a heat sink with a TIM composed of copper nanowire arrays in between. Figure is not drawn to scale.

In sum, two types of TIMs were designed and characterized in this thesis research. The first one, *Designed TIM 1*, is composed of AAO templates filled with intrusive copper nanowires. The second one, *Designed TIM 2*, is composed of thermal grease thin films applied on both sides of *Designed TIM 1*. Low thermal impedance of both designed TIMs is expected due to the following reasons:

(1) One-dimensional low heat resistance path provided by copper nanowires

(2) Few air-filled voids at interfaces

(3) Large surface area of forest-like copper nanowires provide mass thermal conduction path

The fabrication and characterization processes of designed TIMs will be presented in following sections. The thermal performance of our designed TIMs obtained from experimental results will be evaluated to justify the above expectations.

3. METHODOLOGY

3.1 Objective

The objective of this thesis research is to characterize the thermal properties of copper filled AAO templates to evaluate their technical and practical feasibility as thermal interface material. We will follow the standard method regulated by ASTM D5470-06 to measure the thermal properties of TIMs.

First of all, we need to fabricate AAO templates with desired dimensions (pore size=80nm, thickness=25, 40, 60μm). Then, we have to electro-deposit copper into AAO nanochannels followed by etching partial surface AAO to expose desired length (100nm) of copper nanowires (*Designed TIM 1)*. By the application of thermal grease on both sides of *Designed TIM 1*(sandwich structure), the *Designed TIM 2* is also fabricated.

Finally, the thermal properties of our designed TIMs will be compared with existing high performance, high popularity commercial TIMs under various treatments.

3.2 Proposed TIM designs

Figure 3 and Figure 4 illustrate the fabrication process and morphology of designed TIM 1. Basically, we will first fabricate AAO templates followed by the removal of aluminum substrate and barrier layer. Next, with the technique of sputtering deposition, a thin copper layer is coated on the bottom of AAO templates. Then, the electrodeposition of copper into AAO nanochannels takes place. Finally, partial AAO and copper substrate will be removed to expose copper nanowires.

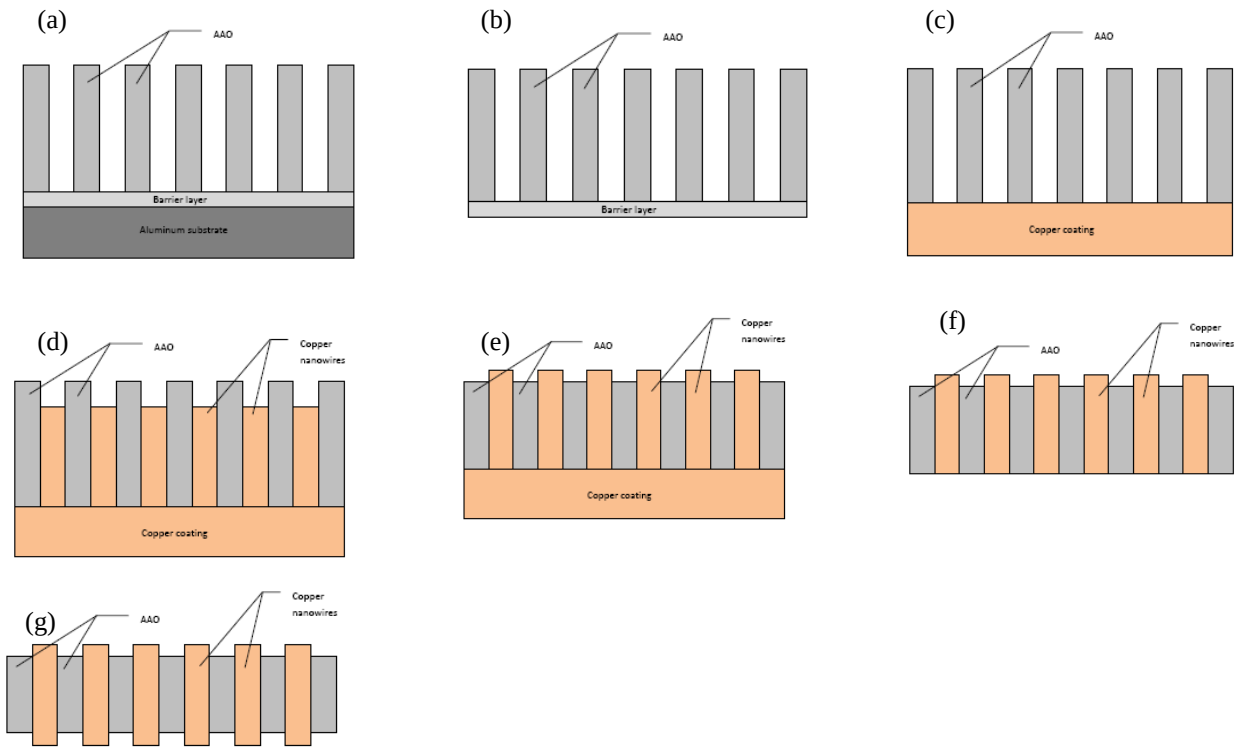

Figure 3 Schematic diagrams showing the fabrication processes of copper nanowire arrays (cross-sectional view). (a) Typical AAO cross-sectional structure before the removal of aluminum substrate and barrier layer, (b) The removal of the aluminum substrate, (c) The removal of barrier layer and the addition of conductive copper coating by sputter deposition, (d) Filling the copper metal into AAO by pulsed electrodeposition, (e) Partial removal of AAO for the top side of the specimen, (f) The removal of copper coating, (g) Partial removal of AAO for the bottom side of the specimen.

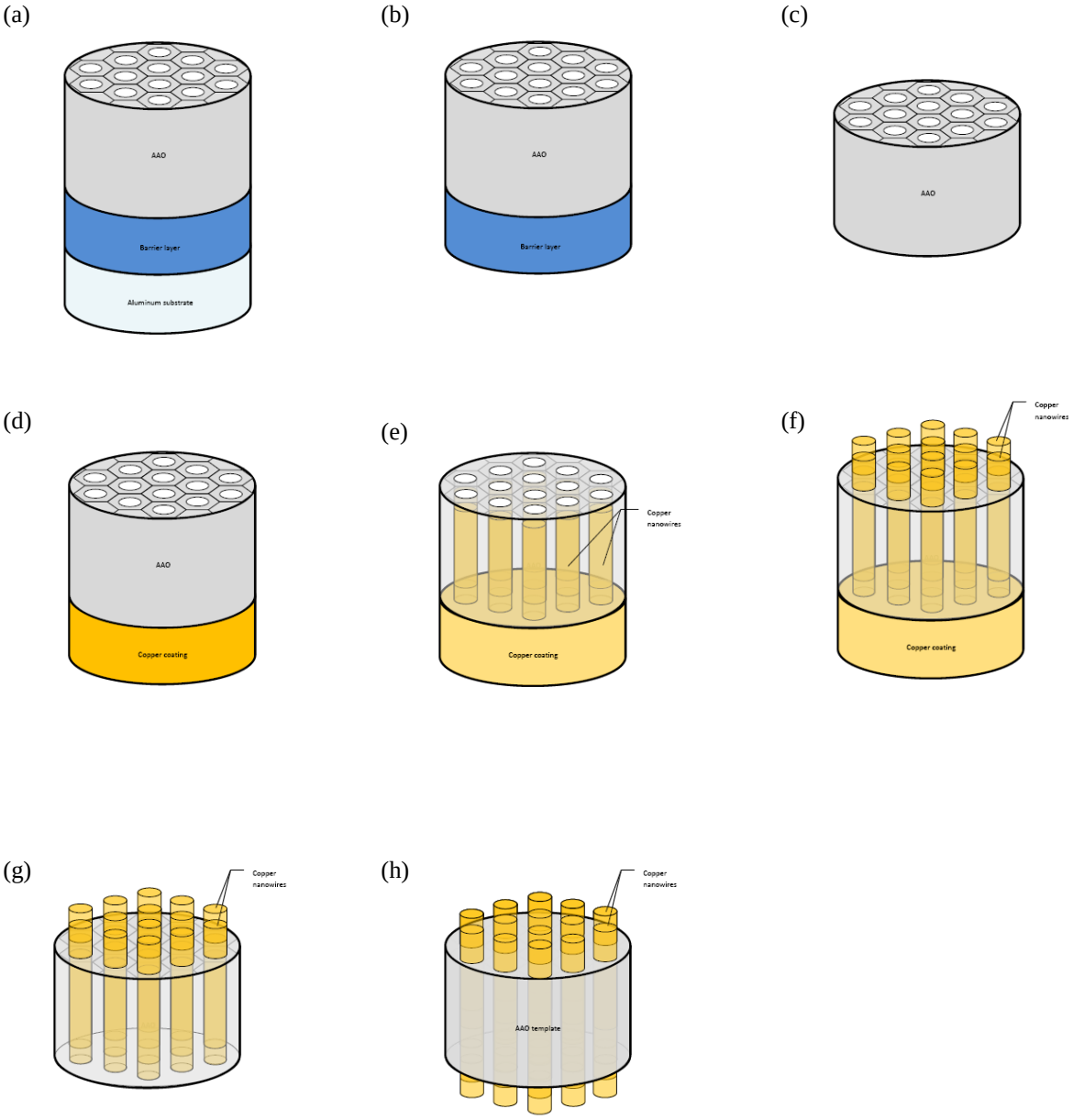

Figure 4 Schematic diagrams showing the fabrication processes of copper nanowire arrays (three-dimensional view). (a) Typical AAO cross-sectional structure before the removal of aluminum substrate and barrier layer, (b) The removal of the aluminum substrate, (c) The removal of barrier layer , (d) The addition of copper coating by sputter deposition, (e) Filling the copper metal into AAO by pulsed electrodeposition, (f) Partial removal of AAO for the top side of the specimen, (g) The removal of copper coating, (h) Partial removal of AAO for the bottom side of the specimen.

3.3 Fabrication process

Basically, the fabrication of designed TIMs consists of two major steps. The first step is the fabrication of AAO templates with desired dimensions, and the second step is the fabrication of intrusive copper nanowires by embedding AAO nanochannels. The step-by-step fabrication processes are described below.

3.3.1 Fabrication of AAO templates

The AAO templates were fabricated by the anodization of general purity (99.7%) aluminum foils, and the whole fabrication process takes less than seven hours in a general chemical laboratory. AAO templates with thickness from 10 to 200μm, and pore-size (diameter of each round nanochannel) from 10 to 500 nm can be successfully fabricated (aspect ratios between 20 and 20,000). The step-by-step procedures are described as follows:

(a) First of all, an aluminum foil is cleaned by acetone to remove grease from the surface. After that, the aluminum foil is rinsed in distilled water and dried in open air. Then, the aluminum foil is uniformly mechanical-polished by a piece of water-proof SiC sandpaper. Sandpapers with decreasing average particle sizes are to be used consecutively to have the aluminum foil increasingly smoothed. Next, the aluminum foil is annealed in a furnace at 550~600℃ under argon for 1 hour to reduce the residual stress in it and promote grain growth and recrystallization. Finally, the annealed specimen is cleaned with pure ethanol and deionized water and then dried out in open air.

(b) The annealed aluminum foil is then electropolished in a bath consisting of perchloric acid ($HClO_4$), ethanol (C_2H_6O), and monobutylether ($CH_3(CH_2)_3OCH_2CH_2OH$) to remove inhomogeneities and roughness of the surface. Two power supplies are required to provide consistent voltage. The anode is the aluminum foil, and the cathode is the pure platinum. Typically, fifteen minutes are required to electropolish the aluminum foil. This process enables the leveling of the aluminum foil surface since high current density areas like metal peaks will be dissolved quickly, and the remaining dirt can also be removed in this process. After the electropolishing of aluminum foil, the specimen needs to be rinsed with pure ethanol and deionized water.

(c) First anodization of the aluminum foil. The AAO template is fabricated by anodizing the electropolished aluminum foil at 40 Volts in oxalic acid ($C_2H_2O_4$) for 30 minutes (different voltages may be applied to achieve different pore sizes). Regular hexagonal array of pores can be formed on the aluminum substrate in this step. However, uniformly distributed vertically-aligned AAO is not well-prepared after this step; therefore, the as-formed AAO needs to be chemically removed by being immersed in a bath consisting of chromic acid (CrO_3) and phosphoric acid (H_3PO_4) at 60℃ for 40 minutes. Regular hexagonal array of scallop-shaped indentations corresponding to just-formed AAO pores will be generated after this operation. The formation mechanism of AAO nanochannel structure may be explained as follows:

When we provide voltage to the electrochemical cell composed of aluminum foil (anode) and platinum (cathode), the aluminum will be ionized (Reaction (1)). Also, in aqueous solution, water will be ionized to H^+ and OH^- (Reaction (2)). Therefore, Al^{+3} can associate with OH^- to form alumina (Al_2O_3) (Reaction (3)). The nanochannel structure of AAO is resulted from hydrogen (H_2) escaping from the bottom of alumina (Reaction (3)).

$$Al_{(s)} \rightarrow Al^{+3} + 3e^- \quad (1)$$

$$H_2O \rightarrow H^+ + OH^- \quad (2)$$

$$2Al^{+3} + 3OH^- \rightarrow Al_2O_{3(s)} + 1.5H_{2(g)} \quad (3)$$

(d) Second anodization of the aluminum foil. The aluminum substrate with regular pattern is anodized again. By introducing this two-step anodization process, an array of ordered hexagonal cells with a central cylindrical pore perpendicular to the membrane surface can be obtained. Again, the AAO template is fabricated by anodizing the regular pattern bearing aluminum foil at 40 Volts in oxalic acid ($C_2H_2O_4$) for 1 to 24 hrs, which correspond to different specimen thicknesses. In other words, the longer the anodization time, the thicker the AAO template. Uniformly-distributed AAO can be formed on the aluminum substrate surface by the end of this step.

(e) The aluminum substrate can be dissolved and then removed by being immersed in a bath consisting of saturated copper chloride ($CuCl_2$), and hydrochloric acid (HCl) for 30 minutes.

(f) The thin oxidative barrier layer (the thickness depends on the applied voltage) between the anodization film and the aluminum substrate can be removed by being immersed in phosphoric acid (H_3PO_4) at 25℃ for 90 minutes.

(g) The pore-widening process. A chemical etching (thinning) treatment to attenuate the nanopore wall thickness can be used to enlarge the nanopores of the AAO template by immersing the AAO template in phosphoric acid (H_3PO_4) at 25℃ for 40 minutes. The number density and the center-to-center distance between pores are maintained after this operation.

(h) The morphology of fabricated AAO specimens will be observed by a field emission scanning electron microscope (FE-SEM) (JEOL JSM-6500F).

The schematic diagrams showing the fabrication process of AAO templates are illustrated in Figure 5.

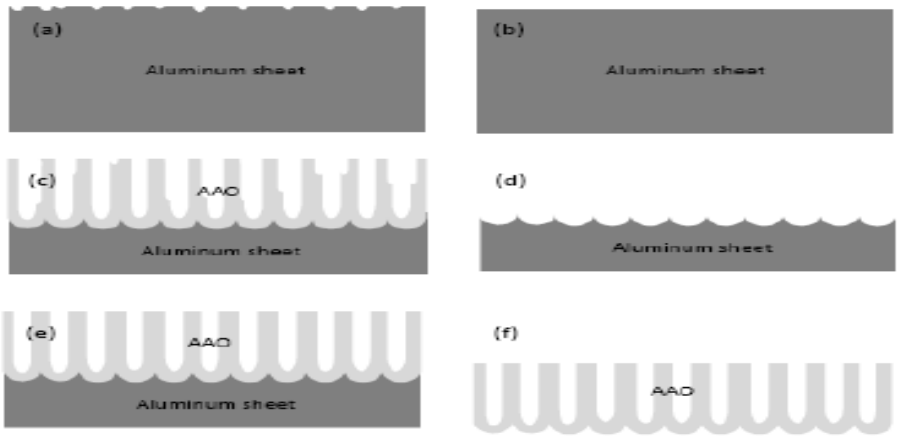

Figure 5 Schematic diagrams illustrating the fabrication processes of AAO templates. (a) 99.7% purity Aluminum foil, (b) Electropolishing of Aluminum foil, (c) First anodization, (d) The removal of AAO formed in the previous step, (e) Second anodization, (f) The removal of Aluminum substrate.

3.3.2 Fabrication of copper nanowire arrays

The fabrication of copper nanowire arrays is accomplished by filling AAO nanochannels with the technique of pulsed DC electrodeposition (PED), one of the common methods used to deposit materials in pores of high aspect ratios. We chose PED instead of alternating current (AC) or direct current (DC) since PED can lead to greater uniformity, homogeneity, and filling fraction of nanowires. Also, PED can compensate for the slow diffusion-driven transport in nanochannels [65-66,104-106]. Furthermore, it was reported that AC sinusoidal waveforms (AC electrodeposition) yields unevenly filled AAO pores. Next, the pulsed AC electrodeposition may damage the AAO templates [107]. Last, the DC electrodeposition is not stable enough and the filling of AAO pores is not uniform [54]. Based on the above research, we chose pulsed DC electrodeposition to fill AAO nanochannels.

Basically, the electrochemical deposition process is based on the cathodic reduction of metal ions dissolved in the electrolyte under electric field [108]. The steps are as follows:

(a) AAO specimens (80 nm in diameter, and 25-60 μm in length) were fabricated according to the procedures described in section 3.1.

(b) The AAO specimen was sputtered on its bottom surface with a thin copper film serving as a working conductive electrode. The specimen rested in a fixture to prevent corrosive attack of acid electrolyte through the deposition process.

(c) The pulsed electrodeposition process was carried out in a typical two electrode electrochemical cell with Platinum (Pt) plate as a counter electrode, and the sputtered thin conductive copper film on the bottom of AAO as a working electrode. The electrolyte was a mixture containing 180g/l $CuSO_4.5H_2O$, 2ml/l H_2SO_4, and 6g/l PEG (Polyethylene Glycol, used as a suppresser) 2000. Also, the bath temperature and pH were maintained at 25℃ and 4, respectively.

(d) During the electrochemical deposition process, the cell was placed in an ultrasonic cleaner (Branson 3510, Figure 6(a)) operated at 40 kHz to facilitate the diffusion process of metal ions into AAO nanochannels. It is expected that metal ion depletion can be prevented by this operation. Also, the delay between pulses enables the replenishment of metal ions.

(e) The power supply was programmed to switch on and off every one second during the entire 1 hr deposition period. In other words, the pulse time was 1 second, and the time period between two consecutive pulses was also 1 second. A potential of -3.5 V was applied between two electrodes with deposition current density of 17mA/cm^2. Also, the potential was -1.2 V during two consecutive pulses.

(f) Most AAO nanochannels were filled with Cu nanowires after 1hr electrodeposition. Specimens were then immersed in 0.5M KOH solution to partially etch away AAO. The longer the immersion time, the longer the exposed length of copper nanowires. Next, specimens were immersed in

deionized water and cleaned by an ultrasonic cleaner to remove any residual alumina on the specimen surfaces.

The copper nanowire arrays fabricated by the above process is *Designed TIM 1*. In order to fabricate *Designed TIM 2*, we used a plastic card to uniformly apply a thin layer of thermal grease on both sides of *Designed TIM 1*. The thickness of thermal grease is measured by a micrometer and controlled at 10μm (top-side thermal grease thickness plus bottom-side thermal grease thickness).

The morphology of as-fabricated copper nanowire array was characterized by field emission scanning electron microscope (FE-SEM) (JEOL JSM-6500F, Figure 6(b)).

Figure 6 Images of instruments used for the fabrication and characterization of copper nanowires. (a) Ultrasonic cleaner (Branson 3510), (b) Field emission scanning electron microscope (FE-SEM) (JEOL JSM-6500F).

3.4 Specimen analysis

3.4.1 Field emission scanning electron microscope (FE-SEM) study

3.4.1.1 SEM images of AAO

The SEM images (top-view) of AAO templates fabricated by the anodization of aluminum foils are shown in Figure 7.

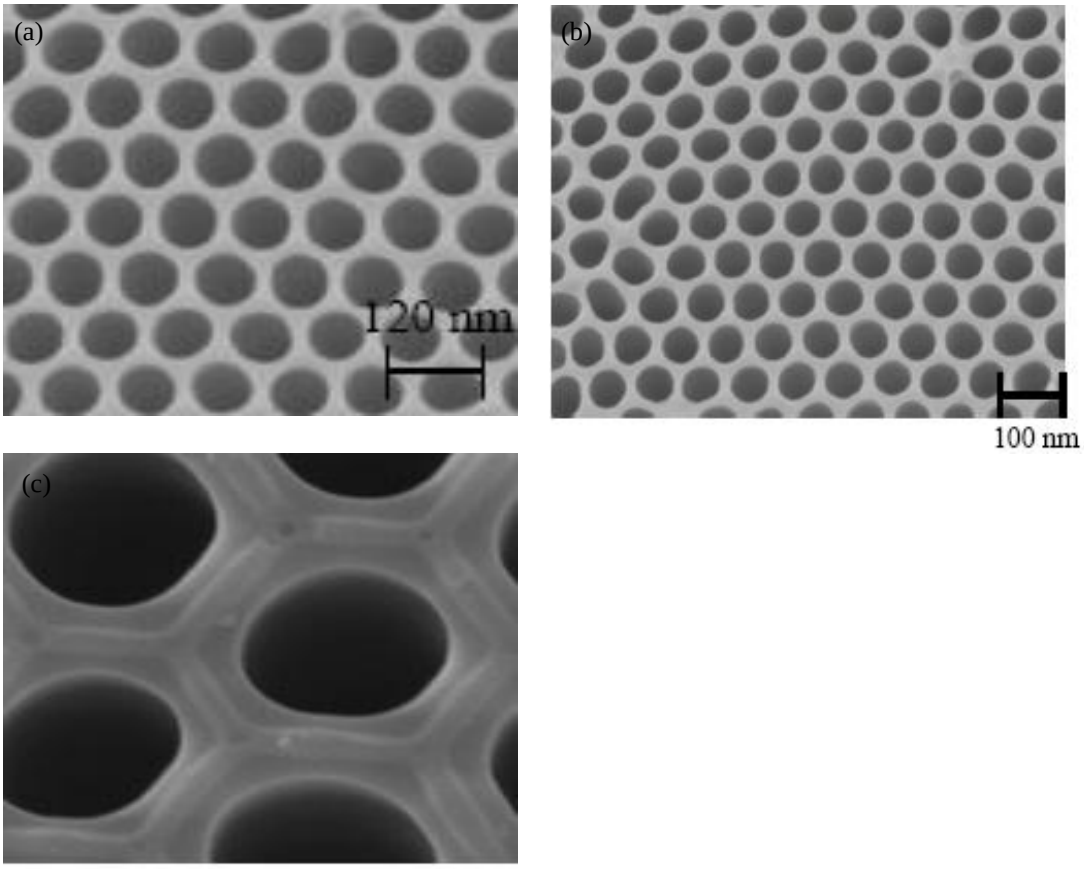

Figure 7 SEM images of AAO fabricated by 99.7% purity aluminum foil (top-view). (a) Hexagonally packed nanopores with diameter=80nm, (b) hexagonally packed nanopores with diameter=60nm, (c) AAO hexagonal pattern image with high magnification.

The SEM images (bottom-view) of AAO templates fabricated by the anodization of aluminum foils are shown in Figure 8.

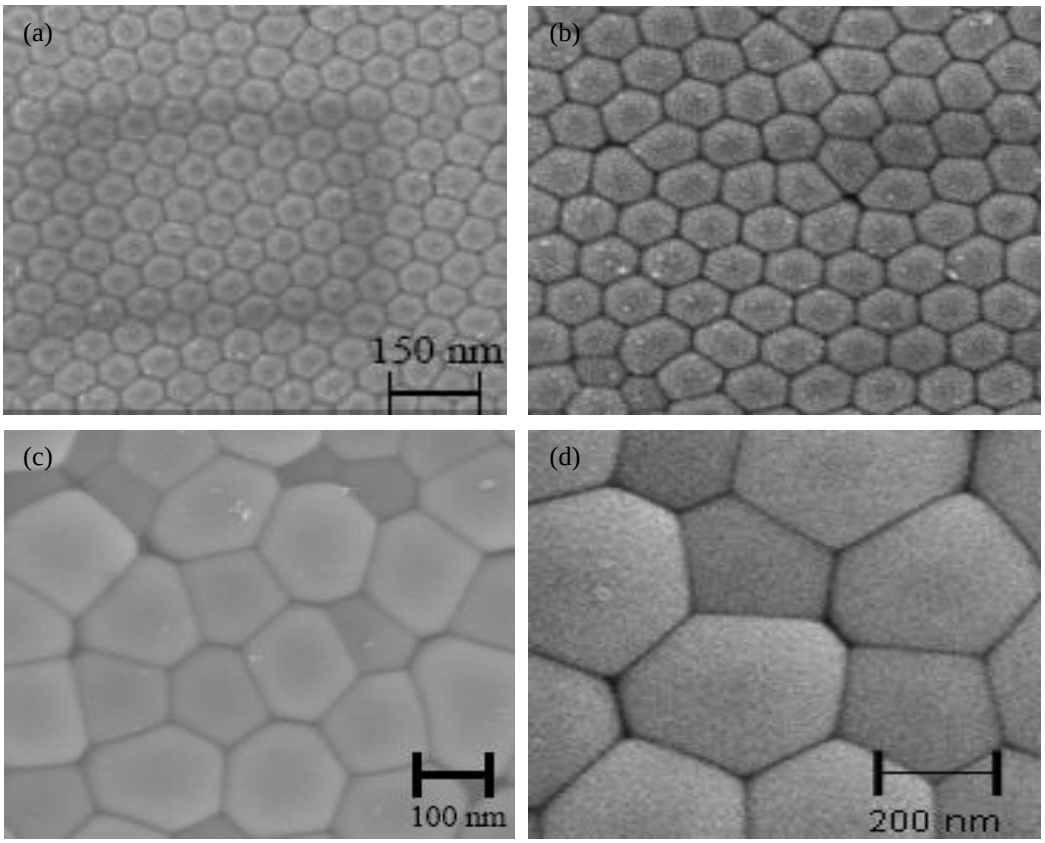

Figure 8 SEM images of AAO fabricated by 99.7% purity aluminum foil (bottom view). (a) Barrier layer with hexagonally packed structure, (b) barrier layer with hexagonally packed structure, (c) barrier layer image with high magnification, (d) barrier layer image with high magnification.

The SEM images (side view) of AAO templates fabricated by the anodization of aluminum foils are shown in Figure 9.

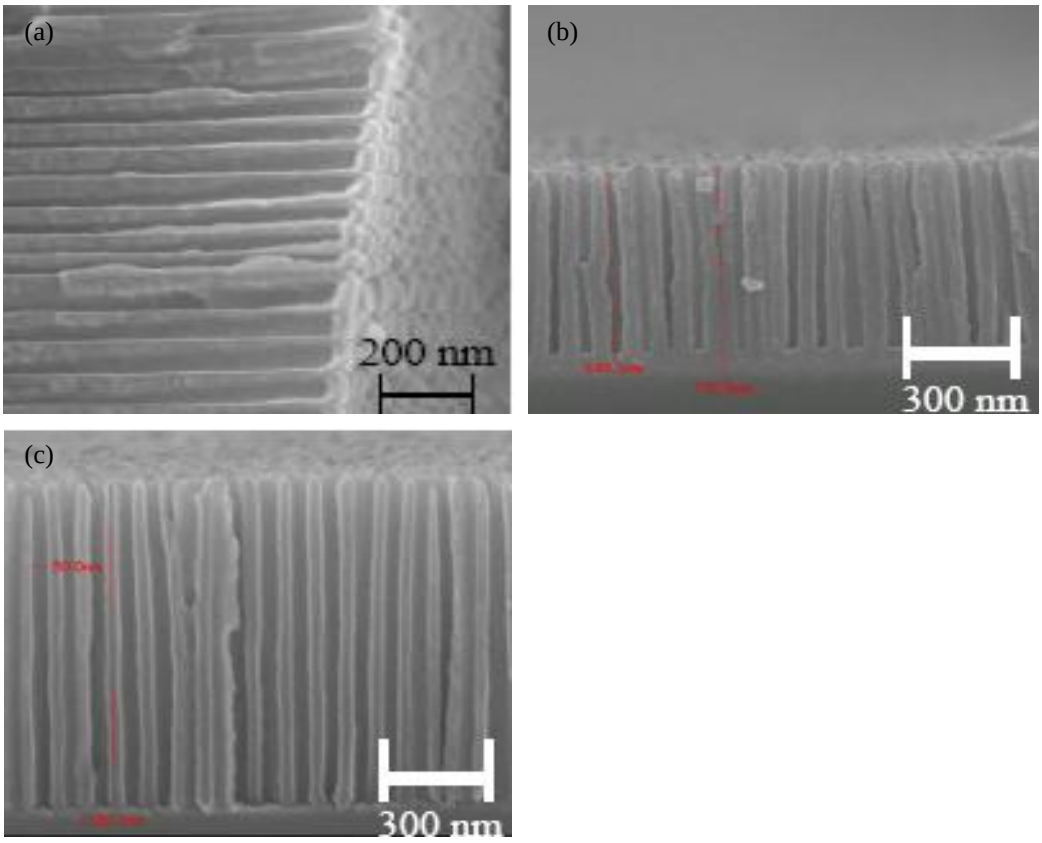

Figure 9 SEM images of AAO fabricated by 99.7% purity aluminum foil (side view). (a) Side view of AAO nanochannels, (b) side view of AAO nanochannels with barrier layer, (c) side view of AAO nanochannels without barrier layer.

3.4.1.2 SEM images of copper nanowires

The SEM images of copper nanowires before testing are shown in Figure 10.

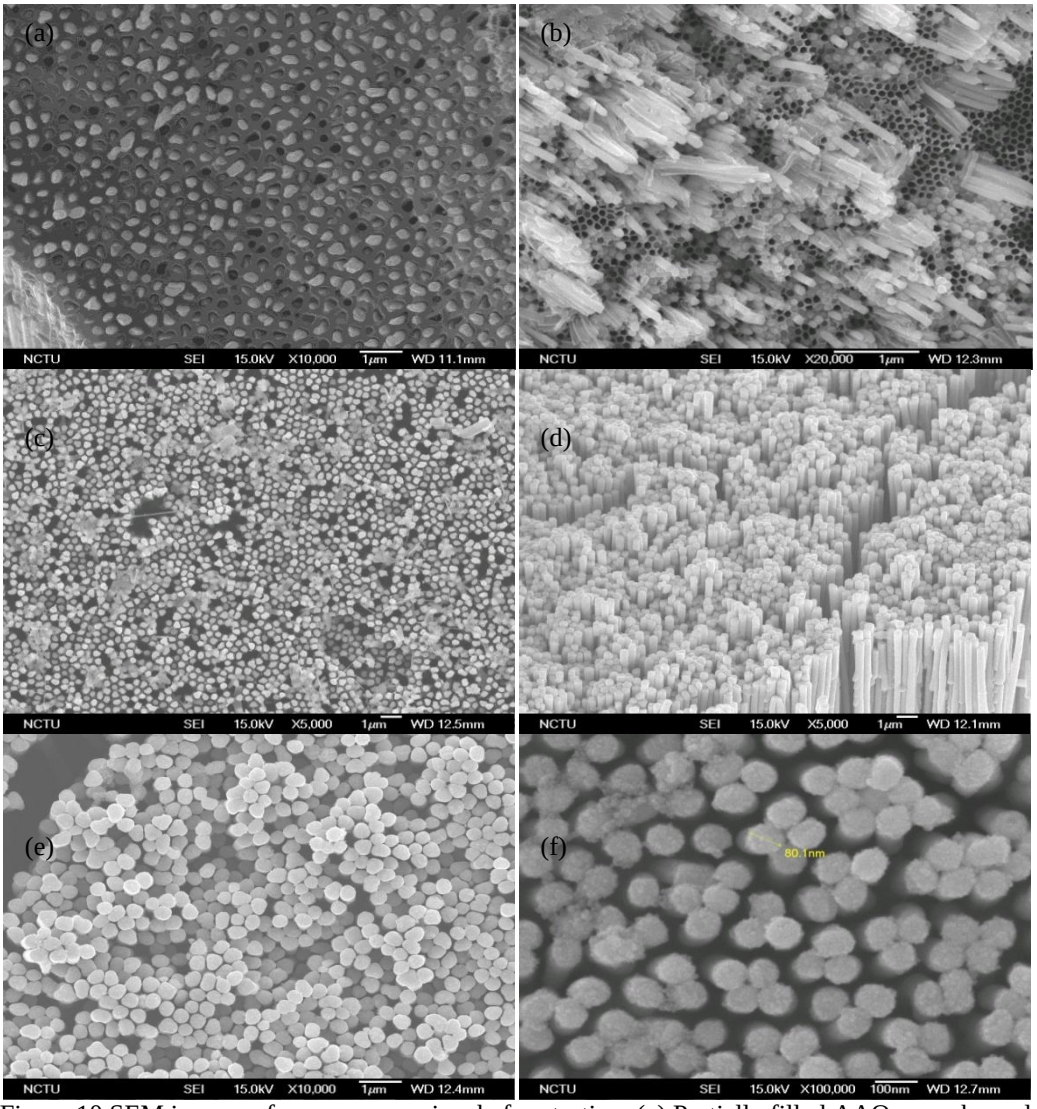

Figure 10 SEM images of copper nanowires before testing. (a) Partially filled AAO nanochannels (top-view), (b) partially filled AAO nanochannels (side-view), (c) highly filled AAO nanochannels, (d) densely-packed copper nanowires, (e) copper nanowires with diameter=80nm, (f) copper nanowires image with high magnification.

The SEM images of copper nanowires after testing are shown in Figure 11.

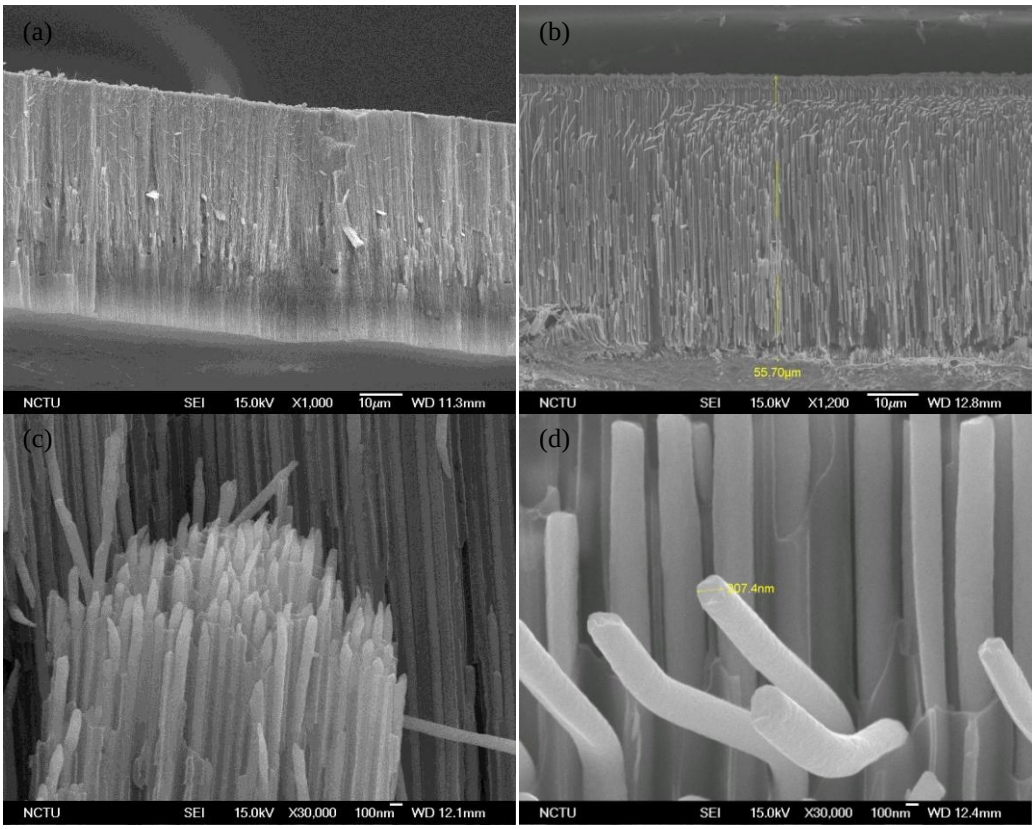

Figure 11 SEM images of copper nanowires after testing. (a) Copper nanowire arrays (side-view), (b) Slightly deflected copper nanowires, (c) densely packed copper nanowires, (d) copper nanowires image with high magnification.

3.5 Calibration process

3.5.1 Calibration of thermocouples

Four thermocouples were used to detect temperature readings along brass meter bars. In order to calibrate temperature readings, Fisher Scientific Isotemp Refrigerated Circulator (FSIRC, Model 9100) with higher resolution than four thermocouples was used. We monitored and recorded temperature readings of these four thermocouples at

different water temperatures, adjustable by tuning the FSIRC. Basically, the water temperatures were elevated from 15℃ to 60℃, with a near 2.5℃ interval between two consecutive adjustments (Table 3). At the same time, the four thermocouple probes were immersed in vicinity of the center of the water tank to take corresponding individual temperature readings. The results are as follows.

Table 3 Temperatures readings of thermocouples at different controlled water bath temperatures.

Water temperature (℃)	$T_{Thermocoule\ 1}$ (℃)	$T_{Thermocoule\ 2}$ (℃)	$T_{Thermocoule\ 3}$ (℃)	$T_{Thermocoule\ 4}$ (℃)	Avg. of four thermocouples (℃)
15.0	12.9	14.0	13.5	14.6	13.8
17.5	15.3	16.4	15.9	17.0	16.2
20.0	17.7	18.8	18.2	19.4	18.5
22.5	20.1	21.2	20.6	21.8	20.9
25.0	22.6	23.5	23.0	24.2	23.3
27.5	25.1	25.9	25.4	26.7	25.8
30.1	27.6	28.5	28.0	29.0	28.3
32.5	29.9	30.9	30.4	31.0	30.6
35.1	32.5	33.4	33.0	33.9	33.2
37.6	35.0	35.9	35.5	36.5	35.7
40.1	37.5	38.5	38.0	39.1	38.3
42.6	40.0	40.9	40.4	41.5	40.7
45.0	42.4	43.3	42.8	44.0	43.1
47.5	44.8	45.8	45.3	46.5	45.6
50.0	47.2	48.3	47.8	49.0	48.1
52.5	49.7	50.8	50.3	51.5	50.6
55.0	52.1	53.3	52.8	54	53.1
57.5	54.7	55.8	55.3	56.5	55.6
60.0	57.2	58.3	57.8	59.1	58.1

With the data listed above, we were able to calibrate temperature readings of four thermocouples based on their values biased from the average temperatures of four

thermocouples at a specific water temperature (as a reference). The results are as listed in Table 4.

Table 4 Adjustments of temperatures readings of thermocouples at different controlled water bath temperatures.

Water temperature (℃)	$T_{Thermocoule\ 1}$ (biased value)[1] (℃)	$T_{Thermocoule\ 2}$ (biased value)[1] (℃)	$T_{Thermocoule\ 3}$ (biased value)[1] (℃)3	$T_{Thermocoule\ 4}$ (biased value)[1] (℃)
15.0	0.85	-0.25	0.25	-0.85
17.5	0.85	-0.25	0.25	-0.85
20.0	0.825	-0.275	0.325	-0.875
22.5	0.825	-0.275	0.325	-0.875
25.0	0.725	-0.175	0.325	-0.875
27.5	0.675	-0.125	0.375	-0.925
30.1	0.675	-0.225	0.275	-0.725
32.5	0.65	-0.35	0.15	-0.45
35.1	0.7	-0.2	0.2	-0.7
37.6	0.725	-0.175	0.225	-0.775
40.1	0.775	-0.225	0.275	-0.825
42.6	0.7	-0.2	0.3	-0.8
45.0	0.725	-0.175	0.325	-0.875
47.5	0.8	-0.2	0.3	-0.9
50.0	0.875	-0.225	0.275	-0.925
52.5	0.875	-0.225	0.275	-0.925
55.0	0.95	-0.25	0.25	-0.95
57.5	0.875	-0.225	0.275	-0.925
60.0	0.9	-0.2	0.3	-1.0

[1] Here the *biased value* means the difference between a thermocouple temperature reading and the one from the average of four thermocouples at a specific water temperature.

Based on the above data, we may calibrate our thermocouples as in Table 5.

Table 5 Calibrations of four thermocouples.

Thermocouples	$T_{Thermocoule\ 1}$ (℃)	$T_{Thermocoule\ 2}$ (℃)	$T_{Thermocoule\ 3}$ (℃)	$T_{Thermocoule\ 4}$ (℃)
Calibration value	+0.8	-0.2	+0.3	-0.9

To ensure the consistency of calibration values, regular calibrations are needed.

3.5.2 Calibration of experimental fixture

In order to test the feasibility of our fixture, we chose and tested on two commercially available TIMs with published thermal properties to see if we can derive consistent and close values as published ones. In regards to TIMs applied between heat sink and computer chip, the following two kinds of TIMs were recommended by *Chomerics*® [15]:

(1) *976*: Best thermal performance

(2) *A580*: High popularity due to its good thermal performance and relatively low cost

In order to test the consistency of our fixture, we repeatedly conducted tests on the above two types of TIMs. The experimental results are as follows (Table 6 and 7):

Table 6 Preliminary experiment results of commercial TIM products #976.

Sample description [15]:
1. Published thermal impedance=3.1($℃-cm^2/W$)at 50psi.
2. Published thermal conductivity=6 W/m-K.
3. Thickness under no pressure=0.1 cm.
4. Thickness under 50psi=0.055 cm
5. Ambient temperature is controlled between 23±2℃.
6. Circulating water bath temperature is maintained at 10℃.

Specimen	1	2	3	4	5	6	7	8	9	10
$T_{1,\,final}$ (℃)	61.1	61.5	59.1	59.3	57.9	56.5	57.1	59.3	60.1	61.5
$T_{2,\,final}$ (℃)	57.7	58.2	55.7	56.2	54.8	53.4	54.1	56.0	56.8	58.0
$T_{3,\,final}$ (℃)	45.0	45.7	43.4	44.6	43.5	42.5	43.1	43.8	44.4	45.2
$T_{4,\,final}$ (℃)	41.4	42.1	39.8	41.2	40.1	39.4	39.9	40.4	41.0	41.7
$T_{Specimen}$ (℃)	51.4	52.0	49.6	50.4	49.2	48.0	48.6	49.9	50.6	51.6
θ ($℃-\frac{cm^2}{W}$)	3.036	3.029	2.893	2.962	2.846	2.895	2.935	3.052	3.127	3.071
% off the published value (%)	-2.06	-2.29	-6.68	-4.45	-8.19	-6.61	-5.32	-1.55	+0.87	-0.94

Table 6 (Continued)

Specimen	11	12	13	14	15	16	17	18	19	20
Ampere (A)	3.15	3.15	3.15	3.15	3.15	3.15	3.15	3.15	3.15	3.15
$T_{1,\ final}$ (℃)	62.5	62.3	60.2	61.6	60.0	59.4	61.4	61.1	58.6	58.2
$T_{2,\ final}$ (℃)	58.7	58.3	56.4	58.1	56.8	56.3	58.3	57.9	55.2	55.0
$T_{3,\ final}$ (℃)	45.2	44.9	43.0	44.8	43.6	42.5	44.8	44.4	43.6	43.3
$T_{4,\ final}$ (℃)	42.0	41.7	39.7	40.8	39.2	38.3	40.4	40.2	40.5	39.9
$T_{Specimen}$ (℃)	52.0	51.6	49.7	51.5	50.2	49.4	51.6	51.2	49.4	49.2
θ $(℃-\frac{cm^2}{W})$	3.321	3.153	3.218	2.933	2.842	3.226	3.000	3.061	2.962	2.932
% off the published value (%)	+7.13	+1.71	+3.81	-5.39	-8.32	+4.06	-3.23	-1.26	-4.45	-5.42

Table 6 (Continued)

Specimen	21	22	23	24	25
Ampere (A)	3.15	3.15	3.15	3.15	3.15
$T_{1,\ final}$ (℃)	57.8	59.0	57.1	58.0	55.8
$T_{2,\ final}$ (℃)	54.6	56.5	54.3	55.2	53.3
$T_{3,\ final}$ (℃)	43.2	46.8	44.2	44.7	43.4
$T_{4,\ final}$ (℃)	40.0	44.3	41.6	41.9	40.8
$T_{Specimen}$ (℃)	48.9	51.7	49.3	50.0	48.4
θ $(℃-\frac{cm^2}{W})$	2.953	3.350	3.176	3.188	3.353
% off the published value (%)	-4.74	+8.06	+2.45	+2.84	+8.16

Table 7 Preliminary experiment results of commercial TIM products #A580.

Sample description [15]:

1. Published thermal impedance≈2.700($℃-cm^2/W$) at 50psi.
2. Published thermal conductivity=3 W/m-K.
3. Thickness under no pressure=0.05 cm.
4. Thickness under 50psi=0.035 cm.
5. Ambient temperature is controlled between 23±2℃.
6. Circulating water bath temperature is maintained at 10℃.

Specimen	1	2	3	4	5	6	7	8	9	10
Ampere (A)	3.15	3.15	3.15	3.15	3.15	3.15	3.15	3.15	3.15	3.15
$T_{1,\ final}$ (℃)	54.5	55.3	56.0	59.7	60.1	59.9	62.4	61.9	62.3	64.1
$T_{2,\ final}$ (℃)	52.6	53.0	53.9	56.7	56.9	56.9	59.4	58.9	59.3	59.1
$T_{3,\ final}$ (℃)	44.0	44.3	45.3	43.3	43.6	43.4	44.3	43.8	44.1	42.4
$T_{4,\ final}$ (℃)	40.9	41.3	42.3	38.4	38.8	38.6	38.3	37.8	38.2	37.3
$T_{Specimen}$ (℃)	48.3	48.7	49.6	50.0	50.3	50.2	51.9	51.4	51.7	50.8
θ $(℃-\frac{cm^2}{W})$	2.800	2.604	2.716	2.741	2.656	2.827	2.694	2.694	2.770	2.634
% off the published value (%)	+3.70	-3.56	+0.59	+1.52	-1.63	+4.70	-0.22	-0.22	+2.59	-2.44

Table 7 (Continued)

Specimen	11	12	13	14	15	16	17	18	19	20
$T_{1,\ final}$ (℃)	64.1	63.8	65.9	65.7	64.3	64.2	64.6	63.8	66.5	66.0
$T_{2,\ final}$ (℃)	59.1	58.3	60.5	60.1	58.9	59.0	59.2	58.4	60.8	60.5
$T_{3,\ final}$ (℃)	42.3	40.7	42.9	42.4	40.9	40.9	41.3	40.3	42.7	42.4
$T_{4,\ final}$ (℃)	37.3	35.7	37.6	37.4	35.8	35.8	36.0	35.1	37.6	37.2
$T_{Specimen}$ (℃)	50.7	49.5	51.7	51.3	49.9	50.0	50.3	49.4	51.8	51.5
θ $(℃ - \frac{cm^2}{W})$	2.700	2.690	2.612	2.675	2.786	2.893	2.682	2.769	2.690	2.729
% off the published value (%)	0.00	-0.37	-3.26	-0.93	+3.19	+7.15	-0.67	+2.56	-0.37	+1.07

Table 7 (Continued)

Specimen	21	22	23	24	25
$T_{1,\ final}$ (℃)	66.8	64.4	63.8	65.1	64.6
$T_{2,\ final}$ (℃)	61.0	58.8	58.4	59.6	59.1
$T_{3,\ final}$ (℃)	42.7	40.7	40.4	41.2	40.7
$T_{4,\ final}$ (℃)	37.6	35.6	35.2	35.9	35.5
$T_{Spcimen}$ (℃)	51.9	49.8	49.4	50.4	49.9
θ $(℃ - \frac{cm^2}{W})$	2.697	2.729	2.745	2.759	2.799
% off the published value (%)	-0.11	+1.07	+1.67	+2.19	+3.67

The preliminary experimental results are summarized in Table 8.

Table 8 Preliminary experimental results of arithmetic mean and standard deviation of thermal impedances of TIM#976 and A580.

TIM	Sample size	Arithmetic mean of thermal impedance ($℃ - cm^2/W$)	Standard deviation
976	25	3.061	0.1536
A580	25	2.724	0.0677

In order to statistically prove whether our experimental fixture can consistently derive thermal impedance values close to published ones for TIM#976 and A580, the following two-tailed hypothesis testing was conducted:

1. Null hypothesis H_0: $\mu_{TIM} = \mu_0$ (manufacturer's published values)

   Alternative hypothesis H_A: $\mu_{TIM} \neq \mu_0$

   where μ_{TIM} and μ_0 represent the true average and manufacturer's published thermal

impedance value, respectively.

Significance level α=0.05

2. Test statistic (TS): $t = \frac{\bar{x}-\mu_0}{s/\sqrt{n}}$ =1.270 (TIM#976) and 1.773 (TIM#A580)

3. Rejection region (RR): For Degree of freedom (DF) =n-1=24,

   reject H_0 if $t \geq t_{\propto/2,n-1}$ or $t \leq -t_{\propto/2,n-1}$

   From the table of the t distribution, $t_{0.025,24}$=2.064

4. For TIM#976, t does not fall in the RR

   For TIM#A580, t does not all in the RR

5. Therefore, the data does not strongly suggest that the true average thermal impedance value of TIM#976 and A580 derived from experiments differ from the manufacturer's published value.

As a result, we may conclude from the above preliminary experimental results and hypothesis testing that our experimental fixture can derive consistent thermal impedance values and can be used for testing our designed TIMs under various treatments.

3.6 Experimental setup

Figure 12 illustrates the experimental fixtures used for the fabrication of AAO templates.

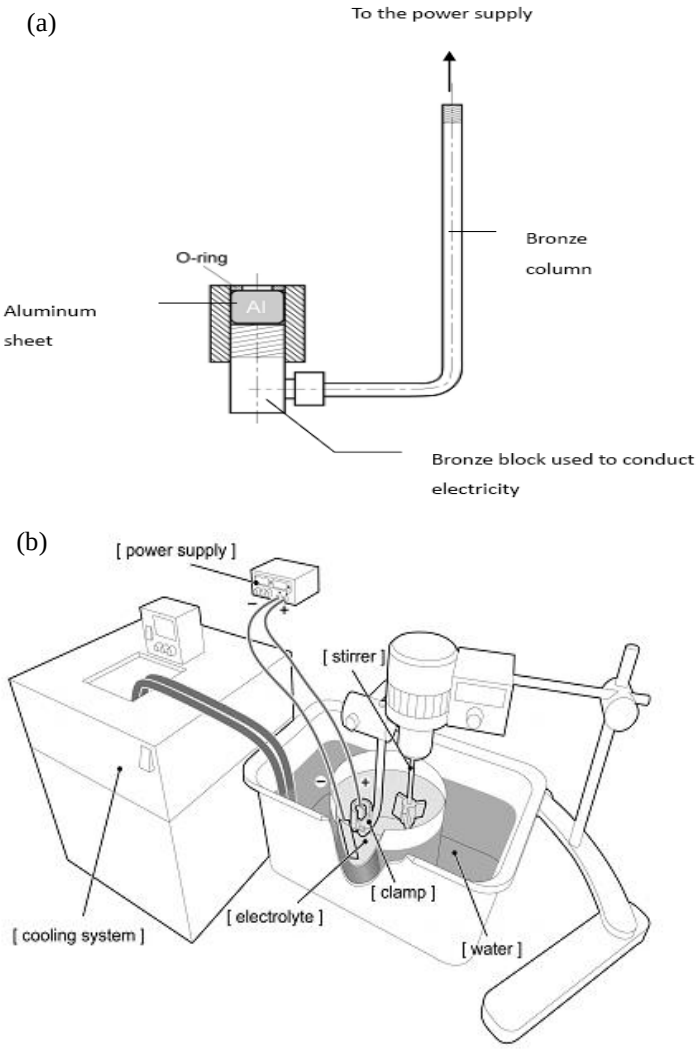

Figure 12 Schematic diagrams of the experimental fixtures used to fabricate AAO templates. (a) Fixture used to secure the aluminum foil throughout the electrodeposition process, (b) experimental fixtures used to fabricate AAO templates.

The experimental setup and testing procedures follow the standards of ASTM D5470-06, which is the standard test method for thermal transmission properties of thermally conductive materials.

Basically, the experimental fixture is composed of a vacuum chamber, a vacuum pump, a power supply, a refrigerated circulator, four thermocouples, pneumatics, and two brass meter bars (Figure 13).

A test specimen of uniform thickness is placed between two parallel, isothermal surfaces. In order to generate the heat flow through the specimen, we need to impose the thermal gradient across the specimen. The lower (hot) meter bar is coiled with electrical resistance wires and connects to a power supply; while the upper (cool) meter bar is coiled with copper coils and connects to a refrigerated circulator (Figure 14). The temperature of hotter meter bar can be controlled by tuning the current input of power supply, and the temperature of cooler meter bar can be tuned by adjusting the target water temperature of refrigerated circulator.

The contact pressure on the specimen will be controlled and maintained by pneumatics, which can be precisely controlled by air regulator between 10-160 psi.

Four K-type thermocouples were used to monitor the temperatures along meter bars for the sake of determining the specimen surface temperatures. The resolution of our thermometer is ±0.1℃.

In order to minimize the effect of thermal convection, a vacuum pump will be used to suck all the air out of the experimental chamber. Furthermore, the experimental chamber will be covered with Mylar sheet to reduce the effect of thermal radiation.

Figure 13 Image of the experimental setup used to determine thermal properties of TIMs.

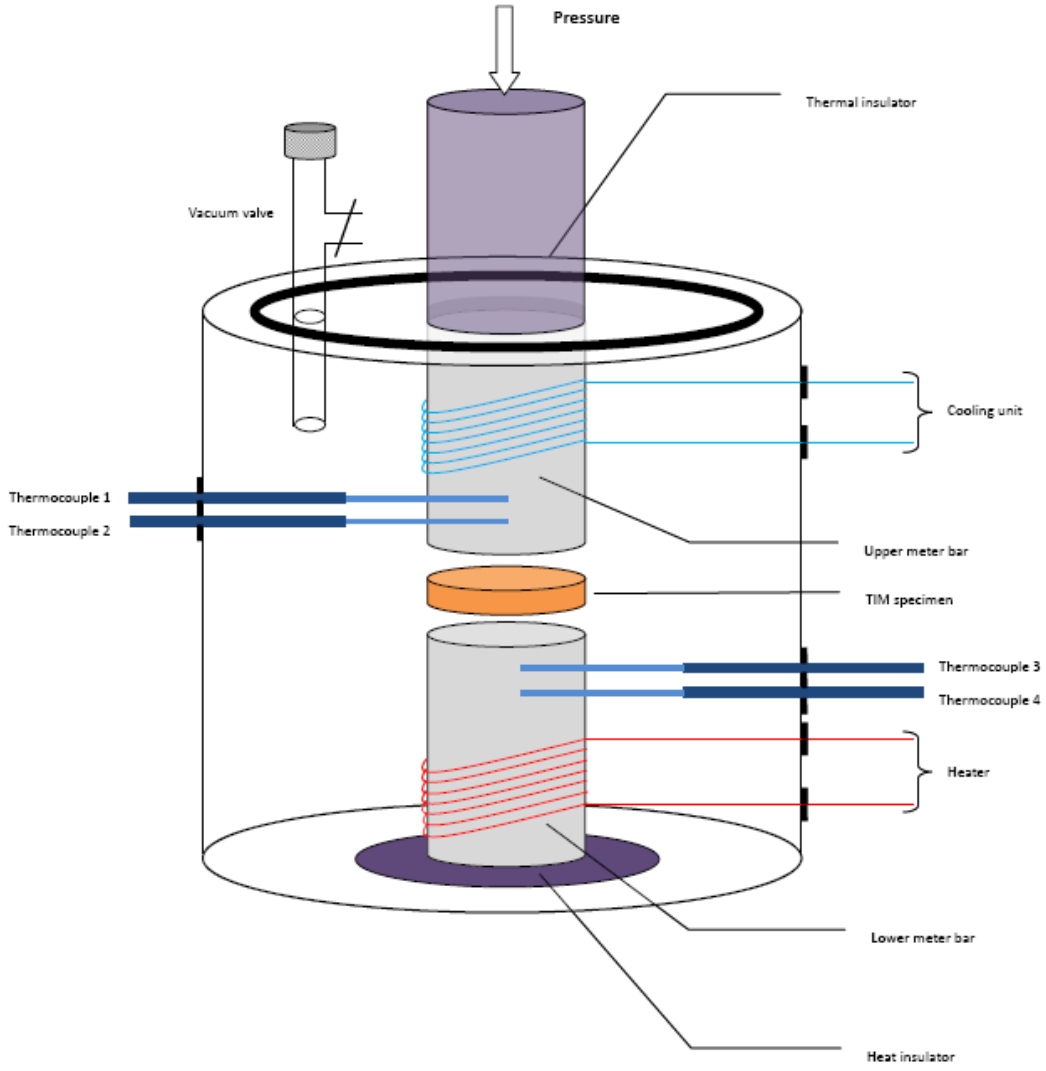

Figure 14 Schematic diagram of the experimental chamber following the regulations of ASTM D5470-06 used to determine the thermal properties of TIMs.

4. DESIGN OF EXPERIMENTS

4.1 Experimental hypothesis

4.1.1 The dominating heat transfer mode in TIMs

There are three heat transfer modes: thermal conduction, thermal convection, and thermal radiation. The physical mechanisms underlying three heat transfer modes are briefly explained below.

4.1.1.1 Thermal conduction

In order to quantify the heat transferred by conduction, the *Fourier's law of thermal conduction* is presented as:

$$Q=K\times A_c\times \frac{\Delta T}{\Delta x} \quad (4)$$

where Q is the heat flow, A_c is the cross-sectional surface area of the material, and $(\Delta T/\Delta x)$ is the temperature gradient in the material. This is the one-dimensional thermal conduction under steady state conditions.

Thermal conduction is the heat transfer mode that relates to atomic and molecular interaction activities. As a result of interactions between particles, the thermal conduction takes place and transfers energies from higher energetic particles to relatively lower ones [110]. The physical mechanism behind this is that higher temperature particles always have higher energies, and when they collide with lower temperature particles with lower energies, the energy will be transferred in the direction of decreasing energies. Therefore, if we focus on the temperature, which is one member of

energy families, the thermal conduction will proceed in the direction of decreasing temperatures.

4.1.1.2 Thermal convection

In order to quantify the heat transferred by convection, the *Newton's law of cooling* is presented as:

$$Q=h\times A_s\times\left(T_s-T_\infty\right) \quad (5)$$

where Q is the heat flow, h is the convection heat transfer coefficient, A_s is the surface area of the material/specimen, T_s is the surface temperature, and T_∞ is the fluid temperature.

Thermal convection is contributed both by random molecular motion and by the bulk motion of fluid within the boundary layer. According to the nature of the flow, convection heat transfer may be classified into two modes. One is free (natural) convection, and the other one is forced convection. Forced convection is caused by external means while free (natural) convection is induced by buoyancy forces [110].

4.1.1.3 Thermal radiation

The heat transferred by radiation can be quantified as:

$$Q=\varepsilon\times\sigma\times A_s\times\left(T_s^4-T_{sur}^4\right) \quad (6)$$

where Q is the heat flow, ε is the emissivity, A_s is the surface area of the material/specimen, T_s is the surface temperature, and T_{sur} is the surrounding temperature.

Thermal radiation is energy emitted by matter that is at a finite temperature. Unlike conduction and convection heat transfers require the presence of a material

medium, radiation is transferred by electromagnetic waves (phonons) and does not require any medium.

Based on the mechanisms of three heat transfer modes, the effects of thermal convection and radiation were neglected in regards to heat transfer in a TIM. The reasons are as follows.

First of all, the thermal convection was neglected due to the fact that the heat transfer coefficient is too small, even though intrusive copper nanowires may have extremely high exposed surface area. Furthermore, the experimental chamber needs to be vacuumed throughout the testing. Without the existence of medium, the effect of thermal convection is negligible.

Next, the thermal radiation was neglected due to the application of Mylar, a polyester film used to shade sun and resist radiation, on the surface of the experimental chamber to reduce the effect of thermal radiation.

4.1.2 Specimen deflection under various pressures

According to ASTM D5470-06 [109], metals and ceramics are classified as *Type-III* materials, which are defined as the elastic solids exhibiting negligible deflection. Since the designed TIMs are composed of copper nanowire arrays (Cu, metals) and alumina (Al_2O_3, ceramics), they are classified as *Type-III* materials. Therefore, the thickness of the designed TIMs was assumed to remain unchanged under moderate clamping pressures.

4.1.3 Surface roughness and parallelism of brass meter bars

The rationale behind ASTM D5470-06 is idealized heat conduction between two parallel isothermal surfaces sandwiching a specimen. The test surfaces are required to be smooth within 0.4 μm and parallel to within 5μm [109]. However, the two brass bar surfaces might not be perfectly smooth over repeated tests if the hardness of specimens is larger than them. Therefore, the heat flow imposed on specimens by temperature difference of two meter bars will not be perfectly perpendicular to specimen surfaces, which may lead to non-uniform heat distribution, lateral heat spreading, and inconsistent specimen thickness. Next, during the application of contact pressure, the meter bars and the specimen were aligned manually. In other words, the alignment of specimen/meter bars was accomplished manually every time. Even slight misalignment of two meter bars may lead to considerable errors since the cross-sectional area and the direction of heat transportation will be influenced (Figure 15). It is postulated that meter bars were well aligned through the whole experiments if we may derive consistent results between tests.

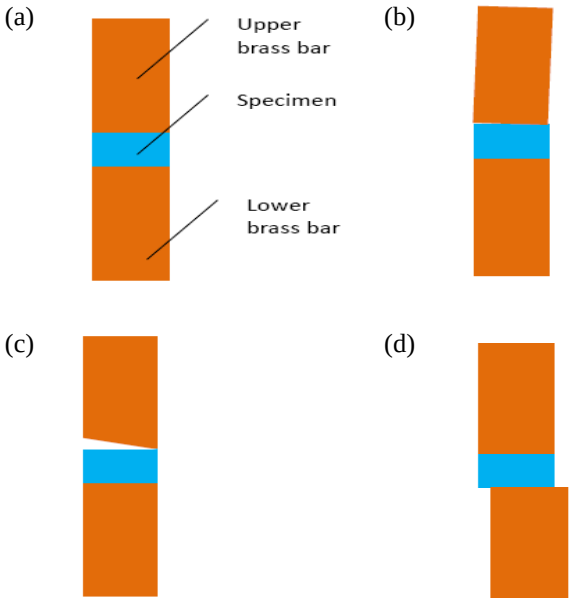

Figure 15 Schematic diagrams showing the physical contact between meter bars and the specimen. (a) Ideal physical contact, (b) Misalignment of meter bars and the specimen, (c) The upper meter bar is not parallel to the lower meter bar, and (d) Misalignment of meter bars and the specimen.

4.1.4 The accuracy of thermocouples

During testing processes, we need to use four thermocouples to measure the temperatures at specific locations of meter bars. The resolution of our four thermocouples is ±0.1℃, which is normal for most of the temperature-measuring devices. However, since the distance (Δx) between two thermocouples is small, the thermal gradient ($\Delta T/\Delta x$) will vary significantly even with slight error of temperature readings from not well-calibrated thermocouples. Therefore, we need to calibrate thermocouples periodically to make sure that readings from them are accurate.

Another source of error resulting from thermocouples is the physical contact between temperature probes and brass bras. The tighter and better the physical contact, the higher the temperature readings (Figure 16). Therefore, it is very important to ensure

consistent contacts all the times. It was assumed that thermocouples are accurate by constantly calibrating their accuracy.

(a) (b)

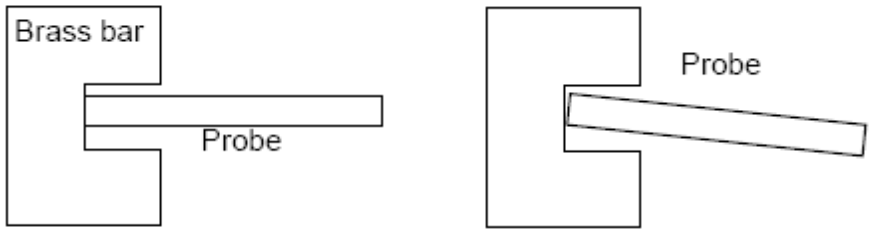

Figure 16 Schematic diagrams showing the physical contact between the temperature probe and the center of the brass bar. (a) Ideal physical contact, (b) Bad physical contact (Figures are not drawn to scale).

4.1.5 The oxidation of copper nanowires

Theoretically, our high thermal conductivity copper nanowires may directly bridge and contact two mating surfaces. However, when copper is placed in a humid environment, two-step oxidation process will take place, as follows:

First step: The formation of a thin Cu_2O layer on the copper surface.

$$4Cu_{(s)} + 2H_2O_{(g)} \rightarrow 2Cu_2O_{(s)} + 2H_{2\,(g)} \quad (7)$$

Second step: The transformation from Cu_2O to CuO

$$2Cu_2O_{(s)} \rightarrow 2CuO_{(s)} + 2Cu_{(s)} \quad (8)$$

The net oxidation reaction equation is then

$$2Cu_{(s)} + O_{2\,(g)} \rightarrow 2CuO_{(s)} \quad (9)$$

Therefore, a thin oxidation (ceramics) layer may top the surface of copper nanowires, which will affect the physical contact between mating surfaces (ceramics is less malleable). Next, the apparent thermal conductivity of our designed TIM will also be affected. In order to reduce the effect of this thin oxidization layer, we need to make use of hydrogen gas or weak nitric acid as reducing agent. The reduction reaction equations are as follows:

$$CuO_{(s)} + H_{2\,(g)} \rightarrow Cu_{(s)} + H_2O_{\,(g)} \quad (10)$$

$$3CuO_{(s)} + 6HNO_{3\,(aq.)} \rightarrow 3Cu(NO_3)_{2\,(aq.)} + 3H_2O_{(l)} \quad (11)$$

We selected nitric acid as our reduction agent due to its easy access. We immerse our designed TIMs in weak nitric acid for 30 sec. It must be pointed out that nitric acid may also oxidize copper, as follows:

$$Cu_{(s)} + 4HNO_{3\,(aq.)} \rightarrow Cu(NO_3)_{2\,(aq.)} + 2NO_{2(g)} + 2H_2O_{(l)} \text{ (concentrated nitric acid)} \quad (12)$$

$$3Cu_{(s)} + 8HNO_{3\,(aq.)} \rightarrow 3Cu(NO_3)_{2\,(aq.)} + 2NO_{(g)} + 4H_2O_{(l)} \text{ (dilute nitric acid)} \quad (13)$$

Therefore, the immersion time must be carefully controlled or some copper nanowires may be dissolved. According to repeated tests and SEM images, it was concluded that 30 seconds is enough to remove the oxidation layer on copper nanowire arrays. Therefore, it is postulated that the oxidization layer on the top of our designed TIMs have been completely removed before testing.

4.2 Measure of performance

The measure of performance in this thesis research is the thermal impedance (θ). The experimental setup and calculations follow the standards of ASTM D5470-06.

Accordingly, if we use two meter bars as calorimeters, then the average heat flow (Q) through specimen can be determined as follows:

$$Q_{12}=\frac{\lambda_{12}\times A}{d}\times\left[T_1-T_2\right] \quad (14)$$

$$Q_{34}=\frac{\lambda_{34}\times A}{d}\times\left[T_3-T_4\right] \quad (15)$$

$$Q=\frac{Q_{12}+Q_{34}}{2} \quad (16)$$

where Q_{12} is the heat flow in hot meter bar (W), Q_{34} is the heat flow in cold meter bar (W), λ_{12} is the thermal conductivity of the hot meter bar (W/m-K), λ_{34} is the thermal conductivity of the cold meter bar (W/m-K), A is the area of meter bars (m^2), T_1 (K) is the temperature measured by thermocouple 1, T_2 (K) is the temperature measured by thermocouple 2, T_3 (K) is the temperature measured by thermocouple 3, T_4 (K) is the temperature measured by thermocouple 4, and d is the distance between thermocouples in meter bars (m).

In order to derive the surface temperatures of the top (hot) and bottom (cold) brass bars in contact with the specimen, the temperature gradients inside both of them need to be calculated by the following equations:

$$\nabla T_{Top,cold}=\frac{T_3-T_4}{d_C}\equiv\alpha \quad (17)$$

$$\nabla T_{bottom,hot}=\frac{T_1-T_2}{d_A}\equiv\beta \quad (18)$$

where $\nabla T_{Top,\ cold}$ (defined as α here for convenience) is the temperature gradient in the top (cold) meter bar (K/m), $\nabla T_{bottom,hot}$ (defined as β here for convenience) is the temperature gradient in the bottom (hot) meter bar (K/m), T_1 (K) is the temperature

measured by thermocouple 1, T_2 (K) is the temperature measured by thermocouple 2, T_3 (K) is the temperature measured by thermocouple 3, T_4 (K) is the temperature measured by thermocouple 4, d_A (m) is the distance between T_1 and T_2, d_B (m) is the distance between T_2 and the surface of the hot meter bar in contact with the specimen, d_C (m) is the distance between T_3 and T_4, and d_D (m) is the distance between T_4 and the surface of the cold meter bar in contact with the specimen.

With the temperature gradients in both the top and bottom meter bars, we are now able to derive the temperatures of their surfaces in contact with the specimen by extrapolating from the known measured temperatures as follows:

$$T_H=T_2-d_B\times\beta \quad (19)$$

$$T_C=T_3+d_D\times\alpha \quad (20)$$

where T_C is the temperature of the cold top meter bar surface in contact with the specimen, and T_H is the temperature of the hot bottom meter bar surface in contact with the specimen. Temperature readings of T_1, T_2, T_3, and T_4 are measured through the testing process, where T_C and T_H are extrapolated from the calculated thermal gradients (Figure 17).

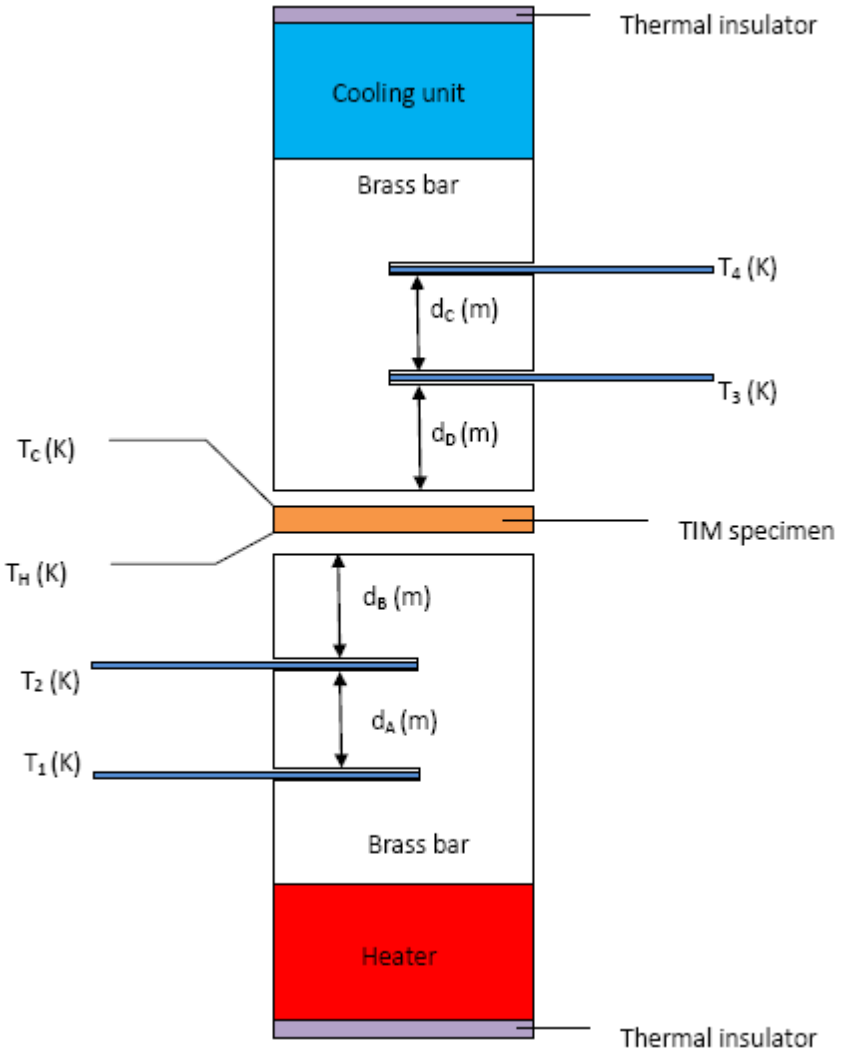

Figure 17 Schematic diagram showing the test stack used for the determination of thermal properties of TIMs.

The thermal impedance is defined as follows:

$$\theta=\frac{A}{Q}\times\left[T_H-T_C\right] \tag{21}$$

where θ is the thermal impedance, and A is the surface area of the specimen (or meter bars). Therefore, the less the temperature difference across the interface between the

CPU and the heat sink, the less is the thermal impedance and the better is the thermal management performance of the TIM.

The thermal impedance, θ, defined as the total resistance that an interface/ material presents to the heat flow from a hot surface to a cold surface, is the sum of its inherent thermal resistance ($R_{material}$) and the thermal contact resistance ($R_{contact}$) exists between it and contact surfaces. The thermal resistance, $R_{material}$, is defined as follows:

$$R_{material}=\frac{d}{K} \tag{22}$$

where *d* is the thickness of the specimen, and *K* is the thermal conductivity. Obviously, two parameters are related to the reduction of the thermal resistance. The first one is the sample thickness, and the second one is the thermal conductivity. By reducing the sample thickness and increasing the thermal conductivity we can lower the thermal resistance.

It must be pointed out that "d" in Equation (14) represents the specimen thickness under contact pressure. In this thesis research, we conducted tests on some polymer-based commercial TIMs. Therefore, the deflection of those commercial TIMs under various contact pressures must be known first. The following data was acquired from *Chomerics* [15] (Table 9 and 10).

Table 9 Percent deflection of TIM#976 and TIM#A580 under various pressures.

Pressure (psi)	A580	976
	% Deflected	%Deflected
10 psi	10%	10%
20 psi	15%	10%
30 psi	20%	16%
40 psi	25%	28%
50 psi	30%	45%

Table 10 Specimen thicknesses of TIM#976 and TIM#A580 before and after the application of contact pressures.

TIM	A580			976		
Thickness (cm) under no pressure	0.05	0.25	0.50	0.10	0.25	0.50
Thickness (cm) under various pressures						
20 psi	0.043	0.213	0.425	0.09	0.225	0.450
30 psi	0.040	0.200	0.400	0.084	0.210	0.420
40 psi	0.038	0.188	0.375	0.072	0.180	0.360
50 psi	0.035	0.175	0.350	0.055	0.138	0.275

The thermal impedance, θ, can be rearranged as follows:

$$\theta = R_{material} + R_{Contact} = \frac{d}{K} + R_{Contact} \quad (23)$$

By plotting thermal impedance (θ) (y-axis) versus specimen thickness (d) (x-axis), we then have a straight line that best fits to the experimental data, whose slope equals to the reciprocal of the apparent thermal conductivity (K), and its intercept at zero thickness equals to the thermal contact resistance ($R_{Contact}$).

4.3 Experimental design

In order to evaluate the thermal performance of TIMs under various conditions, we need to design sets of experiments. The following results will be presented by conducting experiments:

(1) Ambient temperature vs. Thermal impedance of TIMs

(2) Specimen thickness vs. Thermal impedance of TIMs

(3) Contact pressure vs. Thermal impedance of TIMs

(4) Specimen temperature vs. Thermal impedance of TIMs

(5) Thermal impedance of designed TIM vs. Thermal impedance of copper foil

(6) Surface roughness of meter bars vs. Thermal impedance of TIMs

(7) Extreme specimen temperature vs. Thermal impedance of TIMs

(8) Independent experiment for the determination of thermal conductivity of *Designed TIM 1*

(9) Independent experiment for the determination of thermal conductivity of *Designed TIM 2*

The experimental design of each test will be presented below (Figure 18 to 26, Table 11 to 19).

Experiment 1

1. Objective: To determine whether there is a significant linear correlation between the ambient temperature and the thermal impedance of TIMs

2. Performance measurement: Thermal impedance (θ)

3. The sample size of each kind of TIM is 25 for TIM#976, A580, and designed TIM 1; while it is 10 for designed TIM 2. The specimen thickness of TIM#976, A580, designed TIM 1, and designed TIM 2 is 1.0, 0.5, 0.025, and 0.035mm, respectively. The contact pressure is 50 psi. The controlled variable is the ambient temperature, which is controlled between 18.0 and 24.0℃ (Table 11).

4. Test of hypothesis:

H_0: $\rho = 0$ (No significant linear correlation)

H_A: $\rho \neq 0$ (Significant linear correlation)

where ρ represents the linear correlation coefficient for a population

α=0.05

5. TS: $t=\frac{r}{\sqrt{\frac{1-r^2}{n-2}}}$, where *r* represents the linear correlation coefficient for a sample

6. If the absolute value of the test statistic exceeds the critical values, reject H_0. Otherwise, fail to reject H_0

7. If H_0 is rejected, conclude that there is a significant linear relation. Otherwise, there is not sufficient evidence to conclude that there is a linear correlation.

Figure 18 Description of experimental design 1.

Table 11 Experimental design for determining the effect of ambient temperature on thermal impedance of TIMs.

TIM	Sample size	Ambient temperatures (℃)	Specimen thickness (mm)	Contact pressure (psi)
976	25	18.0-24.0	1.0	50
A580	25	18.0-24.0	0.5	50
Designed TIM 1	25	18.0-24.0	0.025	50
Designed TIM 2	10	18.0-24.0	0.035	50

Experiment 2

1. Objective: To determine the effect of specimen thickness on the thermal impedance of TIMs

2. Performance measurement: Thermal impedance (θ)

3. The contact pressure is 50 psi. The sample size is 25 for TIM#976, A580, and designed TIM 1; while it is 10 for designed TIM 2. The controlled variable is the specimen thickness. For TIM#976, the specimen thicknesses are 0.055, 0.138, and 0.275 mm. For TIM#A580, the specimen thicknesses are 0.035, 0.175, and 0.35 mm. For designed TIM 1, the specimen thicknesses are 0.025, 0.040, and 0.060mm. For designed TIM 2, the specimen thicknesses are 0.035, 0.050, and 0.070mm (Table 12)

4. Test of hypothesis (One-way ANOVA followed by the Tukey's procedure):

H_0: $\mu_{\text{thickness }1} = \mu_{\text{thickness }2} = \mu_{\text{thickness }3}$

H_A: at least two of the $\mu_{\text{thickness }i}$'s are different

where μ represents the population mean of thermal impedance values

α=0.05

5. TS: $F=\frac{nS_{\bar{x}}^2}{S_p^2}$, where $S_{\bar{x}}^2$ represents the variance of the sample means and S_p^2 represents the variance within samples.

6. DF with k (3) samples of the same size n (25):

Numerator DF=k-1=2; Denominator DF=k*(n-1) = 72

Critical value equals to 3.1347 (F Distribution Table)

7. If the test statistic exceeds the critical value, reject H_0. Otherwise, fail to reject H_0

8. If H_0 is rejected, there is sufficient evidence to warrant rejection of the claim that the three samples come from populations having the same mean. Otherwise, there is not sufficient evidence to warrant rejection of the claim that the three samples come from populations having the same mean.

9. The Tukey's procedure can help determine which of the $\mu_{\text{thickness }i}$'s are different from one another at a certain defined significance level.

Figure 19 Description of experimental design 2.

Table 12 Experimental design for determining the effect of specimen thickness on thermal impedance of TIMs.

TIM	Sample size	Specimen thickness (mm)	Contact pressure (psi)
976	25	1.0	50
	25	2.5	50
	25	5.0	50
A580	25	0.5	50
	25	2.5	50
	25	5.0	50
Designed TIM 1	25	0.025	50
	25	0.040	50
	25	0.060	50
Designed TIM 2	10	0.035	50
	10	0.050	50
	10	0.070	50

Experiment 3

1. Objective: To determine the effect of contact pressure on the thermal impedance of TIMs

2. Performance measurement: Thermal impedance (θ)

3. The sample size is 25 for TIM#976, A580, and designed TIM 1; while it is 10 for designed TIM 2. The specimen thickness of TIM#976, A580, designed TIM 1, and designed TIM 2 is 1.0, 0.5, 0.025, and 0.035mm, respectively. The controlled variable is the contact pressure, which is controlled at 30, 40, and 50 psi (Table 13).

4. Test of hypothesis (One-way ANOVA followed by Tukey's procedure):

H_0: $\mu_{\text{pressure }1} = \mu_{\text{pressure }2} = \mu_{\text{pressure }3}$

H_A: at least two of the $\mu_{\text{pressure }i}$'s are different

where μ represents the population mean of thermal impedance values

α=0.05

5. TS: $F=\frac{nS_{\bar{x}}^2}{S_p^2}$, where $S_{\bar{x}}^2$ represents the variance of the sample means and S_p^2 represents the variance within samples.

6. DF with k (3) samples of the same size n (25):

Numerator DF=k-1=2; Denominator DF=k*(n-1) = 72

Critical value equals to 3.1347 (F Distribution Table)

7. If the test statistic exceeds the critical value, reject H_0. Otherwise, fail to reject H_0

8. If H_0 is rejected, there is sufficient evidence to warrant rejection of the claim that the three samples come from populations having the same mean. Otherwise, there is not sufficient evidence to warrant rejection of the claim that the three samples come from populations having the same mean.

Figure 20 Description of experimental design 3.

Table 13 Experimental design for determining the effect of contact pressure on thermal impedance of TIMs.

TIM	Sample size	Specimen thickness (mm)	Contact pressure (psi)
976	25	1.0	30,40,50
A580	25	0.5	30,40,50
Designed TIM 1	25	0.025	30,40,50
Designed TIM 2	10	0.035	30,40,50

Experiment 4

1. Objective: To determine whether there is a significant correlation between the specimen temperature and the thermal impedance of TIMs

2. Performance measurement: Thermal impedance (θ)

3. The sample size is 25 for TIM#976, A580, and designed TIM 1; while it is 10 for designed TIM 2. The specimen thickness of TIM#976, A580, designed TIM 1, and designed TIM 2 is 1.0, 0.5, 0.025 and 0.035mm, respectively. The contact pressure is 50 psi. The controlled variable is the specimen temperature, which is controlled at 50±2℃ (Table 14).

4. Test of hypothesis:

H_0: $\rho = 0$ (No significant linear correlation)

H_A: $\rho \neq 0$ (Significant linear correlation)

where ρ represents the linear correlation coefficient for a population

α=0.05

5. TS: $t = \frac{r}{\sqrt{\frac{1-r^2}{n-2}}}$, where *r* represents the linear correlation coefficient for a sample

6. If the absolute value of the test statistic exceeds the critical values, reject H_0. Otherwise, fail to reject H_0

7. If H_0 is rejected, conclude that there is a significant linear relation. Otherwise, there is not sufficient evidence to conclude that there is a linear correlation.

Figure 21 Description of experimental design 4.

Table 14 Experimental design for determining the effect of specimen temperature on thermal impedance of TIMs.

TIM	Sample size	Specimen temperature (℃)	Specimen thickness (mm)	Contact pressure (psi)
976	25	50±2	1.0	50
A580	25	50±2	0.5	50
Designed TIM 1	25	50±2	0.025	50
Designed TIM 2	10	50±2	0.035	50

Experiment 5

1. Objective: To compare the thermal impedance values of designed TIM 1 and copper foil

2. Performance measurement: Thermal impedance (θ)

3. The sample size is 25 for both the designed TIM 1 and copper foil. The specimen thickness of designed TIM and copper foil is 0.04mm. The contact pressure is 50 psi (Table 15).

4. Test of hypothesis:

H_0: $\mu_{\theta,\text{designed TIM 1}} = \mu_{\theta,\text{copper foil}}$

H_A: $\mu_{\theta,\text{designed TIM 1}} < \mu_{\theta,\text{copper foil}}$

where μ_θ represents the true average thermal impedance value for each TIM

α=0.05

5. TS: $t=\frac{\bar{x}-\bar{y}}{S_p\sqrt{\frac{1}{m}+\frac{1}{n}}}$, where S_p represents the pooled estimator of σ^2

6. If the test statistic is less than the critical value, reject H_0. Otherwise, fail to reject H_0

7. If H_0 is rejected, conclude that the true average thermal impedance of designed TIM 1 is smaller than that of the copper foil. Otherwise, there is not sufficient evidence to conclude that the true average thermal impedance of designed TIM is smaller than that of the copper foil.

Figure 22 Description of experimental design 5.

Table 15 Experimental design for comparing the thermal impedance of designed TIM 1 and copper foil.

TIM	Sample size	Specimen thickness (mm)	Contact pressure (psi)
Copper foil	25	0.04	50
Designed TIM 1	25	0.04	50

Experiment 6

1. Objective: To determine the effect of meter bar surface roughness on the thermal impedance of TIMs

2. Performance measurement: Thermal impedance (θ)

3. The sample size of each kind of TIM is 10. The specimen thickness of TIM#976, A580, designed TIM 1, and designed TIM 2 is 1.0, 0.5, 0.025 and 0.035mm, respectively. The contact pressure is 50 psi. The controlled variable is the meter bar surface roughness, which is controlled at R_1 and R_2 (Table 16).

4. Test of hypothesis:

H_0: $\mu_{\theta,\text{surface roughness 1}} = \mu_{\theta,\text{surface rougness 2}}$

H_A: $\mu_{\theta,\text{surface roughness 1}} < \mu_{\theta,\text{surface roughness 2}}$

where μ_θ represents the true average thermal impedance value for each TIM

α=0.05

5. TS: $t=\frac{\bar{x}-\bar{y}}{S_p\sqrt{\frac{1}{m}+\frac{1}{n}}}$, where S_p represents the pooled estimator of σ^2; DF=m+n-2

6. Critical values are found from T-Distribution Table.

7. If the test statistic falls in the rejection region, reject H_0. Otherwise, fail to reject H_0.

8. If H_0 is rejected, conclude that the true average thermal impedance of TIMs derived at surface roughness 1 is not equal to that derived from surface roughness 2. Otherwise, there is not sufficient evidence to conclude that the true average thermal impedance of TIMs derived at surface roughness 1 is not equal to that derived from surface roughness 2.

Figure 23 Description of experimental design 6.

Table 16 Experimental design for determining the effect of meter bar surface roughness on thermal impedance of TIMs.

TIM	Sample size	Specimen thickness (mm)	Contact pressure (psi)	Surface roughness (μm)
976	10	1.0	50	0.4, 25.0
A580	10	0.5	50	0.4, 25.0
Designed TIM 1	10	0.025	50	0.4, 25.0
Designed TIM 2	10	0.035	50	0.4, 25.0

Experiment 7

1. Objective: To determine whether there is a significant linear correlation between the extreme specimen temperature and the thermal impedance of TIMs

2. Performance measurement: Thermal impedance (θ)

3. The sample size of each kind of TIM is 10. The specimen thickness of TIM#976, A580, designed TIM 1, and designed TIM 2 is 1.0, 0.5, 0.025, and 0.035mm, respectively. The contact pressure is 50 psi. The controlled variable is the specimen temperature, which is controlled at 18±1 and 65±1℃ (Table 17).

4. Test of hypothesis:

H_0: $\rho = 0$ (No significant linear correlation)

H_A: $\rho \neq 0$ (Significant linear correlation)

where ρ represents the linear correlation coefficient for a population

α=0.05

5. TS: $t=\frac{r}{\sqrt{\frac{1-r^2}{n-2}}}$, where *r* represents the linear correlation coefficient for a sample

6. If the absolute value of the test statistic exceeds the critical values, reject H_0. Otherwise, fail to reject H_0

7. If H_0 is rejected, conclude that there is a significant linear relation. Otherwise, there is not sufficient evidence to conclude that there is a linear correlation.

Figure 24 Description of experimental design 7.

Table 17 Experimental design for determining the effect of extreme specimen temperature on thermal impedance of TIMs.

TIM	Sample size	Specimen thickness (mm)	Contact pressure (psi)	Specimen temperature (℃)
976	10	1.0	50	18±1, 65±1
A580	10	0.5	50	18±1, 65±1
Designed TIM 1	10	0.025	50	18±1, 65±1
Designed TIM 2	10	0.035	50	18±1, 65±1

Experiment 8

1. Objective: To determine the thermal conductivity of designed TIM 1. The thermal conductivity value derived from this independent test will be used in the mathematical model for the verification of experimental results.

2. The sample size of each specimen thickness is 5. The contact pressure is 50 psi. The controlled variable is the specimen thickness, which is controlled at 0.025, 0.040, and 0.060 mm (Table 18).

Figure 25 Description of experimental design 8.

Table 18 Experimental design for determining the thermal conductivity of designed TIM 1.

TIM	Sample size	Specimen thickness (mm)	Contact pressure (psi)	Specimen temperature (℃)
Designed TIM 1	5	0.025	50	50±2
Designed TIM 1	5	0.040	50	50±2
Designed TIM 1	5	0.060	50	50±2

Experiment 9

1. Objective: To determine the thermal conductivity of designed TIM 2. The thermal conductivity value derived from this independent test will be used in the mathematical model for the verification of experimental results.

2. The sample size of each specimen thickness is 5. The contact pressure is 50 psi. The controlled variable is the specimen thickness, which is controlled at 0.035, 0.050, and 0.070 mm (Table 19).

Figure 26 Description of experimental design 9.

Table 19 Experimental design for determining the thermal conductivity of designed TIM 2.

TIM	Sample size	Specimen thickness (mm)	Contact pressure (psi)	Specimen temperature (℃)
Designed TIM 1	5	0.035	50	50±2
Designed TIM 1	5	0.050	50	50±2
Designed TIM 1	5	0.070	50	50±2

4.4 Experimental procedures

The experimental procedures follow the standards of ASTM D5470-06. This standard is based on idealized thermal conduction between two parallel, isothermal surfaces separated by a test specimen (e.g. TIM) of uniform thickness. The temperature difference between two contact surfaces imposes the thermal gradient across the specimen. It is critical to ensure the heat flow is perpendicular (one dimensional) to the test surfaces and is uniformly distributed across the surfaces. It is assumed that there is no lateral heat spreading during the test. Also, the effects of thermal convection and radiation are minimized by the usage of a vacuum pump and radiation shield, respectively. Some measurements are required to derive the thermal transmission properties of the test specimen.

The procedures are summarized as follows:

(a) Determination of the TIM specimen thickness. Our designed TIM specimen thickness is reflected by various parameters during the chemical fabrication processes.

(b) Metals and ceramics exhibit negligible deflection and are categorized as *Type III* in accordance with the standard. Since our designed TIMs are composed of AAO

templates (ceramics) and copper nanowires (metals), they are hereby classified as *TYPE III*. Therefore, the thickness of our designed TIMs is assumed to be unchanged before and after the application of contact pressure.

(c) Place the specimen on the top of the lower meter bar.

(d) Place the upper meter bar on the top of the specimen. Apply the contact pressure by pneumatics. The value of the contact pressure can be controlled by an air regulator and read by a pressure gauge. To have one dimensional uniform pressure applied on the test specimen, it is very important to make sure that two meter bars are perfectly aligned.

(e) Supply heat to meter bars by using a power supply along with resistance wires wrapped on the surface of the bottom meter bar. At the same time, the upper meter bar will be cooled by using Fisher Scientific Isotemp Refrigerated Circulator (Model 9100). The steady state average specimen temperature can be fine tuned by controlling the power input and/or the water circulator. A controllable thermal gradient will thus be generated.

(f) At equilibrium, record the temperature readings of four thermocouples. According to ASTM D5470-06, equilibrium is defined as, at constant power supply, two sets of temperature readings taken at 5 minutes intervals differ by less than $\pm 0.1℃$.

Calculate the average specimen temperature from temperature readings of four thermocouples. Next, determine the thermal impedance by simple mathematical calculations. In order to determine other thermal transmission properties (e.g. thermal

contact resistance and thermal conductivity), we need to determine the thermal impedance for the same type of specimen at three different thicknesses. The average specimen temperature is controlled at $50 \pm 2℃$ (The average of T_2 and T_3 at equilibrium).

5. EXPERIMENTAL RESULTS AND ANALYSIS

5.1 Experimental results

In this section, the effects of ambient temperatures, contact pressures, specimen temperatures, nanostructured copper, and specimen thicknesses on the thermal performance of commercial and our designed TIMs are presented. Hypothesis testing was conducted after each experiment.

5.1.1 The correlation between ambient temperature and thermal impedance

The plots showing the thermal impedance values of TIMs under various ambient temperatures are shown in Figure 27, 28, 29, and 30.

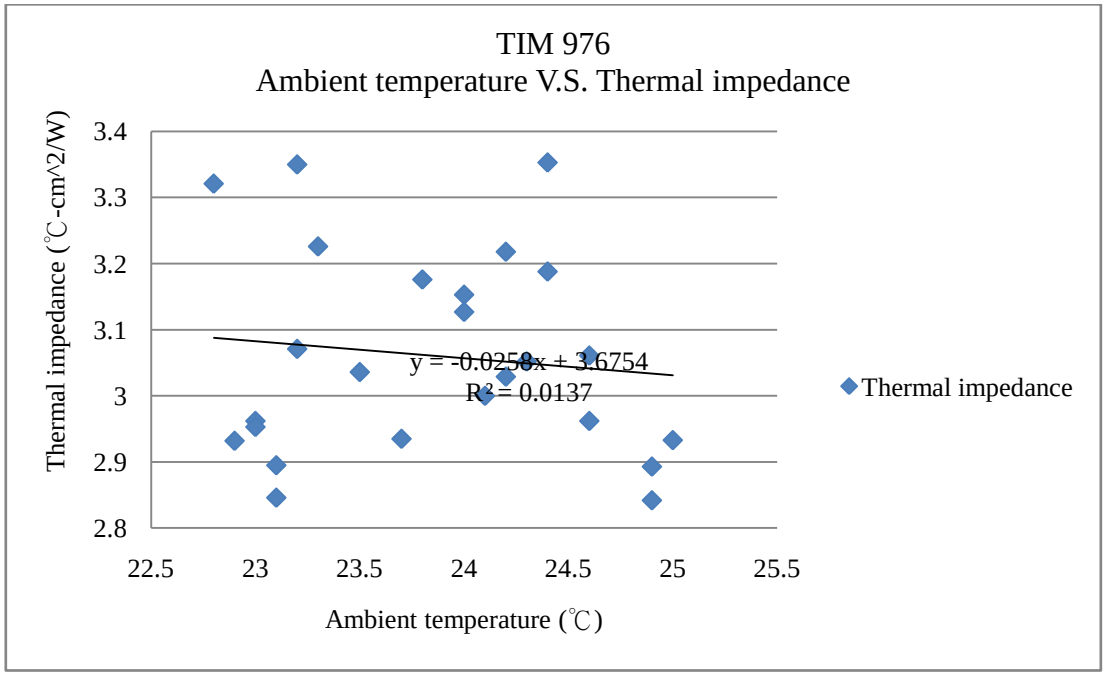

Figure 27 Plot showing the thermal impedance values of TIM#976 under various ambient temperatures.

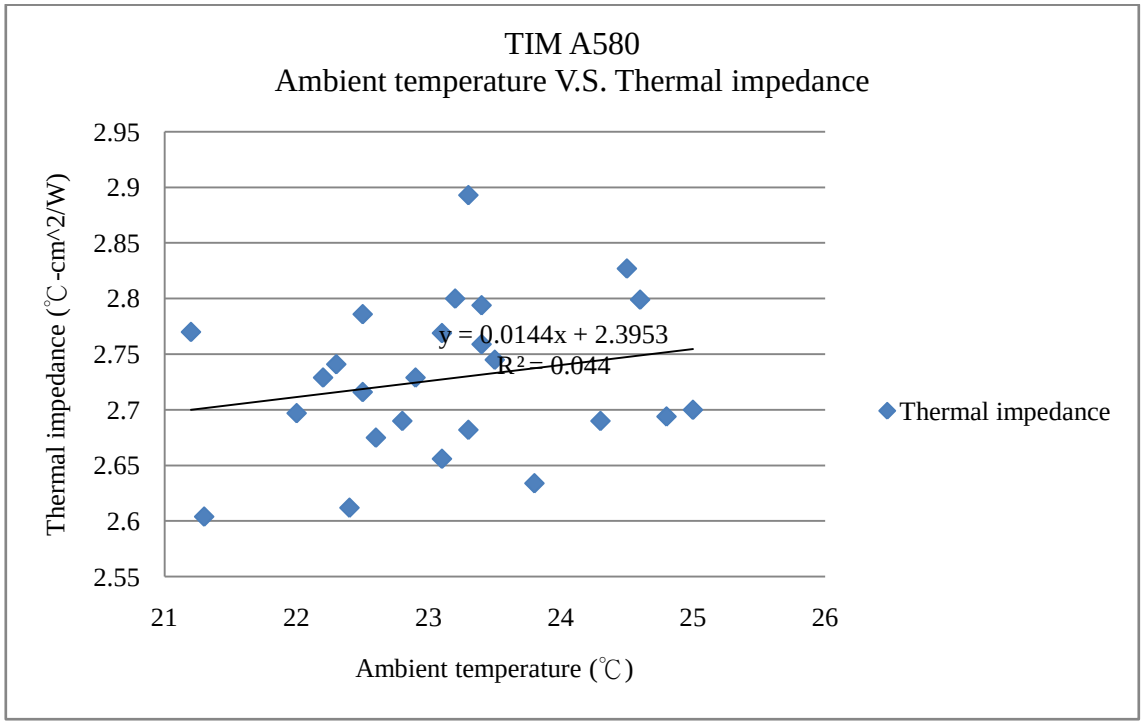

Figure 28 Plot showing the thermal impedance values of TIM#A580 under various ambient temperatures.

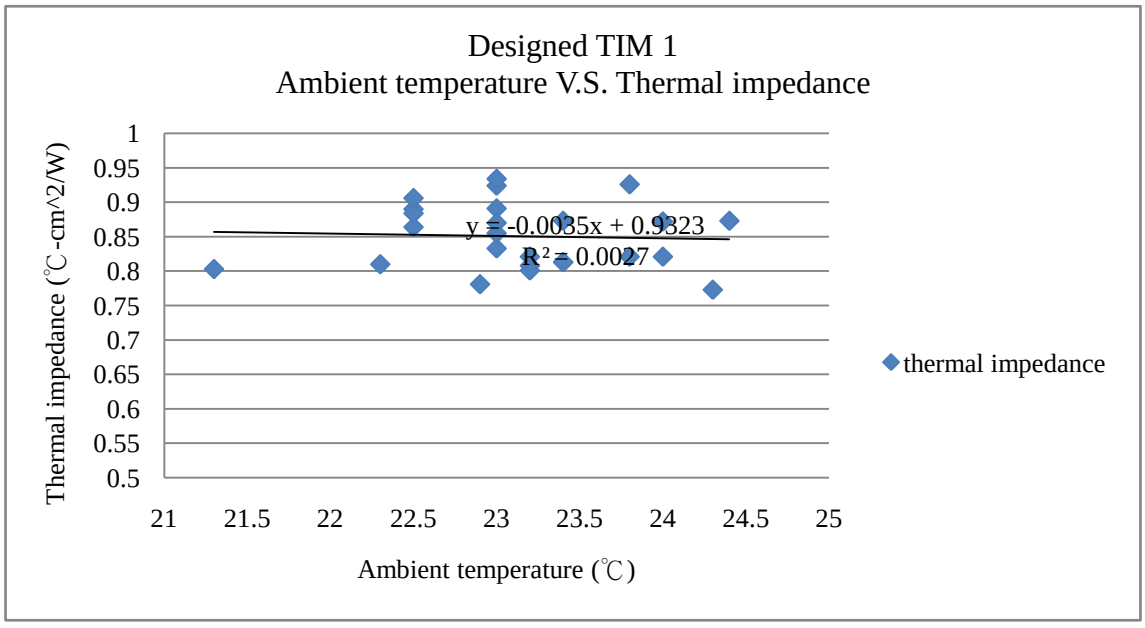

Figure 29 Plot showing the thermal impedance values of designed TIM 1 under various ambient temperatures.

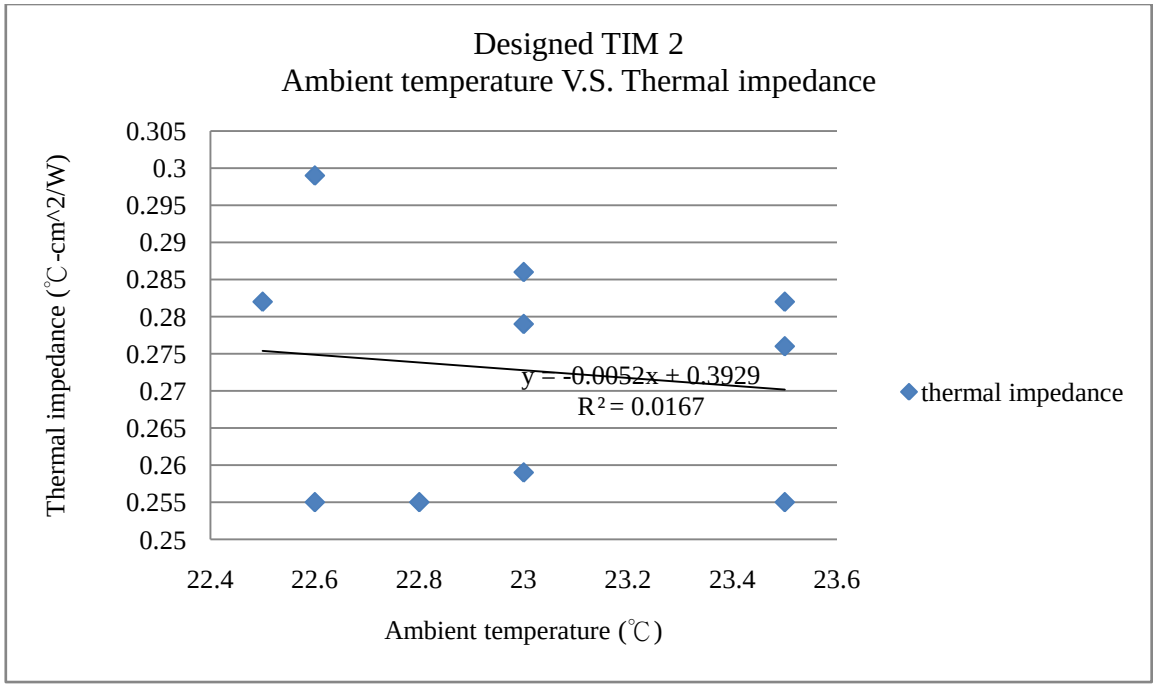

Figure 30 Plot showing the thermal impedance values of designed TIM 2 under various ambient temperatures.

5.1.1.1 Two-tailed hypothesis test

1. Objective: To determine whether there is a significant linear correlation between ambient temperature and thermal impedance

2. H_0: $\rho = 0$ (No significant linear correlation)

   H_A: $\rho \neq 0$ (Significant linear correlation)

   where ρ represents the linear correlation coefficient for a population

   α=0.05

3. TS: $t = \frac{r}{\sqrt{\frac{1-r^2}{n-2}}}$ = 0.565 (TIM#976), 1.030 (TIM#A580), 0.250 (Designed TIM 1), and 0.368 (Designed TIM 2).

   (r represents the linear correlation coefficient for a sample)

4. RR: For DF=n-2=23, reject H_0 if $|t| \geq t_{\alpha/2,n-2} = 2.069$

   For DF=n-2=8, reject H_0 if $|t| \geq t_{\alpha/2,n-2} = 2.306$

   (From the table of the t distribution)

5. For TIM#976, t does not fall in the RR

   For TIM#A580, t does not fall in the RR

   For Designed TIM 1, t does not fall in the RR

   For Designed TIM 2, t does not fall in the RR

6. Therefore, of all the TIMs, H_0 cannot be rejected. There is not sufficient evidence to conclude that there is a linear correlation between ambient temperature and thermal impedance. In other words, the ambient temperature of where the experimental chamber rests in will not affect the experimental results.

5.1.2 The effect of contact pressure on thermal impedance

The plots showing the thermal impedance values of TIMs at different contact pressures are shown in Figure 31, 32, 33, and 34.

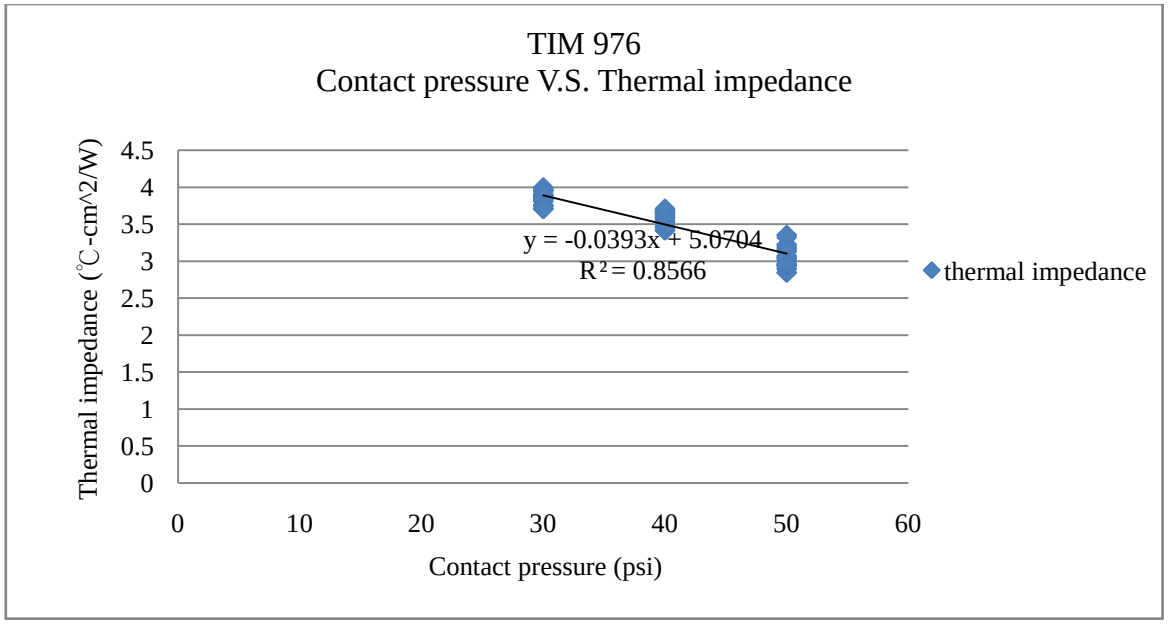

Figure 31 Plot showing the thermal impedance values of TIM#976 at different contact pressures.

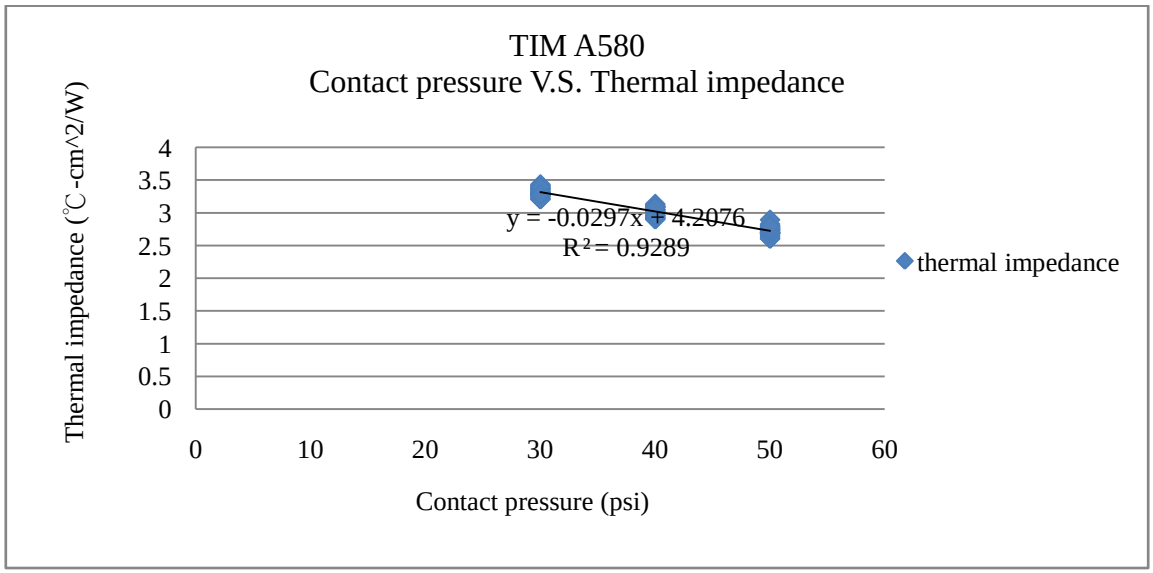

Figure 32 Plot showing the thermal impedance values of TIM#A580 at different contact pressures.

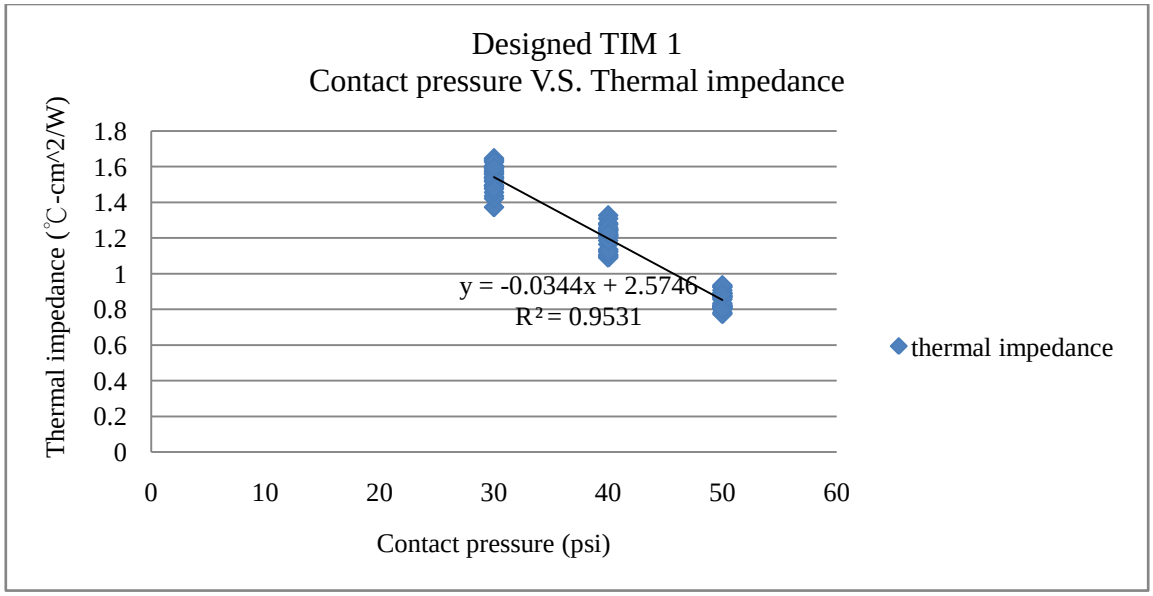

Figure 33 Plot showing the thermal impedance values of designed TIM 1 at different contact pressures.

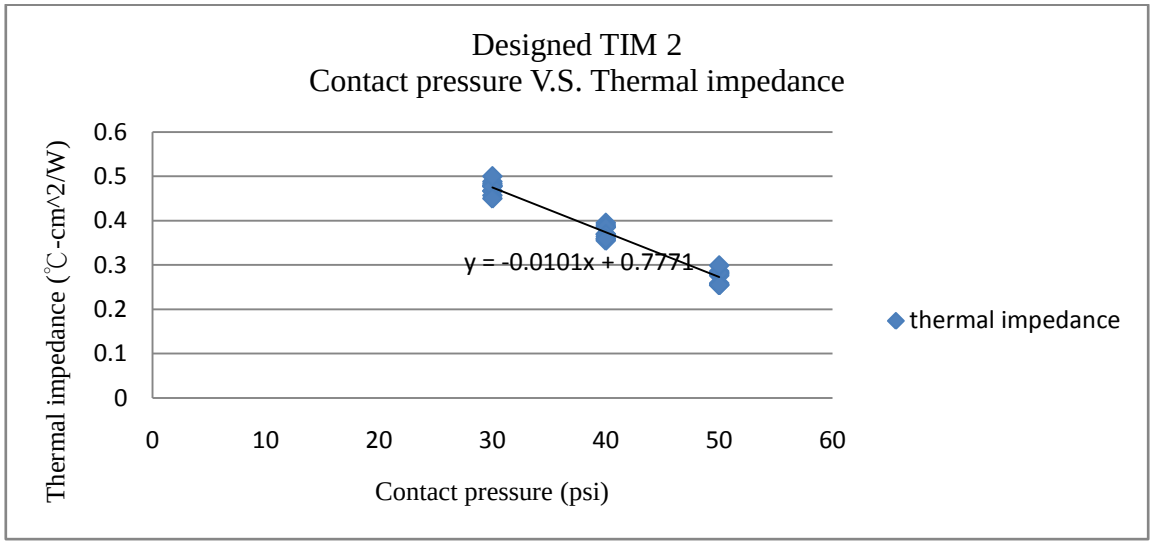

Figure 34 Plot showing the thermal impedance values of designed TIM 2 at different contact pressures.

The arithmetic means and standard deviations of thermal impedance values of TIMs under various contact pressures are summarized in Table 20, 21, 22, and 23.

Table 20 Arithmetic mean and standard deviation of thermal impedances of TIM#976 under various contact pressures.

Contact pressure (psi)	Sample size	Arithmetic mean of thermal impedance ($℃-cm^2/W$)	Standard deviation
30	25	3.847	0.0924
40	25	3.587	0.0967
50	25	3.061	0.1536

Table 21 Arithmetic mean and standard deviation of thermal impedances of TIM#A580 under various contact pressures.

Contact pressure (psi)	Sample size	Arithmetic mean of thermal impedance ($℃-cm^2/W$)	Standard deviation
30	25	3.318	0.0654
40	25	3.014	0.0720
50	25	2.724	0.0677

Table 22 Arithmetic mean and standard deviation of thermal impedances of designed TIM 1 under various contact pressures.

Contact pressure (psi)	Sample size	Arithmetic mean of thermal impedance ($℃-cm^2/W$)	Standard deviation
30	25	1.539	0.0723
40	25	1.202	0.0685
50	25	0.850	0.0467

Table 23 Arithmetic mean and standard deviation of thermal impedances of designed TIM 2 under various pressures.

Contact pressure (psi)	Sample size	Arithmetic mean of thermal impedance ($℃-cm^2/W$)	Standard deviation
30	10	0.475	0.0148
40	10	0.373	0.0146
50	10	0.273	0.0157

5.1.2.1 Hypothesis test (One-way ANOVA followed by Tukey's procedures)

1. Objective: To determine the effect of contact pressure on the thermal impedance of TIMs
2. H_0: $\mu_{\text{pressure } 1} = \mu_{\text{pressure } 2} = \mu_{\text{pressure } 3}$

   H_A: at least two of the $\mu_{\text{pressure } i}$'s are different

where μ represents the population mean of thermal impedance values

α=0.05

3. TS: $F=\frac{nS_{\bar{x}}^2}{S_p^2}$ =290.118 (TIM#976), 471.82 (TIM#A580), 734.820 (Designed TIM 1), and 451.399 (Designed TIM 2).

($S_{\bar{x}}^2$ represents the variance of the sample means and S_p^2 represents the variance within samples)

4. RR: For DF with k (3) samples of the same size n (25)

Numerator degrees of freedom (ν_1) =k-1=2

Denominator degrees of freedom (ν_2) =k*(n-1) = 72

Rejects H_0 if $|F| \geq F_{\alpha, \nu_1, \nu_2}$=3.124

Similarly, for DF with k (3) samples of the same size n (10)

Rejects H_0 if $|F| \geq F_{\alpha, \nu_1, \nu_2}$ =3.354

(F distribution table)

5. For TIM#976, F falls in the RR

For TIM#A580, F falls in the RR

For Designed TIM 1, F falls in the RR

For Designed TIM 2, F falls in the RR

6. Therefore, of all the TIMs, H_0 is rejected. There is sufficient evidence to warrant rejection of the claim that the three samples come from populations having the same mean.

The pair-wise comparisons of TIMs at different contact pressures based on the post-hoc test (Tukey's procedure) are listed in Table 24, 25, 26, and 27.

Table 24 Pair-wise comparisons of TIM#976 at different contact pressures based on the post-hoc test (Tukey's procedure).

Multiple Comparisons

Dependent Variable: Thermal impedance (C-cm^2/W)
Tukey HSD

(I) Contact pressure (psi)	(J) Contact pressure (psi)	Mean Difference (I-J)	Std. Error	Sig.	95% Confidence Interval	
					Lower Bound	Upper Bound
30.00	40.00	.25936*	.03326	.000	.1798	.3390
	50.00	.78612*	.03326	.000	.7065	.8657
40.00	30.00	-.25936*	.03326	.000	-.3390	-.1798
	50.00	.52676*	.03326	.000	.4472	.6064
50.00	30.00	-.78612*	.03326	.000	-.8657	-.7065
	40.00	-.52676*	.03326	.000	-.6064	-.4472

*. The mean difference is significant at the .05 level.

Table 25 Pair-wise comparisons of TIM#A580 at different contact pressures based on the post-hoc test (Tukey's procedure).

Multiple Comparisons

Dependent Variable: Thermal impedance (C-cm^2/W)
Tukey HSD

(I) Contact pressure (psi)	(J) Contact pressure (psi)	Mean Difference (I-J)	Std. Error	Sig.	95% Confidence Interval	
					Lower Bound	Upper Bound
30.00	40.00	.30440*	.01936	.000	.2581	.3507
	50.00	.59452*	.01936	.000	.5482	.6408
40.00	30.00	-.30440*	.01936	.000	-.3507	-.2581
	50.00	.29012*	.01936	.000	.2438	.3364
50.00	30.00	-.59452*	.01936	.000	-.6408	-.5482
	40.00	-.29012*	.01936	.000	-.3364	-.2438

*. The mean difference is significant at the .05 level.

Table 26 Pair-wise comparisons of designed TIM 1 at different contact pressures based on the post-hoc test (Tukey's procedure).

Multiple Comparisons

Dependent Variable: Thermal impedance (C-cm^2/W)
Tukey HSD

(I) Contact pressure (psi)	(J) Contact pressure (psi)	Mean Difference (I-J)	Std. Error	Sig.	95% Confidence Interval	
					Lower Bound	Upper Bound
30.00	40.00	.33664*	.01796	.000	.2936	.3796
	50.00	.68864*	.01796	.000	.6456	.7316
40.00	30.00	-.33664*	.01796	.000	-.3796	-.2936
	50.00	.35200*	.01796	.000	.3090	.3950
50.00	30.00	-.68864*	.01796	.000	-.7316	-.6456
	40.00	-.35200*	.01796	.000	-.3950	-.3090

*. The mean difference is significant at the .05 level.

Table 27 Pair-wise comparisons of designed TIM 2 at different contact pressures based on the post-hoc test (Tukey's procedure).

Multiple Comparisons

Dependent Variable: Thermal impedance (C-cm^2/W)
Tukey HSD

(I) Contact pressure (psi)	(J) Contact pressure (psi)	Mean Difference (I-J)	Std. Error	Sig.	95% Confidence Interval	
					Lower Bound	Upper Bound
30.00	40.00	.10140*	.00672	.000	.0847	.1181
	50.00	.20180*	.00672	.000	.1851	.2185
40.00	30.00	-.10140*	.00672	.000	-.1181	-.0847
	50.00	.10040*	.00672	.000	.0837	.1171
50.00	30.00	-.20180*	.00672	.000	-.2185	-.1851
	40.00	-.10040*	.00672	.000	-.1171	-.0837

*. The mean difference is significant at the .05 level.

Based on the plots and hypothesis testing, we may conclude that both commercial and the designed TIMs have different thermal impedance values at different contact pressures. The higher the contact pressure, the lower the thermal impedance.

5.1.3 The correlation between the specimen temperature and the thermal impedance

The plots showing the thermal impedance values of TIMs at different specimen temperatures are shown in Figure 35, 36, 37, and 38.

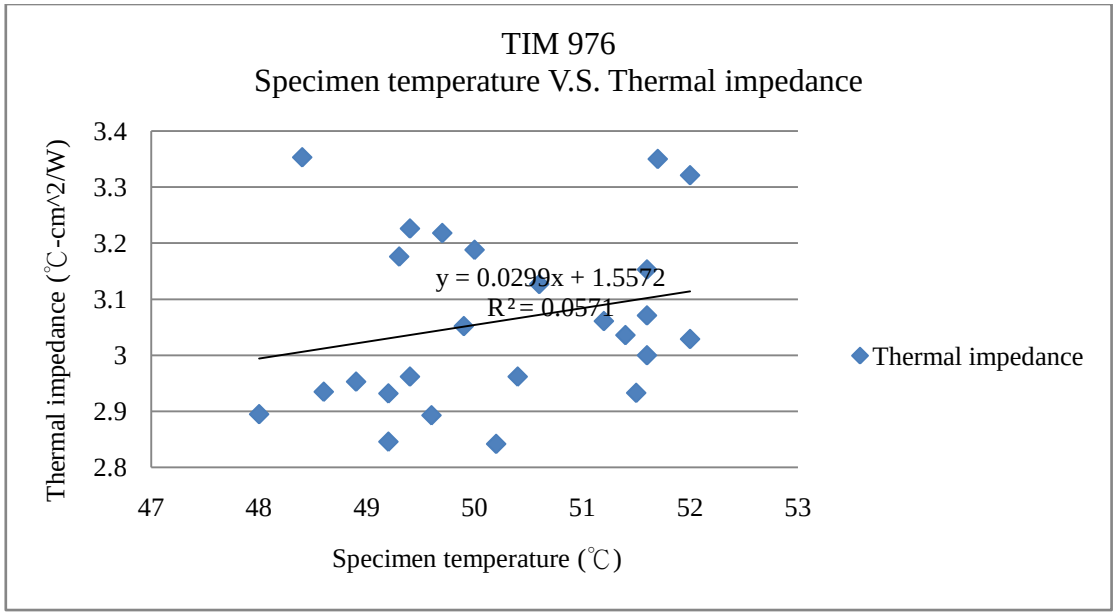

Figure 35 Plot showing thermal impedance values of TIM#976 at different specimen temperatures.

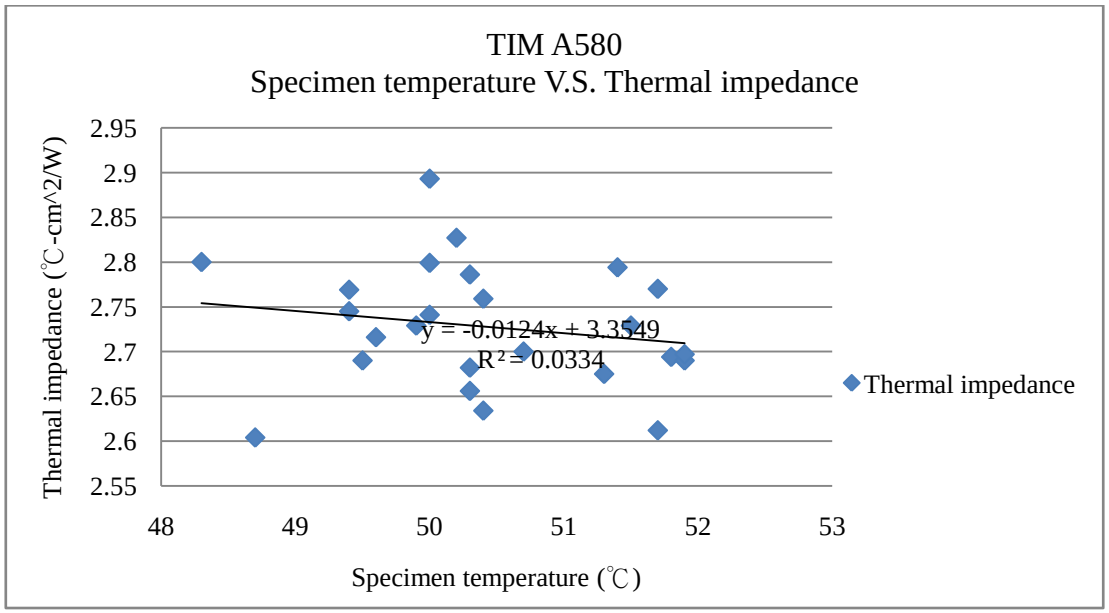

Figure 36 Plot showing thermal impedance values of TIM#A580 at different specimen temperatures.

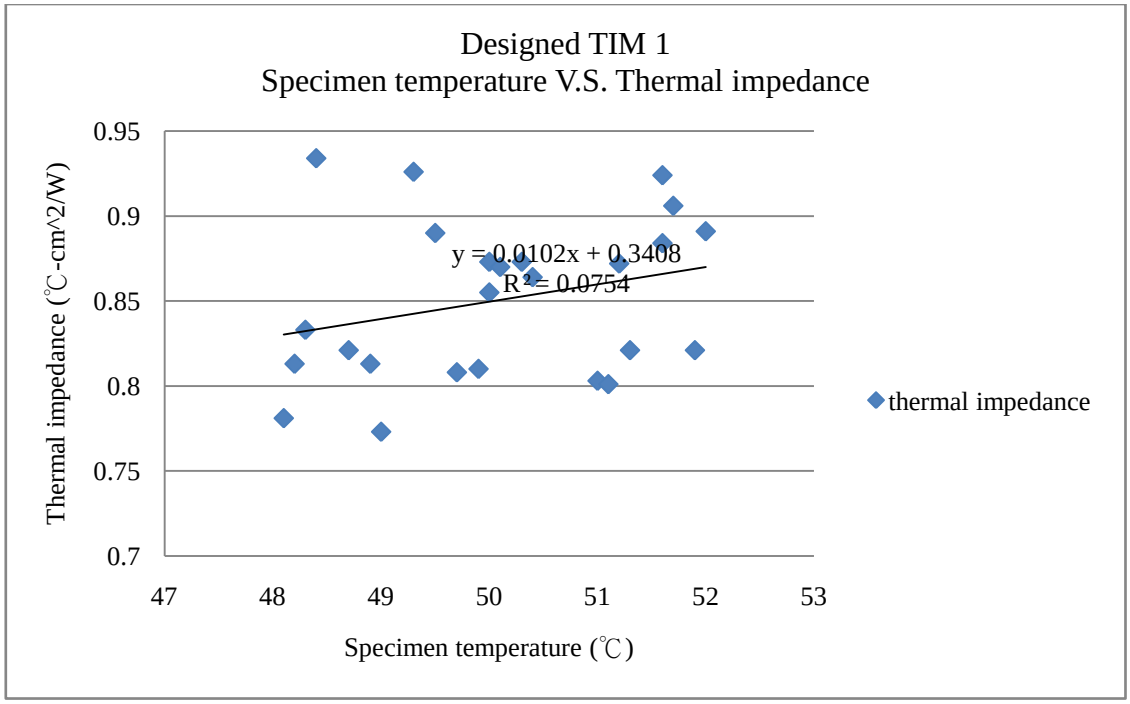

Figure 37 Plot showing thermal impedance values of designed TIM 1 at different specimen temperatures.

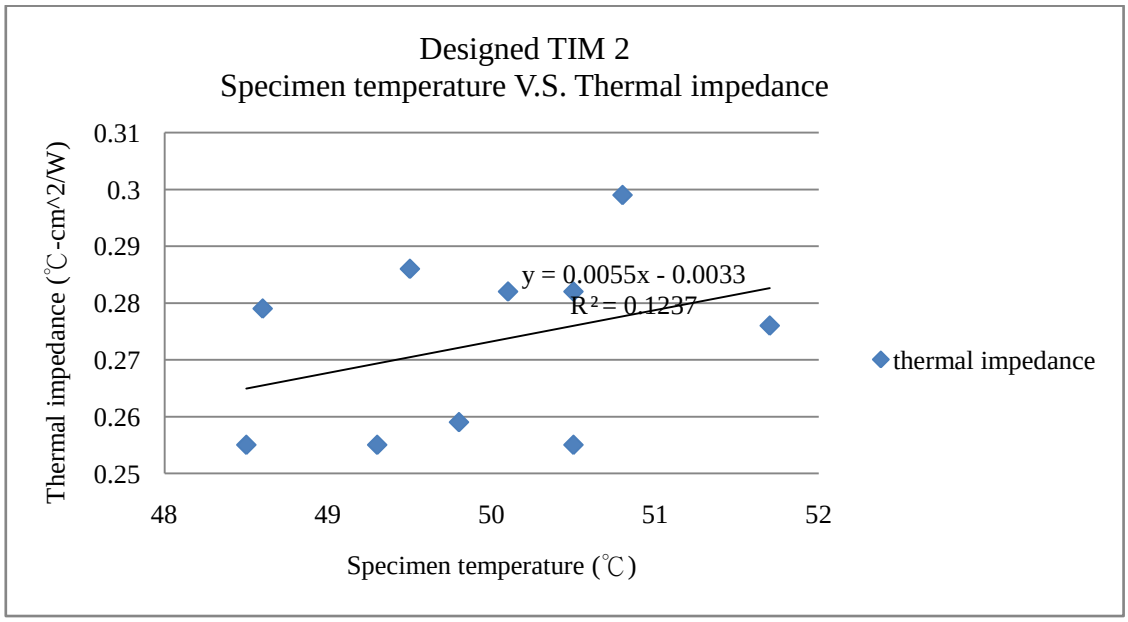

Figure 38 Plot showing thermal impedance values of designed TIM 2 at different specimen temperatures.

5.1.3.1 Hypothesis test

1. Objective: To determine whether there is a significant linear correlation between the specimen temperature and the thermal impedance

2. H_0: $\rho = 0$ (No significant linear correlation)

   H_A: $\rho \neq 0$ (Significant linear correlation)

   where ρ represents the linear correlation coefficient for a population

   α=0.05

3. TS: $t=\frac{r}{\sqrt{\frac{1-r^2}{n-2}}}$ =1.180 (TIM#976), 0.893 (TIM#A580), 1.372 (Designed TIM 1), and 1.063 (Designed TIM 2)

   (r represents the linear correlation coefficient for a sample)

4. RR: For DF=n-2=23, reject H_0 if $|t| \geq t_{\alpha/2,n-2}$ =2.069

   For DF=n-2=8, reject H_0 if $|t| \geq t_{\alpha/2,n-2}$ =2.306

   (From the table of the t distribution)

5. For TIM#976, t does not fall in the RR

   For TIM#A580, t does not fall in the RR

   For Designed TIM 1, t does not fall in the RR

   For Designed TIM 2, t does not fall in the RR

6. Of all the TIMs, H_0 cannot be rejected. Therefore, there is no sufficient evidence to conclude that there is a linear correlation between specimen temperature (50 ± 2℃) and thermal impedance. In other words, linear relationship does not exist between

specimen temperature and thermal impedance when the specimen temperature is within 50±2℃.

5.1.4 The effect of specimen thickness on thermal impedance

The plots showing the thermal impedance values of TIMs with different specimen thicknesses are shown in Figure 39, 40, 41, and 42.

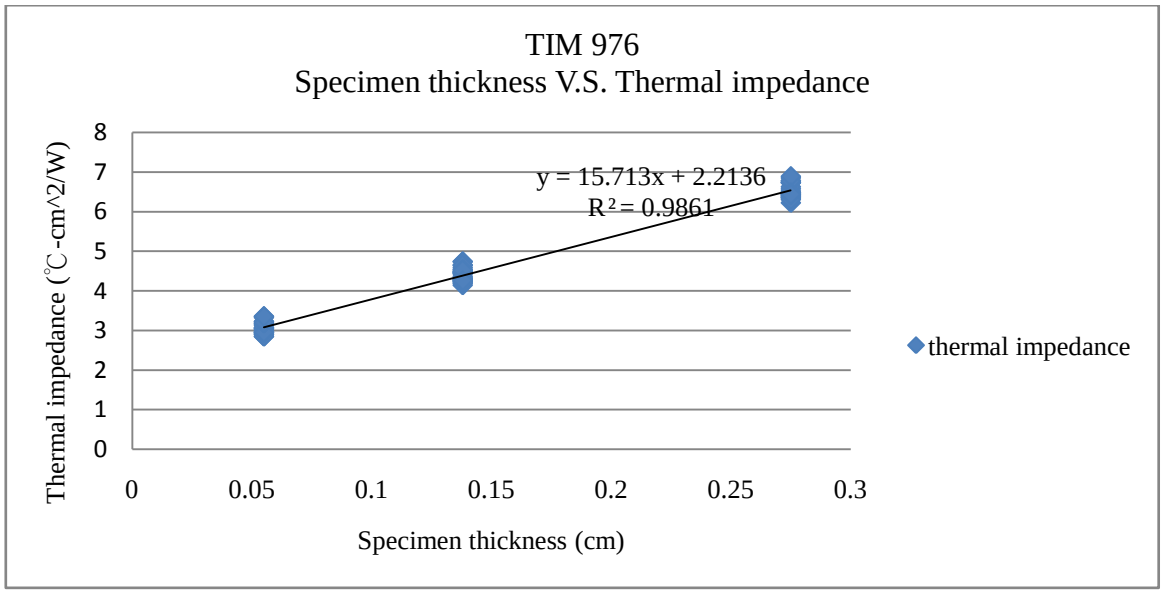

Figure 39 Plot showing the thermal impedance values of TIM#976 with different specimen thicknesses.

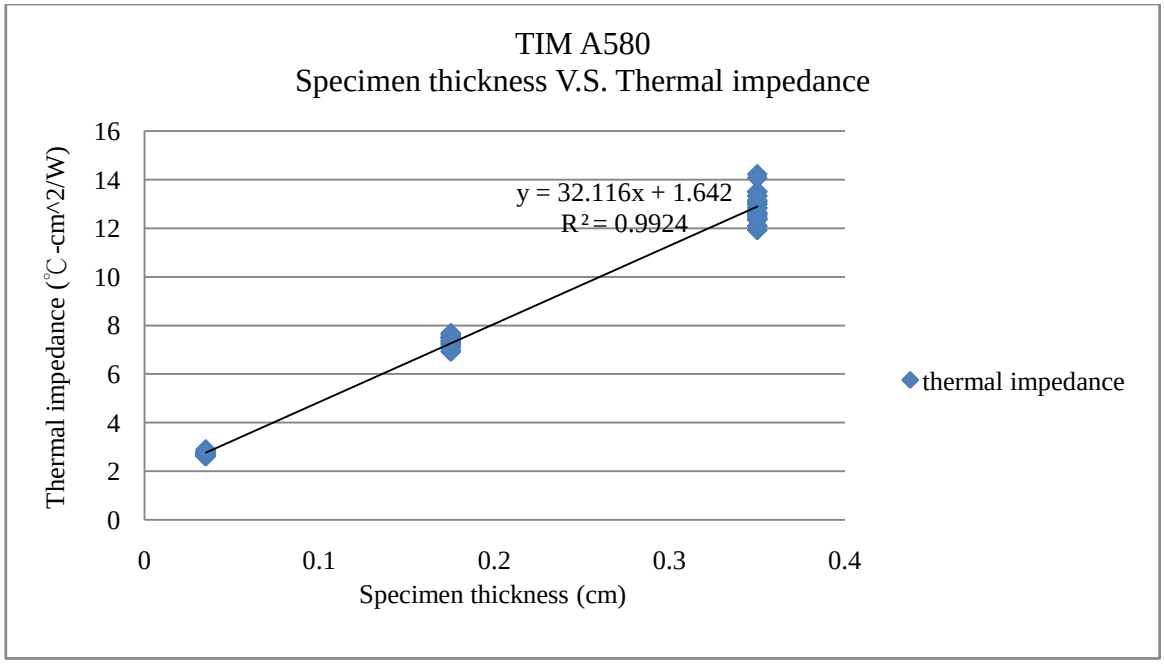

Figure 40 Plot showing the thermal impedance values of TIM#A580 with different specimen thicknesses.

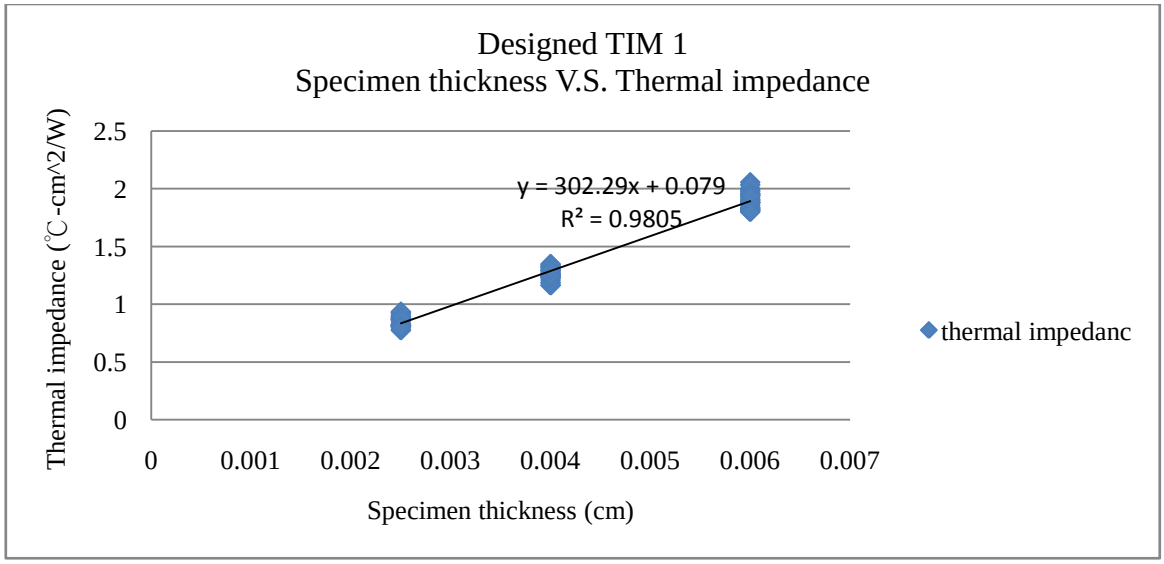

Figure 41 Plot showing the thermal impedance values of designed TIM 1 with different specimen thicknesses.

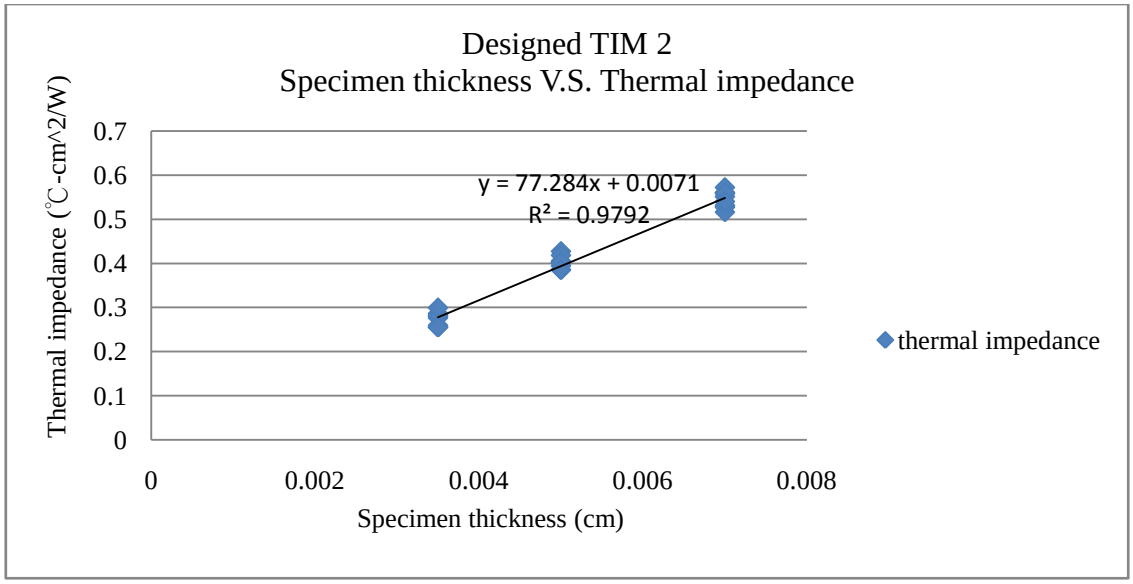

Figure 42 Plot showing the thermal impedance values of designed TIM 2 with different specimen thicknesses.

The arithmetic means and standard deviations of thermal impedance values of TIMs with different thicknesses are summarized in Table 28, 29, 30, and 31.

Table 28 Arithmetic mean and standard deviation of thermal impedances of TIM#976 with different thicknesses.

Thickness (cm)	Sample size	Arithmetic mean of thermal impedance ($℃-cm^2/W$)	Standard deviation
0.055	25	3.061	0.1536
0.138	25	4.410	0.1730
0.275	25	6.524	0.1860

Table 29 Arithmetic mean and standard deviation of thermal impedances of TIM#A580 with different thicknesses.

Thickness (cm)	Sample size	Arithmetic mean of thermal impedance ($℃-cm^2/W$)	Standard deviation
0.035	25	2.724	0.0677
0.175	25	7.339	0.2189
0.35	25	12.849	0.5884

Table 30 Arithmetic mean and standard deviation of thermal impedances of designed TIM 1 with different thicknesses.

Thickness (cm)	Sample size	Arithmetic mean of thermal impedance ($°C - cm^2/W$)	Standard deviation
0.0025	25	0.850	0.0467
0.0040	25	1.261	0.0540
0.0060	25	1.905	0.0734

Table 31 Arithmetic mean and standard deviation of thermal impedances of designed TIM 2 with different thicknesses.

Thickness (cm)	Sample size	Arithmetic mean of thermal impedance ($°C - cm^2/W$)	Standard deviation
0.0035	10	0.273	0.0157
0.0050	10	0.402	0.0131
0.0070	10	0.545	0.0182

5.1.4.1 Hypothesis test (One-way ANOVA followed by Tukey's procedures)

1. Objective: To determine the effect of the specimen thickness on the thermal impedance of TIMs

2. H_0: $\mu_{thickness\ 1} = \mu_{thickness\ 2} = \mu_{thickness\ 3}$

   H_A: at least two of the $\mu_{thickness\ i}$'s are different

   where μ represents the population mean of thermal impedance values

   α=0.05

3. TS: $F=\frac{nS_{\bar{x}}^2}{S_p^2}$ =2594.184 (TIM#976), 4834.077 (TIM#A580), 2022.835 (Designed TIM 1), and 738.788 (Designed TIM 2).

   ($S_{\bar{x}}^2$ represents the variance of the sample means and S_p^2 represents the variance within samples)

4. RR: For DF with k (3) samples of the same size n (25)

   Numerator degrees of freedom (ν_1) =k-1=2

   Denominator degrees of freedom (ν_2) =k*(n-1) = 72

Rejects H_0 if $|F| \geq F_{\alpha, \nu_1, \nu_2} = 3.124$

Similarly, for DF with k (3) samples of the same size n (10)

Rejects H_0 if $|F| \geq F_{\alpha, \nu_1, \nu_2} = 3.354$

(F distribution table)

5. For TIM#976, F falls in the RR

   For TIM#A580, F falls in the RR

   For Designed TIM 1, F falls in the RR

   For Designed TIM 2, F falls in the RR

6. Therefore, of all the TIMs, H_0 is rejected. There is sufficient evidence to warrant rejection of the claim that the three samples come from populations having the same mean.

The pair-wise comparisons of TIMs with different specimen thicknesses based on the post-hoc test (Tukey's procedure) are listed in Table 32, 33, 34, and 35.

Table 32 Pair-wise comparisons of TIM#976 with different specimen thicknesses based on the post-hoc test (Tukey's procedure).

Multiple Comparisons

Dependent Variable: Thermal impedance (C-cm^2/W)
Tukey HSD

(I) Specimen thickness (mm)	(J) Specimen thickness (mm)	Mean Difference (I-J)	Std. Error	Sig.	95% Confidence Interval	
					Lower Bound	Upper Bound
.55	1.38	-1.34916*	.04848	.000	-1.4652	-1.2331
	2.75	-3.46376*	.04848	.000	-3.5798	-3.3477
1.38	.55	1.34916*	.04848	.000	1.2331	1.4652
	2.75	-2.11460*	.04848	.000	-2.2306	-1.9986
2.75	.55	3.46376*	.04848	.000	3.3477	3.5798
	1.38	2.11460*	.04848	.000	1.9986	2.2306

*. The mean difference is significant at the .05 level.

Table 33 Pair-wise comparisons of TIM#A580 with different specimen thicknesses based on the post-hoc test (Tukey's procedure).

Multiple Comparisons

Dependent Variable: Thermal impedance (C-cm^2/W)
Tukey HSD

(I) Specimen thickness (mm)	(J) Specimen thickness (mm)	Mean Difference (I-J)	Std. Error	Sig.	95% Confidence Interval	
					Lower Bound	Upper Bound
.35	1.75	-4.61524*	.10311	.000	-4.8620	-4.3685
	3.50	-10.12516*	.10311	.000	-10.3719	-9.8784
1.75	.35	4.61524*	.10311	.000	4.3685	4.8620
	3.50	-5.50992*	.10311	.000	-5.7567	-5.2632
3.50	.35	10.12516*	.10311	.000	9.8784	10.3719
	1.75	5.50992*	.10311	.000	5.2632	5.7567

*. The mean difference is significant at the .05 level.

Table 34 Pair-wise comparisons of designed TIM 1 with different specimen thicknesses based on the post-hoc test (Tukey's procedure).

Multiple Comparisons

Dependent Variable: Thermal impedance (C-cm^2/W)
Tukey HSD

(I) Specimen thickness (um)	(J) Specimen thickness (um)	Mean Difference (I-J)	Std. Error	Sig.	95% Confidence Interval	
					Lower Bound	Upper Bound
25.00	40.00	-.41028*	.01671	.000	-.4503	-.3703
	60.00	-1.05408*	.01671	.000	-1.0941	-1.0141
40.00	25.00	.41028*	.01671	.000	.3703	.4503
	60.00	-.64380*	.01671	.000	-.6838	-.6038
60.00	25.00	1.05408*	.01671	.000	1.0141	1.0941
	40.00	.64380*	.01671	.000	.6038	.6838

*. The mean difference is significant at the .05 level.

Table 35 Pair-wise comparisons of designed TIM 2 with different specimen thicknesses based on the post-hoc test (Tukey's procedure).

Multiple Comparisons

Dependent Variable: Thermal impedance (C-cm^2/W)
Tukey HSD

(I) Specimen thickness (um)	(J) Specimen thickness (um)	Mean Difference (I-J)	Std. Error	Sig.	95% Confidence Interval	
					Lower Bound	Upper Bound
35.00	50.00	-.12920*	.00707	.000	-.1467	-.1117
	70.00	-.27170*	.00707	.000	-.2892	-.2542
50.00	35.00	.12920*	.00707	.000	.1117	.1467
	70.00	-.14250*	.00707	.000	-.1600	-.1250
70.00	35.00	.27170*	.00707	.000	.2542	.2892
	50.00	.14250*	.00707	.000	.1250	.1600

*. The mean difference is significant at the .05 level.

Based on the experimental results and hypothesis testing, we can conclude that the thermal impedance of TIMs increases as their corresponding thickness increases.

5.1.5 The comparisons of copper foil and designed TIM 1 in thermal impedance

The arithmetic means and standard deviations of thermal impedance values of designed TIM 1 and copper foil are summarized in Table 36. The box-plot showing the thermal impedance of them is illustrated in Figure 43.

Table 36 Arithmetic mean and standard deviation of thermal impedances of designed TIM 1 and copper foil (thickness=40μm).

TIM	Sample size	Arithmetic mean of thermal impedance ($℃-cm^2/W$)	Standard deviation
Designed TIM 1	25	1.261	0.0540
Copper foil	25	2.548	0.0490

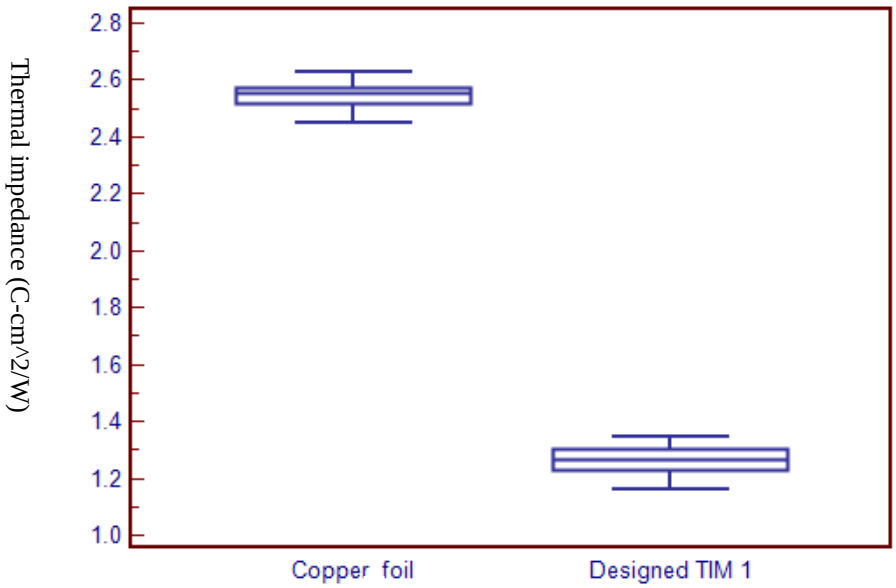

Figure 43 Box-plot showing the thermal impedance values of copper foil and designed TIM 1.

5.1.5.1 One-tail hypothesis testing

1. Objective: To compare the thermal impedance values of designed TIM 1 and copper foil
2. H_0: $\mu_{\theta,\text{designed TIM 1}} = \mu_{\theta,\text{copper foil}}$

   H_A: $\mu_{\theta,\text{designed TIM 1}} < \mu_{\theta,\text{copper foil}}$

   where μ_θ represents the true average thermal impedance value for each TIM

   α=0.05
3. TS: $t=\frac{\bar{x}-\bar{y}}{S_p\sqrt{\frac{1}{m}+\frac{1}{n}}}$ =-88.250

   (S_p represents the pooled estimator of σ^2)
4. RR: For DF=m+n-2=48, reject H_0 if $t \leq -t_{\alpha,m+n-2} = -t_{0.05,48} = -1.679$ (t-distribution table).
5. Because t falls in the RR, H_0 is rejected at the 5% level of significance. The data does strongly suggest that true average thermal impedance of designed TIM 1 (40μm) is smaller than that of copper foil (40μm).

5.1.6 The correlation between the extreme specimen temperature and the thermal impedance of TIMs

The plots showing the thermal impedance values of TIMs at different specimen temperatures are shown in Figure 44, 45, 46, and 47.

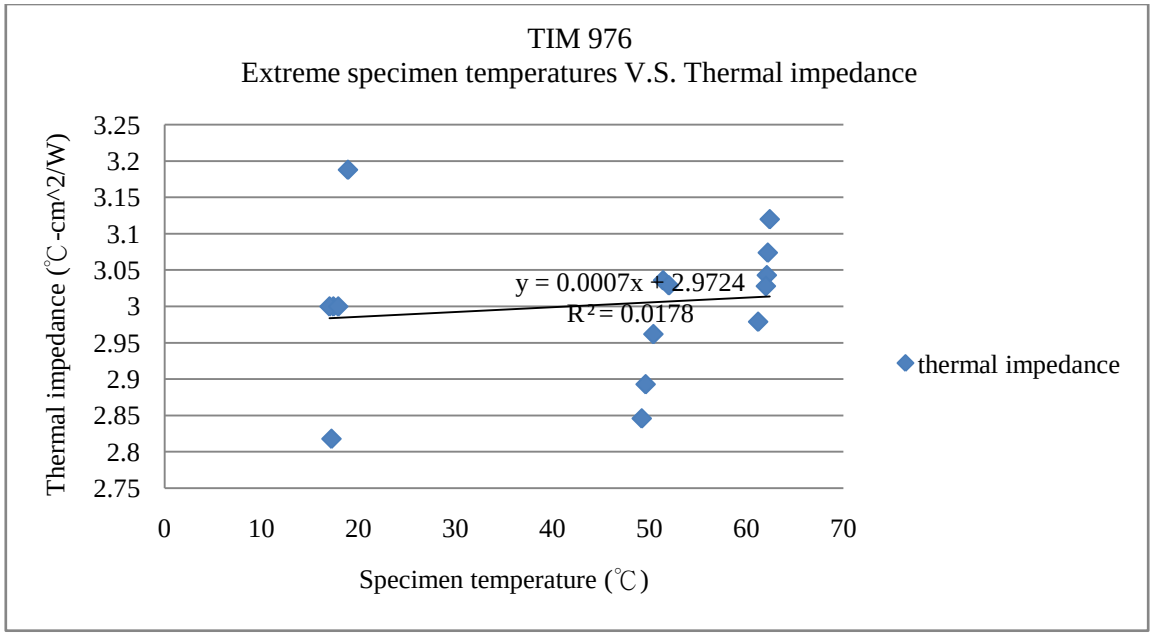

Figure 44 Plot showing the thermal impedance values of TIM#976 at different specimen temperatures.

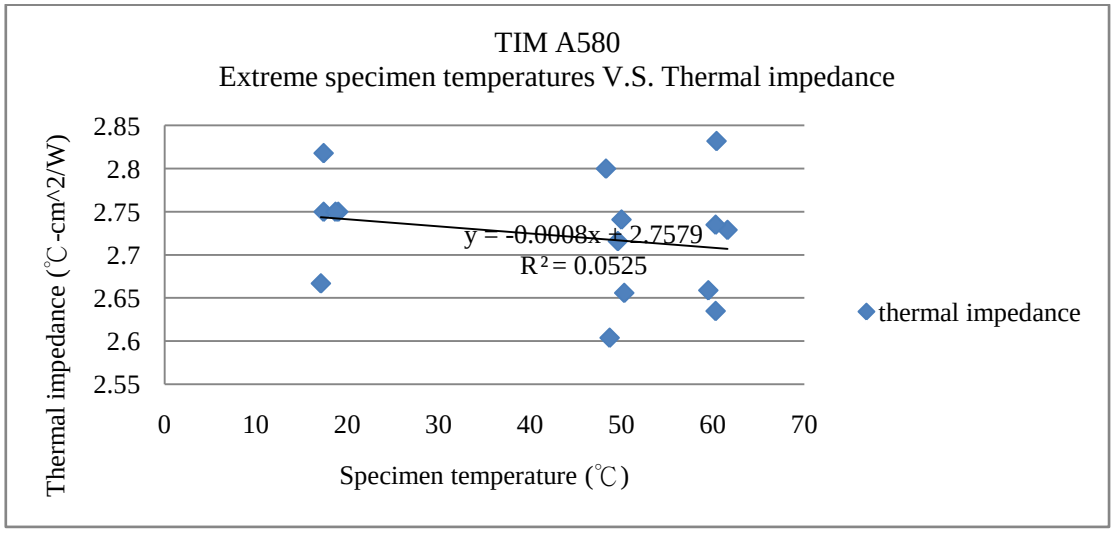

Figure 45 Plot showing the thermal impedance values of TIM#A580 at different specimen temperatures.

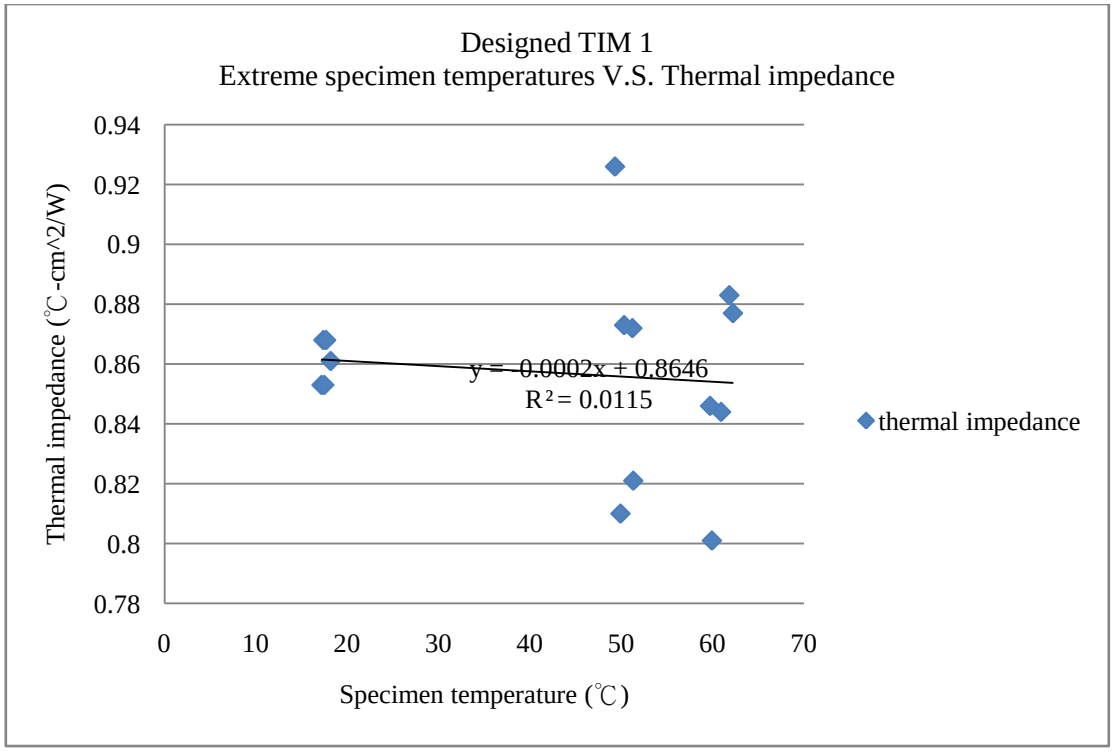

Figure 46 Plot showing the thermal impedance values of designed TIM 1 at different specimen temperatures.

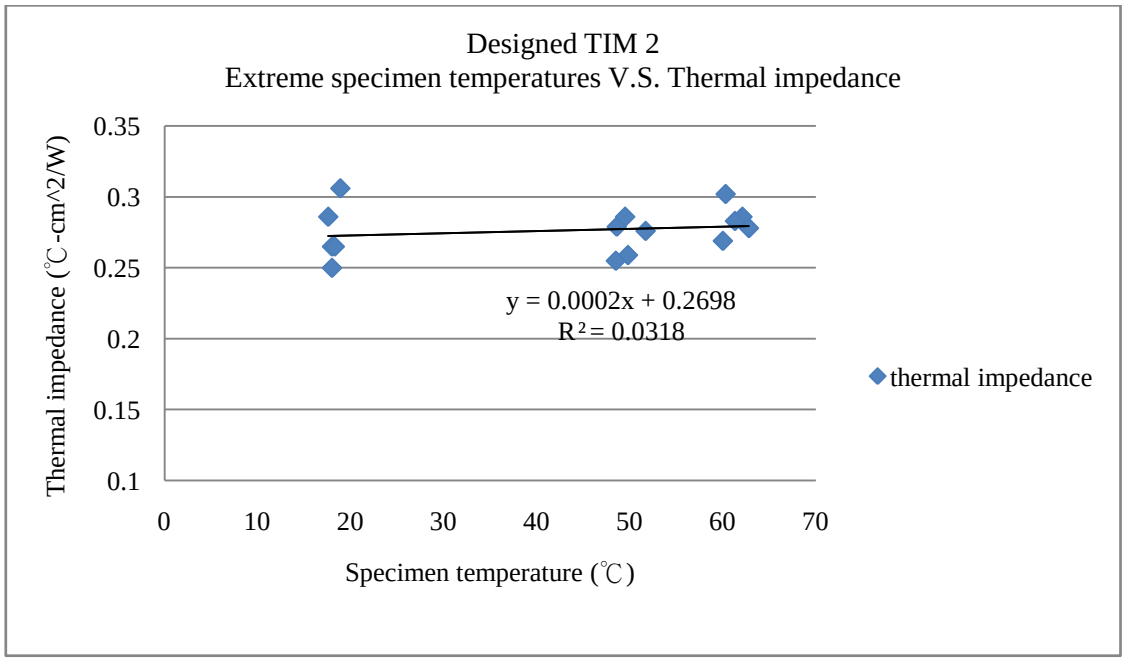

Figure 47 Plot showing the thermal impedance values of designed TIM 2 at different specimen temperatures.

5.1.6.1 Two-tailed hypothesis testing

1. Objective: To determine whether there is a significant linear correlation between the extreme specimen temperature and the thermal impedance
2. H_0: $\rho = 0$ (No significant linear correlation)

   H_A: $\rho \neq 0$ (Significant linear correlation)

   where ρ represents the linear correlation coefficient for a population

   α=0.05
3. TS: $t=\frac{r}{\sqrt{\frac{1-r^2}{n-2}}}$ =0.485 (TIM#976), 0.849 (TIM#A580), 0.389 (Designed TIM 1), and

   0.653 (Designed TIM 2)

   (*r* represents the linear correlation coefficient for a sample)
4. RR: For DF=n-2=13, reject H_0 if $|t| \geq t_{\alpha/2,n-2} = 2.160$

   (t-distribution table)
5. For TIM#976, t does not fall in the RR

   For TIM#A580, t does not fall in the RR

   For Designed TIM 1, t does not fall in the RR

   For Designed TIM 2, t does not fall in the RR
6. Of all the TIMs, H_0 cannot be rejected. Therefore, there is no sufficient evidence to conclude that there is a linear correlation between extreme specimen temperature ($18 \pm 1, 65 \pm 1℃$) and thermal impedance. In other words, linear relationship does not exist between specimen temperature and thermal impedance when the specimen temperature is within 18 ± 1 and$65 \pm 1℃$.

5.1.7 The effect of meter-bar surface roughness on thermal impedance

The arithmetic means and standard deviations of thermal impedance values of TIMs under different surface roughness are summarized in Table 37 and 38.

Table 37 Arithmetic mean and standard deviation of thermal impedance values of TIMs under surface roughness 0.4μm.

TIM	Sample size	Arithmetic mean of thermal impedance ($℃-cm^2/W$)	Standard deviation
976	5	2.953	0.0834
A580	5	2.703	0.0759
Designed TIM 1	5	0.860	0.0466
Designed TIM 2	5	0.271	0.0134

Table 38 Arithmetic mean and standard deviation of thermal impedance values of TIMs under surface roughness 25μm.

TIM	Sample size	Arithmetic mean of thermal impedance ($℃-cm^2/W$)	Standard deviation
976	5	3.007	0.0844
A580	5	2.839	0.0328
Designed TIM 1	5	0.890	0.0222
Designed TIM 2	5	0.325	0.0126

The box-plots showing the comparison of thermal impedance of TIMs under different surface roughness are illustrated in Figure 48, 49, 50, and 51.

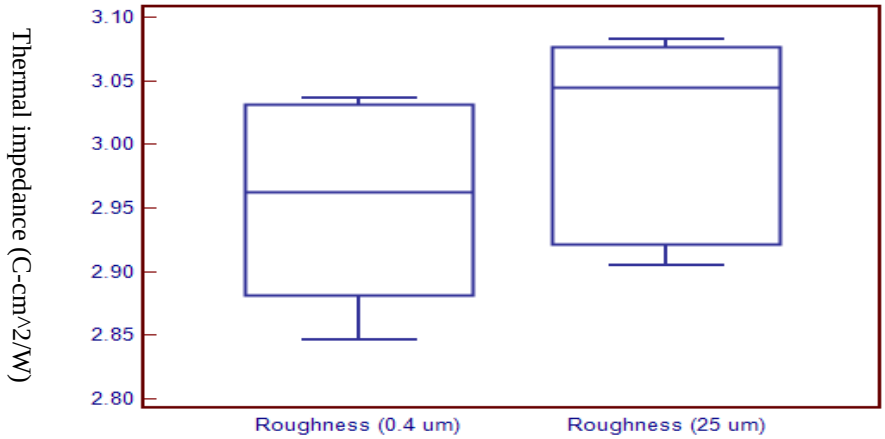

Figure 48 Box-plot showing the comparisons of thermal impedance values of TIM#976 at surface roughness 0.4 and 25 μm.

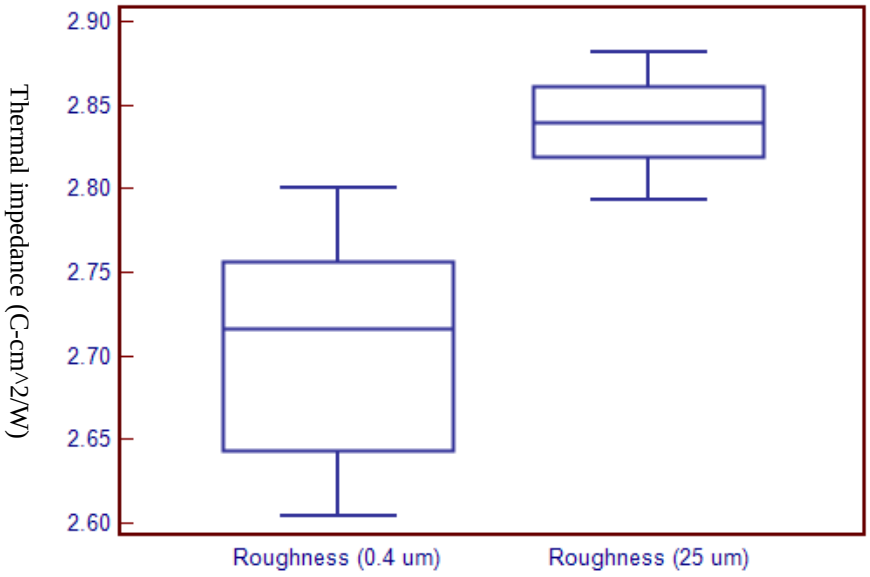

Figure 49 Box-plot showing the comparisons of thermal impedance values of TIM#A580 at surface roughness 0.4 and 25 µm.

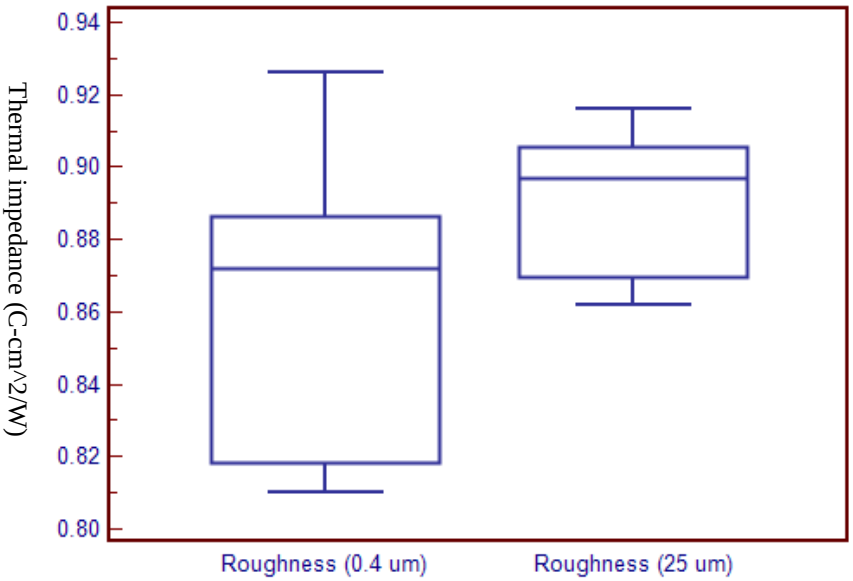

Figure 50 Box-plot showing the comparisons of thermal impedance values of designed TIM 1 at surface roughness 0.4 and 25 µm.

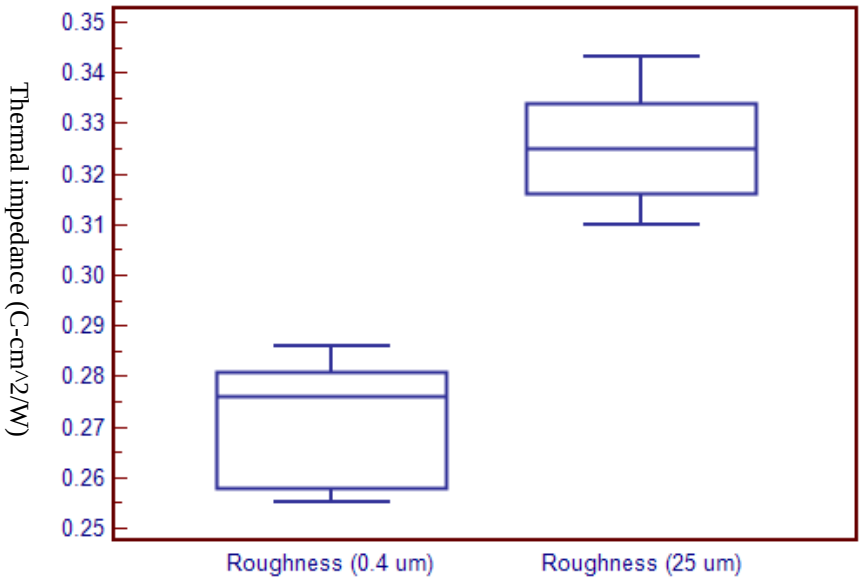

Figure 51 Box-plot showing the comparisons of thermal impedance values of designed TIM 2 at surface roughness 0.4 and 25 μm.

5.1.7.1 Hypothesis testing

1. Objective: To determine the effect of meter bar surface roughness on the thermal impedance of TIMs

2. H_0: $\mu_{\theta,\text{roughness } 0.4\mu m} = \mu_{\theta,\text{roughness } 25\mu m}$

   H_A: $\mu_{\theta,\text{roughness } 0.4\mu m} < \mu_{\theta,\text{roughness } 25\mu m}$

   where μ_θ represents the true average thermal impedance value for each TIM

   α=0.05

3. TS: $t=\frac{\bar{x}-\bar{y}}{S_p\sqrt{\frac{1}{m}+\frac{1}{n}}}$ =-1.108 (TIM#976), -3.678 (TIM#A580), -1.300 (Designed TIM 1), and -6.565 (Designed TIM 2)

   (S_p represents the pooled estimator of σ^2)

4. RR: For DF=m+n-2=8, reject H_0 if $t \leq -t_{\alpha,m+n-2} = -t_{0.05,8} = -1.860$

   (t-distribution table).

5. For TIM#976, t does not fall in the RR

   For TIM#A580, t falls in the RR

   For Designed TIM 1, t does not fall in the RR

   For Designed TIM 2, t falls in the RR

5. Therefore, for TIM#976 and Designed TIM 1, H_0 is not rejected at the 5% level of significance. However, for TIM#A580 and Designed TIM 2, H_0 is rejected at the 5% level of significance. In other words, for TIM#976 and Designed TIM1, there is not sufficient evidence to conclude that there is a difference in true average thermal impedance at surface roughness 0.4 and 25 μm. However, for TIM#A580 and Designed TIM2, the true average thermal impedance at surface roughness 0.4 μm is smaller than that at 25 μm.

5.1.8 The determination of the thermal conductivity of designed TIM 1

The arithmetic means and standard deviations of thermal impedance values of designed TIM 1 with different specimen thicknesses are summarized in Table 39. The plot showing the thermal impedance values of designed TIM 1 with different specimen thicknesses is shown in Figure 52.

Table 39 Arithmetic mean and standard deviation of thermal impedances of designed TIM 1 with different specimen thicknesses.

Thickness (cm)	Sample size	Arithmetic mean of thermal impedance ($℃-cm^2/W$)	Standard deviation
0.0025	5	0.855	0.0172
0.0040	5	1.292	0.0430
0.0060	5	1.925	0.0624

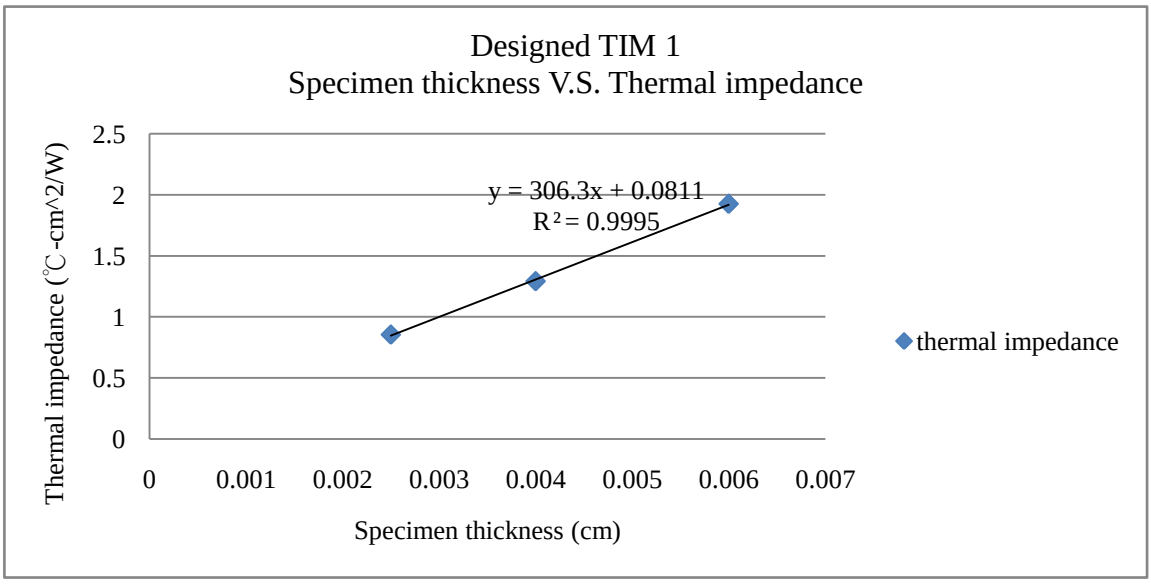

Figure 52 Plot showing the thermal impedance values of designed TIM 1 with different specimen thicknesses. The slope of the straight line is equal to the inverse of the thermal conductivity.

The slope of the linear regression equation in Figure 52 is 306.3. Therefore, the thermal conductivity of designed TIM 1 is equal to 0.00326 W/cm-K, or 0.326 W/m-K. Also, we can have the contact resistance of designed TIM 1 by substituting x with 0. The contact resistance is then 0.0811℃-cm^2/W.

5.1.9 The determination of the thermal conductivity of designed TIM 2

The arithmetic means and standard deviations of thermal impedance values of designed TIM 2 with different specimen thicknesses are summarized in Table 40. The

plot showing the thermal impedance values of designed TIM 2 with different specimen thicknesses is shown in Figure 53.

Table 40 Arithmetic mean and standard deviation of thermal impedances of designed TIM 2 with different specimen thicknesses.

Thickness (cm)	Sample size	Arithmetic mean of thermal impedance (℃ – cm^2/W)	Standard deviation
0.0035	5	0.283	0.0109
0.0050	5	0.395	0.0122
0.0070	5	0.543	0.0112

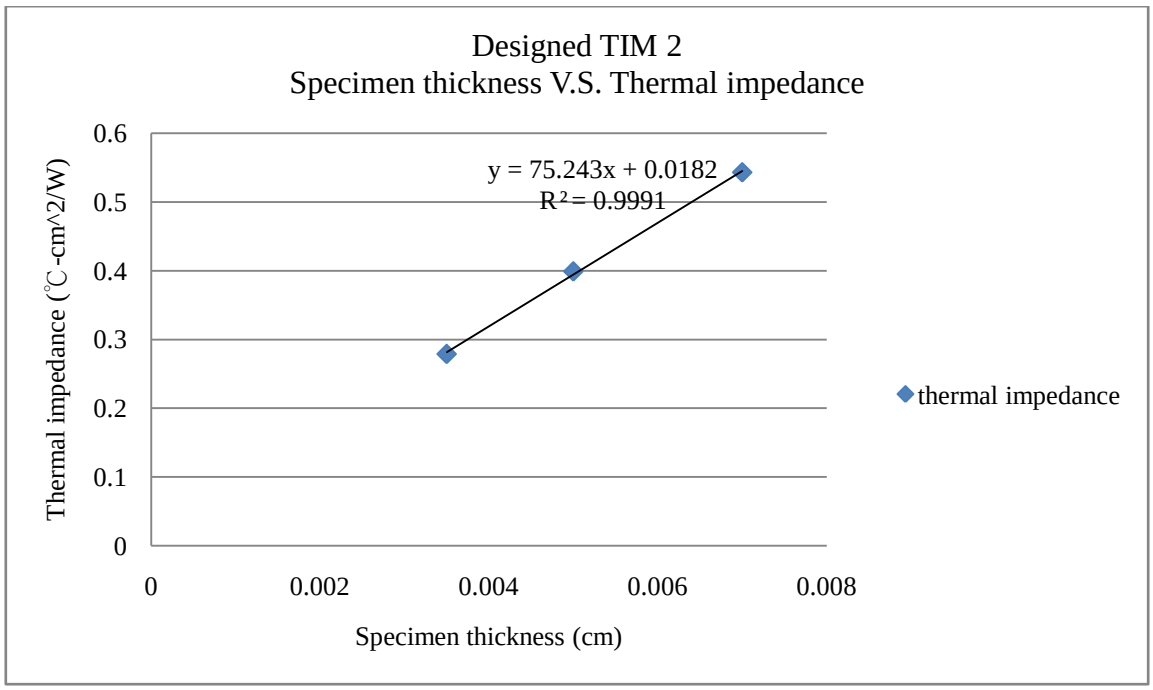

Figure 53 Plot showing the thermal impedance values of designed TIM 2 with different specimen thicknesses. The slope of the straight line is equal to the inverse of the thermal conductivity.

The slope of the linear regression equation in Figure 53 is 75.243. Therefore, the thermal conductivity of designed TIM 2 is equal to 0.01329 W/cm-K, or 1.329 W/m-K.

Also, we can have the contact resistance of designed TIM 2 by substituting x with 0. The contact resistance is then 0.0182℃-cm^2/W.

5.2 Summary of experimental results

Based on the experimental results and statistical analysis, several conclusions can be made. First, there is no linear relationship between ambient temperature and thermal impedance of TIMs. In other words, the ambient temperature at which our experimental chamber sits will not linearly affect the experimental results.

Second, there is no linear relationship between specimen temperature and thermal impedance of TIMs. Four types of TIMs under tests all have uniform and stable thermal performance when the specimen temperate is between 17 and 62℃.

Third, the thermal impedance of a TIM increases as the specimen thickness (d) increases. The reason is that the thermal impedance equals to the summation of the thermal resistance (d/K) of the TIM itself and the contact resistance at the interface. Therefore, increasing d will absolutely increase the thermal impedance value for a TIM.

Fourth, the thermal impedance of a TIM decreases as the contact pressure increases. The reason is that more air-filled voids at the interface can be filled with a TIM when the contact pressure is higher.

Fifth, the intrusive copper nanowires indeed can have lower thermal impedance value compared with a copper foil with the same thickness (40 μm). Even though a copper foil may have higher thermal conductivity than our designed TIMs, the contact

points between two mating surfaces are far less than ours. On the contrary, copper nanowires can provide massive ballistic like heat transportation paths.

Next, the meter bar surface roughness can affect the thermal performance of TIM#A580 and designed TIM 2. On the contrary, the thermal performance of TIM#976 and designed TIM 1 will not be appreciably affected by the meter bar surface roughness. According to the products catalog of Chomerics, the high thermal performance of TIM#976 results from its outstanding conformability at the interface, which is better than that of TIM#A580 (a more popular and cheap thermal management product). Due to the relatively poor conformability of TIM#A580 at the interface, its thermal impedance would be slightly increased as the meter bar surface becomes rougher. For designed TIMs, designed TIM 1 seemed to have better and consistent conformability than designed TIM 2 as the surface becomes rougher. It is postulated that as the meter bar surface becomes rougher, the air-filled voids at the interface cannot be fully filled by thermal grease on both sides of designed TIM 2. The pump-out of thermal grease might be a more serious issue when the surface becomes rougher.

Also, the thermal impedance of thermal grease T670 (product of Chomerics, published thermal impedance value is 0.07℃-cm^2/W) obtained from our tests was around 0.409℃-cm^2/W (Table A-61), which was nearly 6 times of the published value and not as good as our designed TIMs.

According to the correspondence with the applications engineer of *Chomerics*, the thermal performance of thermal grease will not be optimal until it reaches its phase change temperature (For thermal grease T670, the phase change temperature is around

62℃). Furthermore, the pump-out of thermal grease under contact pressure will also affect its thermal performance.

Finally, the arithmetic mean (standard deviation) of thermal impedance value of designed TIM 1 and designed TIM 2 is 0.850 ℃-cm^2/W (0.0467) and 0.273℃-cm^2/W (0.0157), respectively. The lowest thermal impedance value of designed TIM 1 and designed TIM 2 is 0.773 and 0.255℃-cm^2/W, respectively. Also, the thermal conductivity value of designed TIM 1 and designed TIM 2 is 0.326 and 1.329 W/m-K, respectively.

6. MATHEMATICAL MODEL VALIDATION

6.1 Mathematical models for designed TIMs

6.1.1 Designed TIM 1

The schematic diagram showing the structure of designed TIM 1 is illustrated in Figure 54.

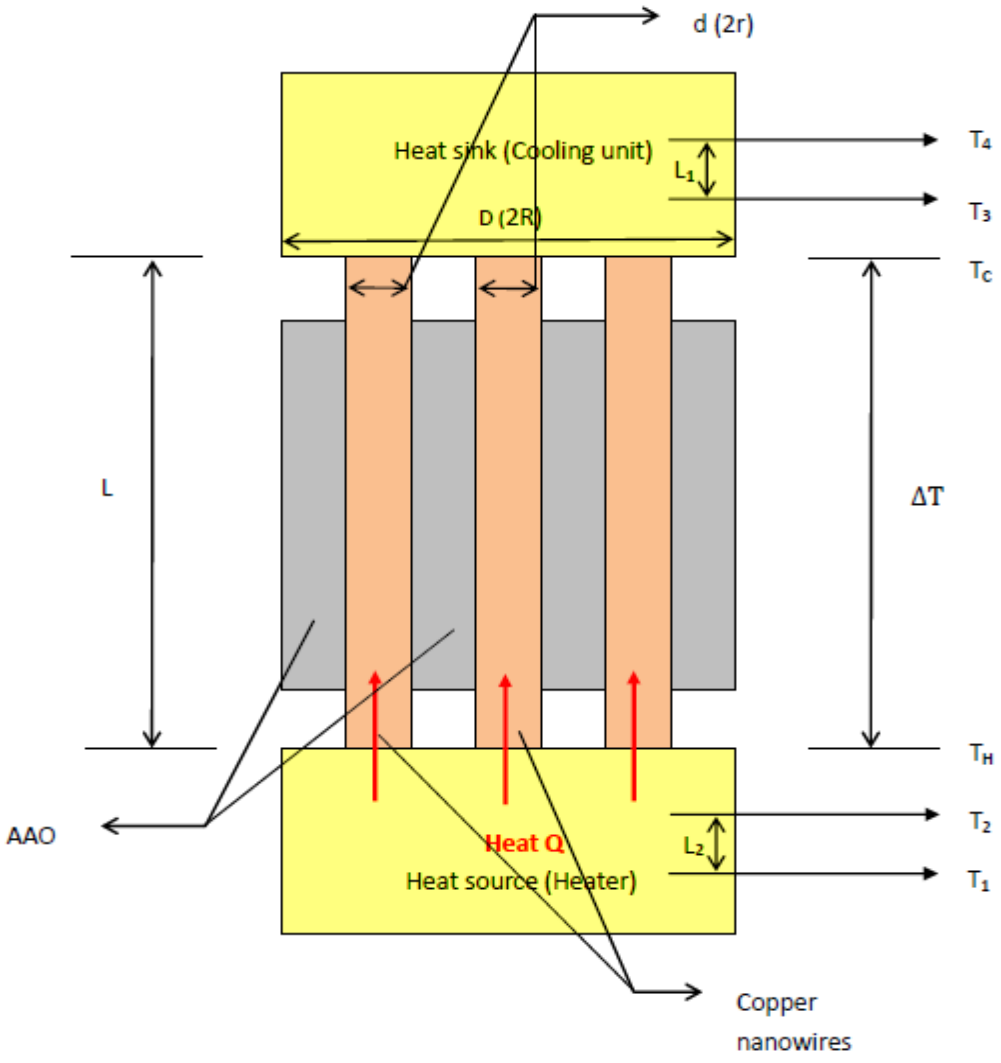

Figure 54 Schematic diagram showing the structure of designed TIM 1. Figure is not drawn to scale.

In this mathematical model, we make some assumptions. First, we assume that all freestanding copper nanowires can bridge two mating surfaces. In other words, exposed copper nanowires will not deflect or collapse under pressure. Second, we assume that the heat is transferred solely by thermal conduction, and the effects of thermal convection and thermal radiation are neglected.

According to the above assumption, we may have

$$Q=Q_{cond.}+Q_{conv.}+Q_{radi.}\cong Q_{cond.} \tag{24}$$

First, the heat transferred by conduction may be determined as

$$Q_{cond.}=K\times A_c\times \frac{\Delta T}{\Delta X}=K\times \left[N\times \frac{\pi d^2}{4}\right]\times \frac{\Delta T}{\Delta X} \tag{25}$$

where *N* is the total number of nanowires/ hexagons which depends on the pore size, and *d* is the diameter of a single nanowire. Both of them can be determined from SEM images.

The heat transferred by conduction may be rearranged as

$$Q_{cond.}=K\times A_c\times \frac{\Delta T}{\Delta X}=KN\frac{\pi d^2}{4}\times \frac{T_H-T_C}{L} \tag{26}$$

Therefore, we may rearrange the total heat Q as

$$Q\cong Q_{cond.}=\frac{KN\pi d^2}{4}\times \frac{T_H-T_C}{L} \tag{27}$$

The temperature difference across our designed TIM can be expressed as

$$\Delta T=\left(T_H-T_C\right)=\frac{4QL}{KN\pi d^2} \tag{28}$$

where Q can be determined from Equation (14) to (16) and can be determined as follows (L_1=L_2):

$$Q=\frac{\lambda A}{L_1}\times\left[\left(T_1-T_2\right)+\left(T_3-T_4\right)\right] \tag{29}$$

where A is the size of the specimen and can be computed as:

$$A=\frac{\pi D^2}{4} \tag{30}$$

Therefore, Q can be rearranged as:

$$Q=\frac{\lambda \pi D^2}{4L_1}\times\left[\left(T_1-T_2\right)+\left(T_3-T_4\right)\right] \tag{31}$$

Substituting Q into Equation (29) leads to the temperature difference (ΔT) as follows:

$$\Delta T=\left(T_H-T_C\right)=\frac{\lambda D^2 L}{L_1 KNd^2}\times\left[\left(T_1-T_2\right)+\left(T_3-T_4\right)\right] \tag{32}$$

The thermal impedance can also be determined according to Equation (8) as:

$$\theta=\frac{A}{Q}\times\left[T_H-T_C\right]=\frac{\left(\frac{\pi D^2}{4}\right)\times\frac{\lambda D^2 L}{L_1 KNd^2}\times\left[\left(T_1-T_2\right)+\left(T_3-T_4\right)\right]}{\frac{\lambda \pi D^2}{4L_1}\times\left[\left(T_1-T_2\right)+\left(T_3-T_4\right)\right]}=\frac{D^2 L}{KNd^2} \tag{33}$$

Next, it is necessary to determine the relationship between the number (N) and the pore size (d) of copper nanowires. It is intuitive to point out that with regards to the same specimen area, the larger the pore size, the less the number density. To derive number density of copper nanowires, we need to make use of SEM images (Figure 55).

With the count of nanowires in a specified small area (1μm×1μm, for example), we can infer the number of nanowires in a larger area (1 cm^2, for example).

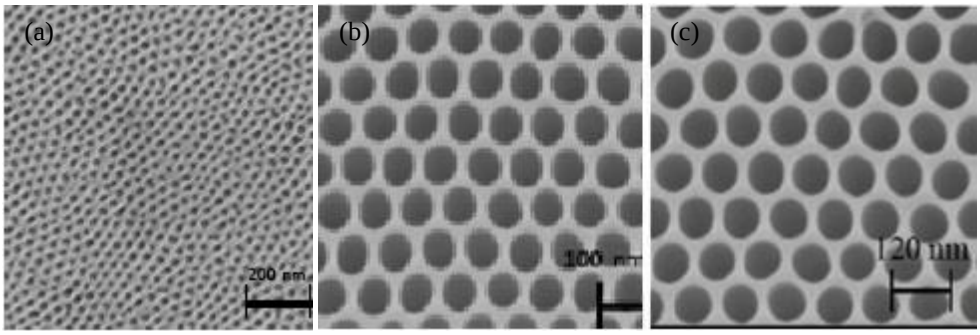

Figure 55 SEM images illustrating the relationship between pore number density (n) and pore size (d); (a) d=15 nm, n≅4.4×10^{11} pores /cm^2, (b) d=60 nm, n≅2.6×10^{10} pores /cm^2, and (c) d=80 nm, n≅1.8×10^{10} pore /cm^2.

In this thesis research, we fabricated AAO templates with uniform pore size equals to80nm. Therefore, the number density of copper nanowires is 1.8×10^{10} per cm^2. Since our specimen area equals 0.950 cm^2, the N value in Equation 10 will be substituted by $0.95\times1.8\times10^{10}=1.711\times10^{10}$.

6.1.2 Designed TIM 2

The schematic diagram showing the structure of designed TIM 2 is illustrated in Figure 56.

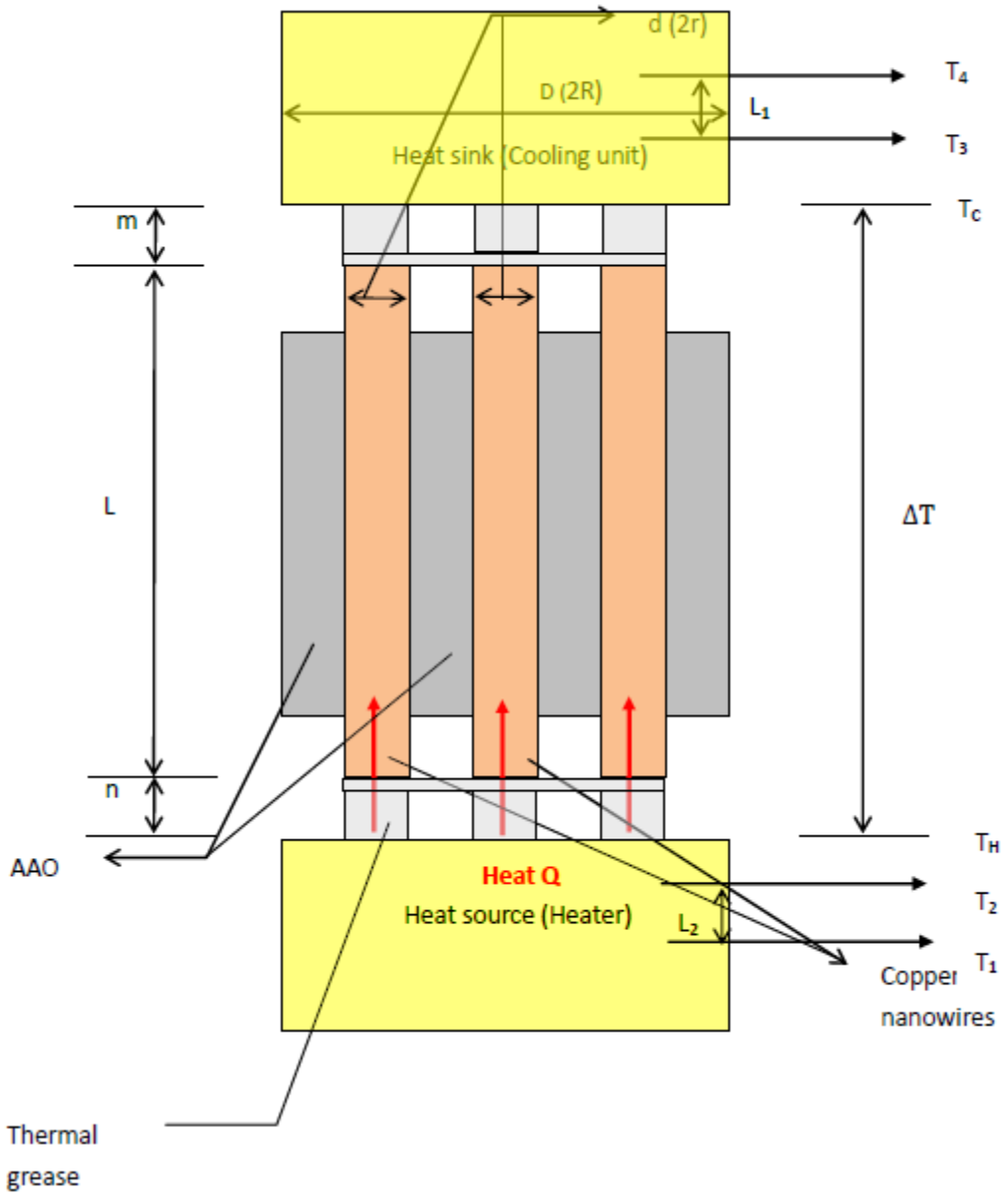

Figure 56 Schematic diagram showing the structure of designed TIM 2. Figure is not drawn to scale.

According to Equation (33), the thermal impedance of the designed TIM 1 structure can be determined by:

$$\theta=\frac{A}{Q}\times[T_H\text{-}T_C]=\frac{D^2L}{KNd^2}$$

Assume that the thermal grease is uniformly applied on both sides of the designed TIM 1 structure as shown in Figure 55, the thermal impedance can be determined by:

$$\theta = \frac{D^2(L+m+n)}{K_cNd^2} \quad (34)$$

where *m* and *n* are the thermal grease thickness applied on top and bottom side of the designed TIM 1 structure, respectively. Also, K_C is the thermal conductivity of the new structure.

6.2 Verification of built mathematical models

6.2.1 Verification of the mathematical model for designed TIM 1

According to Equation (33), the thermal impedance of designed TIM 1 is:

$$\theta=\frac{D^2L}{KNd^2}$$

where *D* is the specimen diameter (1.1cm), *L* is the specimen thickness (0.0025, 0.0040, 0.0060 cm), *K* is the thermal conductivity of the specimen (0.0033 W/cm-K, see Figure 52), *N* is the number of nanowires ($\cong 1.711\times10^{10}$ for pore size 80 nm, see Figure 55), and *d* is the pore size (80 nm).

Table 41 summarizes and compares thermal impedance values of designed TIM 1 derived by experiments and mathematical models:

Table 41 Comparisons of thermal impedance values of designed TIM 1 derived by experiments and built mathematical model.

Thickness (cm)	Pore size (cm)	Experimentally-derived thermal impedance (℃-cm^2/W)	Mathematically-derived thermal impedance (℃-cm^2/W)	%off (%)
0.0025	8×10^{-6}	0.850	0.838	1.4
0.0040	8×10^{-6}	1.261	1.340	-6.3
0.0060	8×10^{-6}	1.905	2.010	-5.5

6.2.2 Verification of the mathematical model for the designed TIM 2

According to Equation (34), the thermal impedance of designed TIM 2 is:

$$\theta = \frac{D^2(L+m+n)}{K_c N d^2}$$

where D is the specimen diameter (1.1cm), L is the specimen thickness (0.0025, 0.0040, 0.0060 cm), $(m+n)$ is the thermal grease thickness (0.0010cm), K_C is the effective thermal conductivity of the specimen (0.0133 W/cm-K, see Figure 53), N is the number of nanowires ($\cong 1.711\times10^{10}$ for pore size 80nm, see Figure 54, and d is the pore size (80 nm).

Table 42 summarizes and compares thermal impedance values of designed TIM 2 derived by experiments and mathematical models:

Table 42 Comparisons of thermal impedance values of designed TIM 2 derived by experiments and built mathematical model.

Thickness (cm)	Pore size (cm)	Experimentally-derived thermal impedance (℃-cm^2/W)	Mathematically-derived thermal impedance (℃-cm^2/W)	%off (%)
0.0035	8×10^{-6}	0.273	0.291	-6.6
0.0050	8×10^{-6}	0.402	0.415	-3.2
0.0070	8×10^{-6}	0.545	0.582	-6.8

7. SUMMARY AND FUTURE DIRECTIONS

7.1 Summary

Thermal insulating material (TIM) is used to reduce thermal impedance between computer chips and heat sinks. For this thesis research, two types of TIMs were designed and characterized. The first type, *Designed TIM 1*, was composed of copper nanowire arrays; while the second, *Designed TIM 2*, combined TIM 1 with thermal grease to form a sandwich structure. The pore size (i.e., the diameter of a single copper nanowire) of our AAO templates was 80 nm; while the thickness was 25, 40, and 60 μm.

The lowest thermal impedance of the designed TIMs was 0.255(℃-cm^2/W), lower than most of the commercially available TIMs (Table 43). Of all the commercially available TIMs listed in Table 43, only thermal grease and phase change material may have better thermal performance than our designed TIMs. However, there are some requirements before those optimal values can be obtained. Considering those requirements, our designed TIMs seem more reliable. The reasons are explained as follows.

Table 43 Published thermal impedance values of commercially available TIMs.

TIM	Thermal impedance ($℃ - cm^2/W$)
Thermal grease	0.07-0.13
Phase change material (PCM)	0.13-2.26
Thermally conductive adhesive tapes	2.0-7.7
Thermally conductive elastomer insulators	2.1-4.1
Thermally conductive pads	1.93-9.1

First, the thermal impedance of thermal grease will not be optimal until it reaches its phase change temperature. For example, the phase change temperature of thermal grease T670 from Chomerics is around 62℃. Therefore, the thermal performance of thermal grease is limited by the operating temperature of the electronics to which it is applied. Furthermore, the pump-out of thermal grease under contact pressure will also affect its thermal performance. If the operating temperature is not higher than the phase change temperature of fillers and the pump-out issue is not solved, the high thermal performance of thermal grease is not guaranteed.

Phase change material (PCM) has the same application limitations as thermal grease. Most PCMs have phase change temperatures around 50℃. The phase change temperature needs to be met before the thermal performance can be optimized. Furthermore, the maximum operating temperature of PCMs is only around 125℃, the lowest among all commercially available TIMs. Therefore, future applications of PCMs will be limited due to the low maximum operating temperature.

Carbon nanotubes (CNTs) have been used in some research as either TIM or TIM fillers. Most of this research employed CNTs as fillers to increase the overall thermal conductivity of the TIMs. The thermal performance of CNT-related TIMs can be as low as 0.052℃-cm^2/W. However, considering the potential health-related issues of CNTs, future applications in real industry are limited.

In sum, the high phase change temperature required for both thermal grease and PCMs is not a problem for our designed TIMs, which have consistent thermal

performance between 17 and 62℃. In addition, our designed TIMs appear to be safer and easier to use than CNTs based TIMs.

In order to evaluate the thermal properties of commercial and our designed TIMs, various treatments were designed. The impact of factors such as ambient temperature, average specimen temperature, contact pressure, specimen thickness, and meter-bar surface roughness on the thermal performance of TIMs were studied.

The experimental results suggest that ambient temperature and average specimen temperature had no significant effects on the thermal performance of either the commercially available on the designed TIMs. However, specimen thickness and contact pressure did affect the thermal performance of the TIMs. Also, meter bar surface roughness affected the thermal performance of TIM#A580 and designed TIM 2, but had no effect on the thermal performance of TIM#976 and designed TIM 1.

According to the product catalog from Chomerics, the operating temperature ranges for TIM#976 and A580 are -65~150℃, and -55~200℃, respectively. Therefore, the thermal performance of TIM#976 and A580 is consistent at our experimental specimen temperatures (17~66℃). As for our designed TIMs, the thermal performance is also consistent in the operating temperature range 17~66℃ due to the fact that they are composed of metal (copper) and ceramics (alumina), both of which are stable in that temperature range. The maximum operating temperature of our designed TIMs is expected to be much higher than 200℃ due to the thermal properties of copper and alumina.

The thermal impedance of a material is defined as the sum of its own thermal resistance (d/K) and any contact resistance between it and the mating surfaces. Assuming that the testing surfaces are consistent, the contact resistance should be the same for the same type of TIM. However, thickness (d) will affect the TIM's own thermal resistance and the overall thermal impedance value. Our experimental results showed this trend. As specimen thickness increases, the thermal impedance of a TIM increases as well.

Another important factor impacting the thermal performance of TIMs is contact pressure. The higher the clamping pressure, the better the conformability at the interface. The reason is that more air-filled voids can be filled with a TIM at higher contact pressure. Our experimental results also showed this trend. For both the commercial and designed TIMs, thermal impedance decreases as contact pressure increases.

The effect of meter bar surface roughness was also studied. The contact resistance of a TIM will be smaller when the surface is smoother. Therefore, the overall thermal impedance of a TIM should be smaller with a smoother surface, unless that TIM has outstanding conformability at the interface. According to the experimental results, the thermal performance of TIM#976 and designed TIM 1 were not significantly impacted by the surface roughness; whereas the thermal performance of TIM#A580 and designed TIM 2 were affected by the surface roughness. According to the product catalog from Chomerics, TIM#976 conforms to surface irregularities under moderate contact pressure. Therefore, it seems justified that TIM#976 has stable and consistent thermal performance at different surface roughness. As for designed TIM 1, the exposed

copper nanowires seemed able to identically bridge mating surfaces under different surface roughness.

Possible reasons for the low thermal impedance of our designed TIMs include:

(1) Copper nanowires can directly bridge mating surfaces

(2) Massive number of highly conductive parallel thermal paths

(3) Ballistic-like one dimensional heat transfer through copper nanowires

(4) Vertically aligned copper nanowires can confine the thermal grease in place

The following sections describe potential research to support future applications of our designed TIMs.

7.2 Future directions

7.2.1 High temperature tests

The maximum operating temperature of commercially available TIMs is around 200℃. Tests on the thermal performance of our designed TIMs under high temperatures (>200℃) are needed to evaluate the feasibility of their use in electronics with extremely high operating temperatures.

7.2.2 Chemical modification of AAO structures

The mechanical properties of ceramic materials limit their applicability. A potential shortcoming of AAO templates is a disposition to catastrophic fracture in a brittle manner with little energy absorption [110]. Therefore, the structural integrity of AAO templates needs to be enhanced to reduce application limitations.

7.2.3 Automated fabrication of AAO templates

AAO templates can be fabricated in a general chemical laboratory. Basically, the fabrication follows a step-by-step process and is easy to control. However, AAO usually takes more than 5 hrs to fabricate manually. Furthermore, the fabrication may not be consistent if it is conducted manually. Therefore, one of our objectives is to automate the fabrication process.

7.2.4 Modification of the experimental fixture

In this research, the experimental chamber used to test the thermal properties of TIMs was composed of glass. The thermal conductivity of glass is around 0.96W/m-K [110], which is small but may lead to some heat loss resulting from thermal conduction from the hot meter bar. Therefore, our group designed a new experimental chamber composed of Polyethylene (PE) (K=0.33 W/m-K) [110] (Figure 57) to reduce heat loss.

Second, the meter bars were aligned manually, which may lead to some error if the alignment was not perfect. In order to fix this problem, our group revised the method for aligning the two meter bars. In our design, the two meter bars perfectly mate to one another when the experimental chamber is closed.

Finally, the thermocouple probes were manually inserted into the center of the meter bars, which was inconsistent with regard to the insertion direction, contact point, and the force. Therefore, it is important to fix the thermocouple probes in the center of meter bars in the revised experimental fixture to reduce errors associated with inconsistent manipulations.

Figure 57 Images of the revised experimental fixture. (a) Thermocouple probes fixed inside copper meter bars, (b) the alignment of copper meter bars, (c) copper meter bars insulated in Polyethylene experimental fixture.

REFERENCES

[1] J.P. Gwinn, R.L. Webb, Performance and testing of thermal interface materials, Microelectronics Journal 34 (2003) 215–222.

[2] T.M. Lee, K.C. Chiou, F.P. Tseng, C.C. Huang, High thermal efficiency carbon nanotube-resin matrix for thermal interface materials, in: Electronic Components and Technology Conference, 2005, pp. 55-59.

[3] R. Saraswati, F.J. Polese, Aluminum matrix composite heat sinks for microchips and microcircuits, in: International Symposium on Microelectronics, 1998, pp. 681-686.

[4] D.D.L. Chung, Advances in thermal interface materials, Advancing Microelectronics 33 (2006) 8-11.

[5] J.R. Lukes, H.L. Zhong, Thermal conductivity of individual single-wall carbon nanotubes, Journal of Heat Transfer 129 (2007) 705-716.

[6] F. Simionescu, D.K. Harris, Estimation of the heat transfer coefficient of a microchannel heat sink using an optimal control technique, in: Proceedings of the 4th International Conference on Nanochannels, Microchannels, and Minichannels, 2006, pp. 901-909.

[7] P. Lall, M. Pecht, E.B. Hakim, Characterization of functional relationship between temperature and microelectronic reliability, Microelectronics and Reliability 35 (1995) 377-402.

[8] G. Dalarozee, Introduction to reliability, Microelectronic Engineering 49 (1999) 3-10.

[9] E.P. Zafiropoulos and E.N. Dialynas, Reliability and cost optimization of electronic devices considering the component failure rate uncertainty, Reliability Engineering and System Safety 84 (2004) 271-284.

[10] O. Salmela, The effect of introducing increased reliability risk electronic components into 3rd generation telecommunications systems, Reliability Engineering and System Safety 89 (2005) 208-218.

[11] C. Glynn, A.J. Robinson, Microscale heat transfer of confined miniature jets, in: Proceedings of the 4th International Conference on Nanochannels, Microchannels, and Minichannels, 2006, pp. 319-327.

[12] R.P. Hodson, A.E. Strevens, A. Drury, H.H. Horhold, W.J. Blau, Nanostructured

metal filled porous alumina as an anode in polymer light-emitting diodes, in: Proceedings of SPIE, 2005, pp. 114-122.

[13] T.H. Ji, S.Y. Kim, J.M. Hyun, Pressure drop and heat transfer correlations for triangular fin heat sinks, IEEE Transactions on Components and Packaging Technologies 30 (2007): 3-8.

[14] A. Desai, S. Mahajan, W. Jones, J. Geer, B. Sammakia, A numerical study of transport in a thermal interface material enhanced with carbon nanotubes, Journal of Electronic Packaging 128 (2006) 92-97.

[15] Chomerics. Parker Hannifin Corp., Woburn, MA. Sept., 2008. http://www.chomerics.com

[16] D.D.L. Chung, Thermal interface materials, Journal of Materials Engineering and Performance 10 (2000) 56-59.

[17] P. Zhou, K.E. Goodson, Modeling and measurement of pressure-dependent junction-spreader thermal resistance for integrated circuits, in: Proceedings of ASME International Mechanical Engineering Congress and Exposition, 2001, pp. 51-67.

[18] R.S. Prasher, Surface chemistry based model for the thermal contact resistance of fluidic interstitial thermal interface materials, Journal of Heat Transfer 123 (2000) 965-975.

[19] Y. Xu, X. Luo, D.D.L. Chuang, Sodium silicate based thermal interface materials for high thermal contact conductance, Journal of Electronic Packaging 122 (2000) 123-131.

[20] F.P. Incropera, D.P. DeWitt, Fundamentals of Heat and Mass Transfer, Fourth ed., Wiley, New York, 1996.

[21] C.P. Chu, G.L. Solbrekken, V. LeBonheur, Y.E. Xu, Application of phase-change materials in Pentium III and Pentium III Xeon processor cartridges, in: International Symposium on Advanced Packaging Materials , 2000, pp. 265-270.

[22] R. Viswanath, V. Wakharkar, A. Watwe, V. Lebonheur, Thermal performance challenges from silicon to systems, Intel Technology Journal 4 (2000).

[23] T. Ollila, 1999. Navigating the maze of thermal interface materials. http://www2.electronicproducts.com/Navigating_the_maze_of_thermal_interface_materials-article-NSUPCHO-NOV1999.aspx

[24] B.A. Cola, X.F. Xu, T.S. Fisher, Increased real contact in thermal interfaces: A carbon nanotube/foil material, Applied Physics Letters 90 (2007) 093513.

[25] Intel Pentium 4 Processor in the 423-pin package at 1.30, 1.40, 1.50, 1.60, 1.70, 1.80, 1.90, and 2 GHz. Datasheet. Aug., 2008. http://developer.intel.com/design/pentium4/datashts/249198.htm

[26] M. deSorgo, 1996. Thermal interface materials. http://www.electronics-cooling.com/articles/1996/sep/sep96_01.php

[27] M. deSorgo, 2001. Private correspondence with Chomerics, October 8.

[28] J.J. Park, M. Taya, Design of thermal interface material with high thermal conductivity and measurement apparatus, Journal of Electronic Packaging 128 (2006) 46-52.

[29] Q. Ngo, B.A. Cruden, A.M. Cassell, G. Sims, M. Meyyappan, J. Li, C.Y. Yang, Thermal interface properties of cu-filled vertically aligned carbon nanofiber arrays, Nano Letters 4 (2004) 2403-2407.

[30] J. Xu, T.S. Fisher, Enhancement of thermal interface materials with carbon nanotube arrays, International Journal of Heat and Mass Transfer. 49 (2006) 1658-1666.

[31] T. Tong, Y. Zhao, L. Delzeit, A. Kashani, M. Meyyappan, Dense vertically aligned multiwalled carbon nanotube arrays as thermal interface materials, Components and Packaging Technologies 30 (2007) 92-100.

[32] R.C. Johnson, Carbon-nanotube arrays take heat off chips, Electrical Engineering Times 1423 (2006) 38.

[33] D.B. Cho, J.H. Suhr, N.A. Koratkar, Carbon nanotube thin film coating for improved thermal management in piezoceramic sheet actuators, Journal of Intelligent Material Systems and Structures 17 (2006) 209-216.

[34] H. Huang, C.H. Liu, Y. Wu, Shoushan, Aligned carbon nanotube composite films for thermal management, Advanced Materials 17 (2005) 1652-1656.

[35] A. Rae, Using nanotechnology to enhance thermal material properties, Advancing Microelectronics 33 (2006) 12-14.

[36] X.J. Hu, L. Jiang, K.E. Goodson, Thermal conductance enhancement of particle-filled thermal interface materials using carbon nanotube inclusions, in: Inter Society Conference on Thermal Phenomena, 2004, pp. 63-69.

[37] S. Shaikh, K. Lafdi, E. Silver, The effect of a CNT interface on the thermal resistance of contact surfaces, Carbon 45 (2007): 695-703.

[38] Q. Ngo, B.A. Cruden, A.M. Cassell, G. Sims, J.L. Li, M. Meyyappan, C.Y. Yang, Nano-engineered carbon nanofiber-copper composite thermal interface material for efficient heat transfer, in: Proceedings of a Symposium Sponsored by the Surface Engineering Committee of the MPMD, 2005, pp. 75-82.

[39] S. Berber, Y.K. Kwon, D. Tomanek, Unusually high thermal conductivity of carbon nanotubes, Phys. Rev. Lett. 84 (2000) 4613-4616.

[40] J.W. Che, T. Cagıın, W.A. Goddard III, Thermal conductivity of carbon nanotubes, Nanotechnology 11 (2000): 65-69.

[41] R. Inguanta, M. Butera, C. Sunseri, S. Piazza, 2007, Fabrication of metal nanostructures using anodic alumina membranes grown in phosphoric acid solution: tailoring template morphology, Applied Surface Science 253 (2007) 5447-5456.

[42] A. Desai, J. Geer, B. Sammakia, Models of steady thermal conduction in multiple cylindrical domains, Journal of Electronic Packaging 128 (2006) 10-17.

[43] Y.S. Xu, G. Ray, B. Abdel-Magid, Thermal behavior of single-walled carbon nanotube polymer-matrix composites, Composites Part A 37 (2006) 114-121.

[44] S.T. Stern, S.E. McNeil, Nanotechnology safety concerns revisited, Society of Toxicology (2007) 1-56.

[45] D.B. Warheit, What is currently known about the health risks related to carbon nanotube exposures? Carbon 44 (2006) 1064-1069.

[46] J.A. Isaacs, A. Tanwani, M.L. Healy, Environmental assessment of SWNT production, in: Proceedings of the IEEE International Symposium on Electronics and the Environment, , 2006, pp. 38-41.

[47] L. Guo, X.Y. Liu, V. Sanchez, C. Vaslet, A.B. Kane, R.H. Hurt, A window of opportunity: designing carbon nanomaterials for environmental safety and health (2007).

[48] S.E. Iyuke, Safety, health, and environmental awareness in nanotechnology training, NSTI-Nanotech 1 (2006): 547-549.

[49] K. Datta, M. Field, Current knowledge about nanotechnology safety, in: Proceedings of Annul Reliability and Maintainability Symposium, 2006, pp. 70-

74.

[50] S. Fiorito, A. Serafino, F. Andreola, A. Togna, G. Togna, Toxicity and biocompatibility of carbon nanoparticles, Journal of Nanoscience and Nanotechnology 6 (2006) 591-599.

[51] C.F. Diniz, K. Balzuweit, N.D. Santina Mohallem, Alumina nanotubes: preparation and textural, structural and morphological characterization, Journal of Nanoparticle Research 9 (2007) 293-300.

[52] D.R. Askeland, P.P. Phule, The Science and Engineering of Materials, Fifth ed., Thompson, New York, 2006.

[53] C.C. Wang, C.C. Kei, Y.W. Yu, T.P. Perng, Organic nanowire-templated fabrication of alumina nanotubes by atomic layer deposition, Nano Letters 7 (2007) 1566-1569.

[54] B.C. Cheng, S.C. Qu, H.Y. Zhou, Z.G. Wang, Al_2O_3: Cr3+ Nanotubes synthesized via homogenization precipitation followed by heat treatment, J. Phys. Chem. B 110 (2006) 15749-15754.

[55] G.S. Huang, X.L. Wu, F. Kong, Y.C. Cheng, In situ fabrication of alumina nanotube array and photoluminescence, Applied Physics Letters 89 (2006) 073114.

[56] X.F. Shao, X.L. Wu, G.S. Huang, T. Qiu, M. Jiang, J.M. Hong, Alumina nanotubes and nanowires from Al-based porous alumina membranes, Appl. Phys. A 81 (2005) 621-625.

[57] G.S. Huang, Y. Xie, X.L. Wu, L.W. Yang, Y. Shi, G.G. Siu et al., Formation mechanism of individual alumina nanotubes wrapping metal (Cu and Fe) nanowires, Journal of Crystal Growth 289 (2006) 295-298.

[58] J. Zhang, Y. Huang, J. Lin, X.X. Ding, C. Tang, S.R. Qi, Large-scale preparation of aluminum borate-coated aluminum oxide nanowires, Journal of Solid State Chemistry 178 (2005) 2262-2266.

[59] J.S. Lee, B. Min, K. Cho, S. Kim, J. Park, Y.T. Lee et al., Al_2O_3 nanotubes and nanorods fabricated by coating and filling of carbon nanotubes with atomic-layer deposition, Journal of Crystal Growth 254 (2003) 443-448.

[60] L. Zhang, B. Cheng, W. Shi, E.T. Samulski, In-situ electrochemical synthesis of 1-D alumina nanostructures, J. Mater Chem. 15 (2005) 4889-4893.

[61] J.H. Zhou, J.P. He, G.W. Zhao, C.X. Zhang, J.S. Zhao, H.P. Hu, Alumina nanostructures prepared by two-step anodization process, Transactions of Nonferrous Metals Society of China 17 (2007) 82-86.

[62] C.C. Chen, C.G. Kuo, J.H. Chen, C.G. Chao, Nanoparticles of Pb-Bi eutectic nucleation and growth on alumina template, Japanese Journal of Applied Physics 43 (2004) 8354-8359.

[63] S.K. Hwang, S.H. Jeong, O.J. Lee, and K.H. Lee, Fabrication of vacuum tube arrays with a submicron dimension using anodic aluminum oxide nanotemplates, Microelectronic Engineering 77 (2005) 2-7.

[64] W.X. Li, and T.H. Shen, Nanomagnet arrays fabricated by electrodeposition using self-assembled anodic aluminum oxide templates, Microelectronic Engineering 84 (2007) 1436-1439.

[65] K. Kim, M. Kim, S.M. Cho, Pulsed electrodeposition of palladium nanowire arrays using AAO template, Materials Chemistry and Physics 96 (2006) 278-282.

[66] Y. Zhang, G.H. Li, Y.C. Wu, B. Zhang, W.H. Song, and L. Zhang, Antimony nanowire arrays fabricated by pulsed electrodeposition in anodic alumina membranes, Adv. Mater. 14 (2002) 1227-1230.

[67] Y.T. Tian, G.W. Meng, T. Gao, S.H. Sun, T. Xie, X.S. Peng et al., Alumina nanowire arrays standing on a porous anodic alumina membrane, Institute of Physics Publishing 15 (2004) 189-191.

[68] R.S. Liu, S.C. Chang, I. Baginskiy, S.F. Hu, C.Y. Huang, Synthesis and magnetic properties of multilayer Ni/Cu and NiFe/Cu nanowires, Journal of Physics 67 (2006) 85-91.

[69] X.Y. Zhang, L.D. Zhang, W. Chen, G.W. Meng, M.J. Zheng, L.X. Zhao, Electrochemical fabrication of highly ordered semiconductor and metallic nanowire arrays, Chem. Mater. 13 (2001) 2511-2515.

[70] L. Pu, X.M. Bao, J.P. Zou, D. Feng, Individual alumina nanotubes, Angew. Chem. Int. Ed. 40 (2001) 1490-1493.

[71] V.F. Surganov, G.G. Gorokh, A.M. Mozelev, A.A. Poznyak, S.K. Metto, Method of determining the dissolution rate of anodic oxide films during aluminum anodizing, Industry Lab. 53 (1988) 1062-1063.

[72] J. Hitzig, K. Juttner, W.J. Lorenz, AC-impedance measurements on corroded

porous aluminum oxide films, J. Electrochem. Soc. 133 (1986) 887-892.

[73] D. Routkevitch, T.L. Haslett, L. Ryan, T. Bigioni, C. Douketis, M. Moskovits, Synthesis and resonance Raman spectroscopy of CdS nanowire arrays, Chemical Physics 210 (1996) 343-352.

[74] C.C. Lin, F.M. Pan, Mei Liu, K.C. Chang, P.L. Chen, C.T. Kuo et al., Anodic aluminum oxide as a template for CNT field emitters and AAO-CNT triode structure, in: Proc. 12th International Display Workshops, 2005, pp. 1687-1689.

[75] F.L. Qu, M.H. Yang, G.L. Shen, R.Q. Yu, Electrochemical biosensing utilizing synergic action of carbon nanotubes and platinum nanowires prepared by template synthesis, Biosensors and Bioelectronics 22 (2007) 1749–1755.

[76] S.H. Jeong, H.Y. Hwang, S.K. Hwang, K.H. Lee, Carbon nanotubes based on anodic aluminum oxide nano-template, Carbon 42 (2004) 2073–2080.

[77] J.S. Lee, G.H. Gu, H. Kim, K.S. Jeong, J. Bae, J.S. Suh, Growth of carbon nanotubes on anodic aluminum oxide templates: fabrication of a tube-in-tube and linearly joined tube, Chem. Mater. 13 (2001) 2387-2391.

[78] Z. Wang, Y.K. Su, H.L. Li, AFM study of gold nanowire array electrodeposited within anodic aluminum oxide template, Appl. Phys. A 74 (2002) 563-565.

[79] W. Lee, R. Scholz, K. Nielsch, U. Gosele, A template-based electrochemical method for the synthesis of multisegmented metallic nanotubes, Angew. Chem. Int. Ed. 44 (2005) 6050-6054.

[80] R.L. Zong, J. Zhou, B. Li, M. Fu, S.K. Shi, L.T. Li, Optical properties of transparent copper 125anorods and nanowire arrays embedded in anodic alumina oxide, The Journal of Chemical Physics 123 (2005) 094710.

[81] K.S. Napolskii, A.A. Eliseev, N.V. Yesin, A.V. Lukashin, Y.D. Tretyakov, N.A. Grigorieva et al., Ordered arrays of Ni magnetic nanowires: Synthesis and investigation, Physica E 37 (2007) 178-183.

[82] T. Ohgai, L. Gravier, X. Hoffer, M. Lindeberg, K. Hjort,R Spohr, J. Ansermet, Template synthesis and magnetoresistance property of Ni and Co single nanowires electrodeposited into nanopores with a wide range of aspect ratios, J. Phys. D: Appl. Phys. 36 (2003) 3109–3114.

[83] A. Saedi, M. Ghorbani, Electrodeposition of Ni–Fe–Co alloy nanowire in modified AAO template, Materials Chemistry and Physics 91 (2005) 417–423.

[84] J.G. Wang, M.L. Tian, N. Kumar, T.E. Mallouk, Controllable template synthesis of superconducting Zn nanowires with different microstructures by electrochemical deposition, Nano Letters 5 (2005) 1247-1253.

[85] Z. Hu, C. Kong, Y. Han, H. Zhao, Y. Yang, H. Wu, Large-scale synthesis of defect-free silver nanowires by electrodeless deposition, Materials Letters 61 (2007) 3931-3934.

[86] Y.S. Shin, J.H. Yang, C.Y. Park, M.H. Kwon, J.B. Yoo, C.W. Yang, Synthesis of crystalline carbon nanotube arrays on anodic aluminum oxide using catalyst reduction with low pressure thermal chemical vapor deposition, Japanese Journal of Applied Physics 45 (2006) 1869-1872.

[87] J.P. Ge, Y.D. Li, Selective atmospheric pressure chemical vapor deposition route to CdS arrays, nanowires, and nanocombs, Adv. Func. Mater. 14 (2004) 157-162.

[88] H. Zhang, X.Y. Ma, J. Xu, J. Niu, J. Sha, D. Yang, Directional CdS nanowires fabricated by chemical bath deposition, Journal of Crystal Growth 246 (2002) 108–112.

[89] M. DaSilva, 2004. M. DaSilva's research photos. http://cobweb.ecn.purdue.edu/~mdasilva/Research_Photos.shtml

[90] P. Kim, L. Shi, A. Majumdar, P. McEuen, Thermal transport and energy dissipation in carbon nanotubes, Phys B 323 (2002)67–70.

[91] J. Hone, M.C. Laguno, M.J. Biercuk, A.T. Johnson, B. Batlogg, Z. Benes et al., Thermal properties of carbon nanotubes and nanotube-based materials, Appl. Phys. A 74 (2002)339–343.

[92] J. Hone, B. Batlogg, Z. Benes, M.C. Laguno, N.M. Nemes, A.T. Johnson, Thermal properties of single-walled carbon nanotubes, in: Materials Research Society Symposium, 2001, pp. A1711–A17112.

[93] F. Mohammad, S. Bengt, Heat and Fluid Flow in Microscale and Nanoscale Structures. Wit Press, Billerica, MA, 2004.

[94] D.J. Yang, Q. Zhang, G. Chen, S.F. Yoon, J. Ahn, S.G. Wang et al., Thermal conductivity of multiwalled carbon nanotubes, Physical Review B 66 (2002) 165440.

[95] X. Wang, Z. Zhong, J. Xu, Non-contact thermal characterization of individual multi- wall carbon nanotubes, in: Proc. 37th AIAA Thermophysics Conference,

2004, pp. 2465.

[96] J. Hone, M. Whitney, C. Piskoti, A. Zettl, Thermal conductivity of single-walled carbon nanotubes, Phys. Review B 59 (1999) R2514.

[97] A.B. Cruden, A.M. Cassell, Q. Ye, M. Meyyappan, Reactor design considerations in the hot filament/direct current plasma synthesis of carbon nanofibers, J. Appl. Phys. 94 (2003) 4070.

[98] A. Balandin, K.L. Wang, Significant decrease of the lattice thermal conductivity due to phonon confinement in a free-standing semiconductor quantum well, Physical Review B 55 (1998) 1544-1549.

[99] A. Khitun, A. Balandin, K.L. Wang, Modification of the lattice thermal conductivity in silicon quantum wires due to spatial confinement of acoustic phonons, Superlattices and Microstructures 26 (1999) 181-193.

[100] J. Zou, A. Balandin, Phonon heat conduction in a semiconductor nanowire, Journal of Applied Physics 89 (2001) 2932-2938.

[101] M.S. Dresselhaus, G. Dresselhaus, K. Sugihara, I.L. Spain, H.A. Goldberg, Graphite fibers and filaments, Spring Series in Materials Science 5 (1988) 97-103.

[102] A. Potts, M.J. Kelly, D.G. Hasko, C.G. Smith, J. Cleaver, H. Ahmed et al., Thermal transport in free-standing semiconductor fine wires, Supperlattices and Microstructures 9 (1991) 315-318.

[103] T.S. Tighe, J.W. Worlock, M.L. Roukes, Direct thermal conductance measurements on suspended nanocrystalline nanostructures, Applied Physics Letters 70 (1997) 2687-2689.

[104] S. Tao, D.Y. Li, Tribological, mechanical and electrochemical properties of nanocrystalline copper deposits produced by pulse electrodeposition, Institute of Physics Publishing 17 (2006) 65-78.

[105] K.H. Saber, C.C. Koch, P.S. Fedkiw, Pulse current electrodeposition of nanocrystalline zinc, Materials Science and Engineering A 341 (2003) 174-181.

[106] G.P. Sklar, K. Paramguru, M. Misra, J.C. LaCombe, Pulsed electrodeposition into AAO templates for CVD growth of carbon nanotube arrays, Nanotechnology 16 (2005) 1265-1271.

[107] R.M. Metzger, S. Ming, G. Zangari, Shamsuzzoha, Magnetic nanoparticle arrays

with ultra-uniform length electrodeposited in highly ordered alumina nanopores, in: Materials Research Society Symposium Proceedings, 2001, pp. 1-6.

[108] J.W. Park, S.H. Ryu, C.N. Chu, Pulsed electrochemical deposition for 3D micro structuring, International Journal of Precision Engineering and Manufacturing 6 (2005) 49-54.

[109] American Society of Testing and Materials (ASTM) test D5470. Standard test method for thermal transmission properties of thermally conductive electrical insulation materials (2006).

[110] William D. Callister, Jr., Materials Science and Engineering: An Introduction. 6th edition, Wiley, New York, 2003.

APPENDIX

1. Experimental data of thermal impedance values of TIMs under various ambient temperatures.

Table A-1 Representative experimental result showing the thermal impedance values of TIM#976 under various ambient temperatures.

Thickness under no pressure=0.1 cm Thickness under 50psi=0.055 cm Published thermal impedance=3.1 ($℃-cm^2/W$) Published thermal conductivity (K)=6 W/m-K T_w=10℃ Contact pressure=50psi Ambient temperatures are between 21.0-25.0 ℃					
Specimen	1	2	3	4	5
$T_{Ambient}$ (℃)	23.5	24.2	24.9	23.1	23.1
T_1 (℃)	61.1	61.5	59.1	59.3	57.9
T_2 (℃)	57.7	58.2	55.7	56.2	54.8
T_3 (℃)	45.0	45.7	43.4	44.6	43.5
T_4 (℃)	41.4	42.1	39.8	41.2	40.1
Specimen temp. (℃)	51.4	52.0	49.6	50.4	49.2
Thermal impedance ($℃-cm^2/W$)	3.036	3.029	2.893	2.962	2.846

Table A-2 Representative experimental results showing the thermal impedance values of TIM#A580 under various ambient temperatures.

Thickness under no pressure=0.05 cm Thickness under 50psi=0.035 cm Published thermal impedance=2.700 ($℃-cm^2/W$) Published thermal conductivity (K)=3 W/m-K T_w=10℃ Contact pressure=50psi Ambient temperatures are between 21.0-25.0 ℃					
Specimen	1	2	3	4	5
$T_{Ambient}$ (℃)	23.2	21.3	22.5	22.3	23.1
T_1 (℃)	54.5	55.3	56.0	59.7	60.1
T_2 (℃)	52.6	53.0	53.9	56.7	56.9
T_3 (℃)	44.0	44.3	45.3	43.3	43.6
T_4 (℃)	40.9	41.3	42.3	38.4	38.8
Specimen temp. (℃)	48.3	48.7	49.6	50.0	50.3
Thermal impedance ($℃-cm^2/W$)	2.800	2.604	2.716	2.741	2.656

Table A-3 Representative experimental result showing the thermal impedance values of designed TIM 1 under various ambient temperatures.

Thickness=0.0025 cm T_w=10℃ Contact pressure=50psi Ambient temperatures are between 21.0-25.0 ℃					
Specimen	1	2	3	4	5
$T_{Ambient}$ (℃)	22.3	24.0	23.8	23.8	24.4
T_1 (℃)	58.0	59.4	56.3	58.4	58.6
T_2 (℃)	53.5	54.9	52.6	54.5	54.0
T_3 (℃)	46.2	47.5	46.0	48.0	46.5
T_4 (℃)	42.8	44.2	42.9	44.9	43.2

Table A-3 (Continued)

Specimen temp. (℃)	49.9	51.2	49.3	51.3	50.3
Thermal impedance (℃ − cm^2/W)	0.810	0.872	0.926	0.821	0.873

Table A-4 Representative experimental result showing the thermal impedance values of designed TIM 2 under various ambient temperatures.

Thickness=0.0035 cm T_w=10℃ Contact pressure=50psi Ambient temperatures are between 21.0-25.0 ℃					
Specimen	1	2	3	4	5
$T_{Ambient}$ (℃)	23.0	23.0	23.5	23.0	22.6
T_1 (℃)	57.1	58.6	60.5	58.1	56.9
T_2 (℃)	52.3	53.6	55.5	53.2	52.1
T_3 (℃)	44.9	46.0	47.9	45.7	44.8
T_4 (℃)	39.3	40.2	42.2	40.1	39.2
Specimen temp. (℃)	48.6	49.8	51.7	49.5	48.5
Thermal impedance (℃ − cm^2/W)	0.279	0.259	0.276	0.286	0.255

2. Experimental data of thermal impedance values of TIMs under various contact pressures.

Table A-5 Representative experimental result showing the thermal impedance values of TIM#976 under contact pressure 30psi.

Thickness under no pressure=0.1 cm Thickness under 30psi=0.084 cm T_w=10℃ Contact pressure=30, 40, 50 psi Ambient temperature is maintained between 22±3℃					
Specimen	1	2	3	4	5
Contact pressure (psi)	30	30	30	30	30
T_1 (℃)	58.8	58.4	57.4	57.3	56.7
T_2 (℃)	57.1	56.7	55.6	55.5	55.1
T_3 (℃)	43.8	43.6	42.9	42.9	42.6
T_4 (℃)	39.3	39.3	38.6	38.8	38.5
Specimen temp. (℃)	50.5	50.2	49.3	49.2	48.9
Thermal impedance (℃ − cm^2/W)	3.863	3.958	3.705	3.839	3.982

Table A-6 Representative experimental result showing the thermal impedance values of TIM#976 under contact pressure 40psi.

Thickness under no pressure=0.1 cm Thickness under 40psi=0.072 cm T_w=10℃ Contact pressure=30, 40, 50 psi Ambient temperature is maintained between 22±3℃					
Specimen	1	2	3	4	5
Contact pressure (psi)	40	40	40	40	40
T_1 (℃)	61.3	60.8	62.1	61.7	62.7
T_2 (℃)	57.3	57.0	58.2	57.8	58.8
T_3 (℃)	40.4	40.1	41.0	40.7	41.5
T_4 (℃)	36.1	35.7	36.6	36.2	37.1
Specimen temp. (℃)	48.9	48.6	49.6	49.3	50.2
Thermal impedance (℃ − cm^2/W)	3.590	3.652	3.681	3.589	3.711

Table A-7 Representative experimental result showing the thermal impedance values of TIM#976 under contact pressure 50psi.

Thickness under no pressure=0.1 cm Thickness under 50psi=0.055 cm T_w=10℃ Contact pressure=30, 40, 50 psi Ambient temperature is maintained between 22±3℃					
Specimen	1	2	3	4	5
Contact pressure (psi)	50	50	50	50	50
T_1 (℃)	61.1	61.5	59.1	59.3	57.9
T_2 (℃)	57.7	58.2	55.7	56.2	54.8
T_3 (℃)	45.0	45.7	43.4	44.6	43.5
T_4 (℃)	41.4	42.1	39.8	41.2	40.1
Specimen temp. (℃)	51.4	52.0	49.6	50.4	49.2
Thermal impedance (℃ − cm^2/W)	3.036	3.029	2.893	2.962	2.846

Table A-8 Experimental result showing the thermal impedance values of TIM#A580 under contact pressure 30 psi.

Thickness under no pressure=0.05 cm Thickness under 30psi=0.040 cm T_w=10℃ Contact pressure=30, 40, 50 psi (25 specimens each) Ambient temperature is maintained between 22±3℃					
Specimen	1	2	3	4	5
Contact pressure (psi)	30	30	30	30	30
T_1 (℃)	61.1	62.6	63.3	63.1	61.1
T_2 (℃)	58.0	59.4	60.1	60.1	57.8
T_3 (℃)	42.7	43.4	43.9	43.8	41.7
T_4 (℃)	37.7	38.2	38.7	38.5	36.6
Specimen temp. (℃)	50.4	51.4	52.0	52.0	49.8
Thermal impedance (℃ − cm^2/W)	3.222	3.262	3.321	3.410	3.292

Table A-9 Representative experimental result showing the thermal impedance values of TIM#A580 under contact pressure 40 psi.

Thickness under no pressure=0.05 cm Thickness under 40psi=0.038 cm T_w=10℃ Contact pressure=30, 40, 50 psi (25 specimens each) Ambient temperature is maintained between 22±3℃					
Specimen	1	2	3	4	5
Contact pressure (psi)	40	40	40	40	40
T_1 (℃)	60.2	57.9	59.2	57.6	60.0
T_2 (℃)	57.1	55.0	56.3	54.8	57.2
T_3 (℃)	43.9	42.1	43.3	41.9	43.9
T_4 (℃)	39.5	37.7	39.9	37.6	39.4
Specimen temp. (℃)	50.5	48.6	49.8	48.4	50.6
Thermal impedance (℃ − cm^2/W)	2.900	2.918	3.014	3.042	3.055

Table A-10 Representative experimental result showing the thermal impedance values of TIM#A580 under contact pressure 50 psi.

Thickness under no pressure=0.05 cm Thickness under 50psi=0.035 cm T_w=10℃ Contact pressure=30, 40, 50 psi (25 specimens each) Ambient temperature is maintained between 22±3℃					
Specimen	1	2	3	4	5
Contact pressure (psi)	50	50	50	50	50
T_1 (℃)	54.5	55.3	56.0	59.7	60.1
T_2 (℃)	52.6	53.0	53.9	56.7	56.9
T_3 (℃)	44.0	44.3	45.3	43.3	43.6
T_4 (℃)	40.9	41.3	42.3	38.4	38.8
Specimen temp. (℃)	48.3	48.7	49.6	50.0	50.3
Thermal impedance ($℃-cm^2/W$)	2.800	2.604	2.716	2.741	2.656

Table A-11 Representative experimental result showing the thermal impedance values of designed TIM 1 under contact pressure 30 psi.

Thickness=0.0025 cm T_w=10℃ Contact pressure=30, 40, 50psi (25 specimens each) Ambient temperature is maintained between 22±3℃					
Specimen	1	2	3	4	5
Contact pressure (psi)	30	30	30	30	30
T_1 (℃)	58.8	61.2	59.7	61.2	61.6
T_2 (℃)	54.5	56.9	55.4	56.4	56.8
T_3 (℃)	44.7	47.0	44.6	45.6	45.9
T_4 (℃)	41.0	43.4	40.2	41.2	41.6
Specimen temp. (℃)	49.6	52.0	50.0	51.0	51.4
Thermal impedance ($℃-cm^2/W$)	1.563	1.633	1.603	1.435	1.495

Table A-12 Representative experimental result showing the thermal impedance values of designed TIM 1 under contact pressure 40 psi.

Thickness=0.0025 cm T_w=10℃ Contact pressure=30, 40, 50psi (25 specimens each) Ambient temperature is maintained between 22±3℃					
Specimen	1	2	3	4	5
Contact pressure (psi)	40	40	40	40	40
T_1 (℃)	58.2	58.8	58.9	59.3	59.9
T_2 (℃)	54.2	54.6	54.5	54.9	55.5
T_3 (℃)	46.4	46.9	46.3	46.8	47.4
T_4 (℃)	43.5	43.7	43.2	43.4	44.5
Specimen temp. (℃)	50.3	50.8	50.4	50.9	51.5
Thermal impedance ($℃-cm^2/W$)	1.326	1.101	1.233	1.096	1.274

Table A-13 Representative experimental result showing the thermal impedance values of designed TIM 1 under contact pressure 50 psi.

Thickness=0.0025 cm T_w=10℃ Contact pressure=30, 40, 50psi (25 specimens each) Ambient temperature is maintained between 22±3℃					
Specimen	1	2	3	4	5
Contact pressure (psi)	50	50	50	50	50
T_1 (℃)	58.0	59.4	56.3	58.4	58.6
T_2 (℃)	53.5	54.9	52.6	54.5	54.0
T_3 (℃)	46.2	47.5	46.0	48.0	46.5
T_4 (℃)	42.8	44.2	42.9	44.9	43.2
Specimen temp. (℃)	49.9	51.2	49.3	51.3	50.3
Thermal impedance ($℃-cm^2/W$)	0.810	0.872	0.926	0.821	0.873

Table A-14 Representative experimental result showing the thermal impedance values of designed TIM 2 under contact pressure 30 psi.

Thickness=0.0035 cm T_w=10℃ Contact pressure=30, 40, 50psi (10 specimens each) Ambient temperature is maintained between 22±3℃					
Specimen	1	2	3	4	5
Contact pressure (psi)	40	40	40	40	40
T_1 (℃)	62.9	61.7	60.9	62.0	60.6
T_2 (℃)	56.8	55.6	54.7	56.1	54.8
T_3 (℃)	47.2	45.9	45.1	46.9	45.7
T_4 (℃)	41.1	39.8	39.1	41.2	40.0
Specimen temp. (℃)	52.0	50.8	49.9	51.5	50.3
Thermal impedance ($℃-cm^2/W$)	0.467	0.488	0.467	0.483	0.478

Table A-15 Representative experimental result showing the thermal impedance values of designed TIM 2 under contact pressure 40 psi.

Thickness=0.0035 cm T_w=10℃ Contact pressure=30, 40, 50psi (10 specimens each) Ambient temperature is maintained between 22±3℃					
Specimen	1	2	3	4	5
Contact pressure (psi)	30	30	30	30	30
T_1 (℃)	61.6	62.1	59.7	62.7	58.2
T_2 (℃)	55.5	55.9	53.9	56.5	52.3
T_3 (℃)	46.3	46.5	45.4	47.0	43.6
T_4 (℃)	40.1	40.3	39.8	40.6	37.8
Specimen temp. (℃)	50.9	51.2	49.7	51.8	48.0
Thermal impedance ($℃-cm^2/W$)	0.370	0.395	0.364	0.385	0.359

Table A-16 Representative experimental result showing the thermal impedance values of designed TIM 2 under contact pressure 50 psi.

Thickness=0.0035 cm T_w=10℃ Contact pressure=30, 40, 50psi (10 specimens each) Ambient temperature is maintained between 22±3℃					
Specimen	1	2	3	4	5
Contact pressure (psi)	50	50	50	50	50
T_1 (℃)	57.1	58.6	60.5	58.1	56.9
T_2 (℃)	52.3	53.6	55.5	53.2	52.1
T_3 (℃)	44.9	46.0	47.9	45.7	44.8
T_4 (℃)	39.3	40.2	42.2	40.1	39.2
Specimen temp. (℃)	48.6	49.8	51.7	49.5	48.5
Thermal impedance (℃ − cm^2/W)	0.279	0.259	0.276	0.286	0.255

3. Experimental data of thermal impedance values of TIMs at different specimen temperatures

Table A-17 Representative experimental result showing the thermal impedance values of TIM#976 under various specimen temperatures.

Thickness under no pressure=0.1 cm Thickness under 50psi=0.055 cm T_w=10℃ Contact pressure=50 psi Ambient temperature is maintained between 22±3℃					
Specimen	1	2	3	4	5
T_1 (℃)	61.1	61.5	59.1	59.3	57.9
T_2 (℃)	57.7	58.2	55.7	56.2	54.8
T_3 (℃)	45.0	45.7	43.4	44.6	43.5
T_4 (℃)	41.4	42.1	39.8	41.2	40.1
Specimen temp. (℃)	51.4	52.0	49.6	50.4	49.2
Thermal impedance (℃ − cm^2/W)	3.036	3.029	2.893	2.962	2.846

Table A-18 Representative experimental result showing the thermal impedance values of TIM#A580 under various specimen temperatures.

Thickness under no pressure=0.05 cm Thickness under 50psi=0.035 cm T_w=10℃ Contact pressure=50 psi Ambient temperature is maintained between 22±3℃					
Specimen	1	2	3	4	5
T_1 (℃)	54.5	55.3	56.0	59.7	60.1
T_2 (℃)	52.6	53.0	53.9	56.7	56.9
T_3 (℃)	44.0	44.3	45.3	43.3	43.6
T_4 (℃)	40.9	41.3	42.3	38.4	38.8
Specimen temp. (℃)	48.3	48.7	49.6	50.0	50.3
Thermal impedance (℃ − cm^2/W)	2.800	2.604	2.716	2.741	2.656

Table A-19 Representative experimental result showing the thermal impedance values of designed TIM 1 under various specimen temperatures.

Thickness=0.0025 cm T_w=10℃ Contact pressure=50 psi Ambient temperature is maintained between 22±3℃					
Specimen	1	2	3	4	5
T_1 (℃)	58.0	59.4	56.3	58.4	58.6
T_2 (℃)	53.5	54.9	52.6	54.5	54.0
T_3 (℃)	46.2	47.5	46.0	48.0	46.5
T_4 (℃)	42.8	44.2	42.9	44.9	43.2
Specimen temp. (℃)	49.9	51.2	49.3	51.3	50.3
Thermal impedance ($℃-cm^2/W$)	0.810	0.872	0.926	0.821	0.873

Table A-20 Representative experimental result showing the thermal impedance values of designed TIM 2 under various specimen temperatures.

Thickness=0.0025 cm T_w=10℃ Contact pressure=50 psi Ambient temperature is maintained between 22±3℃					
Specimen	1	2	3	4	5
T_1 (℃)	57.1	58.6	60.5	58.1	56.9
T_2 (℃)	52.3	53.6	55.5	53.2	52.1
T_3 (℃)	44.9	46.0	47.9	45.7	44.8
T_4 (℃)	39.3	40.2	42.2	40.1	39.2
Specimen temp. (℃)	48.6	49.8	51.7	49.5	48.5
Thermal impedance ($℃-cm^2/W$)	0.279	0.259	0.276	0.286	0.255

4. Experimental data of thermal impedance values of TIMs with different specimen thicknesses

Table A-21 Representative experimental result showing the thermal impedance values of TIM#976 with specimen thickness 0.055 cm.

Thickness under no pressure=0.1cm Thickness under 50psi=0.055cm T_w=10℃ Contact pressure=50 psi Ambient temperature is maintained between 22±3℃					
Specimen	1	2	3	4	5
Thickness (cm)	0.055	0.055	0.055	0.055	0.055
T_1 (℃)	61.1	61.5	59.1	59.3	57.9
T_2 (℃)	57.7	58.2	55.7	56.2	54.8
T_3 (℃)	45.0	45.7	43.4	44.6	43.5
T_4 (℃)	41.4	42.1	39.8	41.2	40.1
Specimen temp. (℃)	51.4	52.0	49.6	50.4	49.2
Thermal impedance ($℃-cm^2/W$)	3.036	3.029	2.893	2.962	2.846

Table A-22 Representative experimental result showing the thermal impedance values of TIM#976 with specimen thickness 0.138 cm.

Thickness under no pressure=0.25cm Thickness under 50psi= 0.138cm T_w=10℃ Contact pressure=50 psi Ambient temperature is maintained between 22±3℃					
Specimen	1	2	3	4	5
Thickness (cm)	0.138	0.138	0.138	0.138	0.138
T_1 (℃)	65.3	63.0	63.5	66.1	65.8
T_2 (℃)	61.0	58.5	58.8	61.8	61.3
T_3 (℃)	40.5	38.2	38.5	40.6	40.3
T_4 (℃)	36.2	33.8	34.2	36.4	36.0
Specimen temp. (℃)	50.8	48.4	48.7	51.2	50.8
Thermal impedance (℃ − cm^2/W)	4.459	4.202	4.139	4.735	4.466

Table A-23 Representative experimental result showing the thermal impedance values of TIM#976 with specimen thickness 0.275 cm.

Thickness under no pressure=0.50 cm Thickness under 50psi=0.275 cm T_w=10℃ Contact pressure=50 psi Ambient temperature is maintained between 22±3℃					
Specimen	1	2	3	4	5
Thickness (cm)	0.275	0.275	0.275	0.275	0.275
T_1 (℃)	69.8	67.4	68.0	68.4	67.6
T_2 (℃)	65.6	63.2	63.4	64.5	63.3
T_3 (℃)	35.2	32.9	33.2	36.4	35.4
T_4 (℃)	29.8	27.9	28.3	31.4	31.0
Specimen temp. (℃)	50.4	48.1	48.3	50.5	49.4
Thermal impedance (℃ − cm^2/W)	6.417	6.734	6.447	6.393	6.517

Table A-24 Representative experimental result showing the thermal impedance values of TIM#A580 with specimen thickness 0.035 cm.

Thickness under no pressure=0.05cm Thickness under 50psi=0.035cm T_w=10℃ Contact pressure=50 psi Ambient temperature is maintained between 22±3℃					
Specimen	1	2	3	4	5
Thickness (cm)	0.035	0.035	0.035	0.035	0.035
T_1 (℃)	54.5	55.3	56.0	59.7	60.1
T_2 (℃)	52.6	53.0	53.9	56.7	56.9
T_3 (℃)	44.0	44.3	45.3	43.3	43.6
T_4 (℃)	40.9	41.3	42.3	38.4	38.8
Specimen temp. (℃)	48.3	48.7	49.6	50.0	50.3
Thermal impedance (℃ − cm^2/W)	2.800	2.604	2.716	2.741	2.656

Table A-25 Representative experimental result showing the thermal impedance values of TIM#A580 with specimen thickness 0.175 cm.

Thickness under no pressure=0.25cm Thickness under 50psi=0.175cm T_w=10℃ Contact pressure=50 psi Ambient temperature is maintained between 22±3℃					
Specimen	1	2	3	4	5
Thickness (cm)	0.175	0.175	0.175	0.175	0.175
T_1 (℃)	66.9	64.9	66.0	65.4	67.9
T_2 (℃)	63.6	61.9	63.6	63.0	64.7
T_3 (℃)	39.3	36.4	37.4	35.5	34.8
T_4 (℃)	35.4	32.2	32.3	30.4	29.7
Specimen temp. (℃)	51.5	49.2	50.5	49.3	49.8
Thermal impedance (℃ − cm^2/W)	6.938	7.354	7.233	7.667	7.506

Table A-26 Representative experimental result showing the thermal impedance values of TIM#A580 with specimen thickness 0.350 cm.

Thickness under no pressure=0.50 cm Thickness under 50psi=0.350 cm T_w=10℃ Contact pressure=50 psi Ambient temperature is maintained between 22±3℃					
Specimen	1	2	3	4	5
Thickness (cm)	0.350	0.350	0.350	0.350	0.350
T_1 (℃)	63.9	64.7	61.4	63.7	64.2
T_2 (℃)	61.6	62.8	59.3	61.6	62.2
T_3 (℃)	39.6	40.6	38.1	40.4	40.4
T_4 (℃)	37.8	38.5	36.3	38.8	38.6
Specimen temp. (℃)	50.6	51.7	48.7	51.0	51.3
Thermal impedance (℃ − cm^2/W)	11.915	12.375	12.090	12.824	12.842

Table A-27 Representative experimental result showing the thermal impedance values of designed TIM 1 with specimen thickness 0.0025 cm.

Thickness=0.0025cm T_w=10℃ Contact pressure=50 psi Ambient temperature is maintained between 22±3℃					
Specimen	1	2	3	4	5
Thickness (cm) 10^3	2.5	2.5	2.5	2.5	2.5
T_1 (℃)	58.0	59.4	56.3	58.4	58.6
T_2 (℃)	53.5	54.9	52.6	54.5	54.0
T_3 (℃)	46.2	47.5	46.0	48.0	46.5
T_4 (℃)	42.8	44.2	42.9	44.9	43.2
Specimen temp. (℃)	49.9	51.2	49.3	51.3	50.3
Thermal impedance (℃ − cm^2/W)	0.810	0.872	0.926	0.821	0.873

Table A-28 Representative experimental result showing the thermal impedance values of designed TIM 1 with specimen thickness 0.0040 cm.

Thickness=0.0040cm T_w=10℃ Contact pressure=50 psi Ambient temperature is maintained between 22±3℃					
Specimen	1	2	3	4	5
Thickness (cm) 10^3	4	4	4	4	4
T_1 (℃)	61.0	63.0	62.6	63.2	60.3
T_2 (℃)	55.5	57.2	56.6	57.1	54.3
T_3 (℃)	44.2	45.7	45.0	45.5	42.6
T_4 (℃)	39.7	41.2	40.5	40.7	37.9
Specimen temp. (℃)	49.9	51.5	50.8	51.3	48.5
Thermal impedance (℃ − cm^2/W)	1.325	1.291	1.262	1.161	1.234

Table A-29 Representative experimental result showing the thermal impedance values of designed TIM 1 with specimen thickness 0.0060 cm.

Thickness=0.0060 cm T_w=10℃ Contact pressure=50 psi Ambient temperature is maintained between 22±3℃					
Specimen	1	2	3	4	5
Thickness (cm) 10^3	6	6	6	6	6
T_1 (℃)	58.6	60.8	59.7	61.4	61.0
T_2 (℃)	54.5	56.7	55.4	57.0	56.6
T_3 (℃)	44.5	46.5	44.4	45.7	45.4
T_4 (℃)	41.2	43.2	40.4	41.8	41.4
Specimen temp. (℃)	49.5	51.6	49.9	51.4	51.0
Thermal impedance (℃ − cm^2/W)	1.878	1.946	1.813	1.904	1.833

Table A-30 Representative experimental result showing the thermal impedance values of designed TIM 2 with specimen thickness 0.0035 cm.

Thickness=0.0035cm T_w=10℃ Contact pressure=50 psi Ambient temperature is maintained between 22±3℃					
Specimen	1	2	3	4	5
Thickness (cm) 10^3	3.5	3.5	3.5	3.5	3.5
T_1 (℃)	57.1	58.6	60.5	58.1	56.9
T_2 (℃)	52.3	53.6	55.5	53.2	52.1
T_3 (℃)	44.9	46.0	47.9	45.7	44.8
T_4 (℃)	39.3	40.2	42.2	40.1	39.2
Specimen temp. (℃)	48.6	49.8	51.7	49.5	48.5
Thermal impedance (℃ − cm^2/W)	0.279	0.259	0.276	0.286	0.255

Table A-31 Representative experimental result showing the thermal impedance values of designed TIM 2 with specimen thickness 0.0050 cm.

Thickness=0.0050cm T_w=10℃ Contact pressure=50 psi Ambient temperature is maintained between 22±3℃					
Specimen	1	2	3	4	5
Thickness (cm) 10^3	5	5	5	5	5
T_1 (℃)	65.0	61.5	61.9	63.3	62.0
T_2 (℃)	57.2	54.2	54.6	56.3	55.3
T_3 (℃)	46.7	44.2	44.5	46.7	46.1
T_4 (℃)	40.7	38.3	38.7	41.1	40.6
Specimen temp. (℃)	52.0	49.2	49.6	51.5	50.7
Thermal impedance (℃ − cm^2/W)	0.402	0.394	0.427	0.405	0.385

Table A-32 Representative experimental result showing the thermal impedance values of designed TIM 2 with specimen thickness 0.0070 cm.

Thickness=0.0070 cm T_w=10℃ Contact pressure=50 psi Ambient temperature is maintained between 22±3℃					
Specimen	1	2	3	4	5
Thickness (cm) 10^3	7	7	7	7	7
T_1 (℃)	59.7	59.2	58.9	60.5	59.6
T_2 (℃)	53.4	53.1	52.7	54.0	54.2
T_3 (℃)	44.1	44.1	43.6	44.4	46.7
T_4 (℃)	39.1	39.1	38.6	39.2	42.8
Specimen temp. (℃)	48.8	48.6	48.2	49.2	50.5
Thermal impedance (℃ − cm^2/W)	0.558	0.527	0.531	0.551	0.516

5. Experimental data of thermal impedance values of designed TIM 1 and copper foil with the same specimen thickness

Table A-33 Representative experimental result showing the thermal impedance values of designed TIM 1 with thickness 0.0040 cm.

Thickness=0.0040 cm T_w=10℃ Contact pressure=50 psi Ambient temperature is maintained between 22±3℃					
Specimen	1	2	3	4	5
Thickness (cm) 10^3	4.0	4.0	4.0	4.0	4.0
T_1 (℃)	61.0	63.0	62.6	63.2	60.3
T_2 (℃)	55.5	57.2	56.6	57.1	54.3
T_3 (℃)	44.2	45.7	45.0	45.5	42.6
T_4 (℃)	39.7	41.2	40.5	40.7	37.9
Specimen temp. (℃)	49.9	51.5	50.8	51.3	48.5
Thermal impedance (℃ − cm^2/W)	1.325	1.291	1.262	1.161	1.234

Table A-34 Representative experimental result showing the thermal impedance values of copper foil with thickness 0.0040 cm.

Thickness=0.0040 cm T_w=10℃ Contact pressure=50 psi Ambient temperature is maintained between 22±3℃					
Specimen	1	2	3	4	5
Thickness (cm) 10^3	4.0	4.0	4.0	4.0	4.0
T_1 (℃)	61.5	61.4	61.1	60.9	59.5
T_2 (℃)	56.0	57.2	56.9	56.8	56.0
T_3 (℃)	41.0	43.6	43.5	43.4	42.6
T_4 (℃)	37.4	39.4	39.4	39.3	37.8
Specimen temp. (℃)	48.5	50.4	50.2	50.1	49.3
Thermal impedance (℃ − cm^2/W)	2.621	2.548	2.536	2.585	2.536

6. Experimental data of thermal impedance values of TIMs at extreme specimen temperatures

Table A-35 Representative experimental result showing the thermal impedance values of TIM#976 at 18±1℃.

Thickness under no pressure=0.1 cm Thickness under 50psi=0.055 cm Specimen temperature is controlled at 18±1℃ T_w=10℃ Contact pressure=50 psi Ambient temperature is maintained at 22±3℃					
Specimen	1	2	3	4	5
Thickness (cm)	0.055	0.055	0.055	0.055	0.055
T_1 (℃)	19.9	18.8	18.4	18.7	19.4
T_2 (℃)	19.6	18.3	17.9	18.1	18.8
T_3 (℃)	18.1	16.5	16.1	16.2	17.0
T_4 (℃)	17.6	16.0	15.6	15.7	16.6
Specimen temp. (℃)	18.9	17.4	17.0	17.2	17.9
Thermal impedance (℃ − cm^2/W)	3.188	3.000	3.000	2.818	3.000

Table A-36 Representative experimental result showing the thermal impedance values of TIM#976 at 50±2℃.

Thickness under no pressure=0.1 cm Thickness under 50psi=0.055 cm Specimen temperature is controlled at 50±2℃ T_w=10℃ Contact pressure=50 psi Ambient temperature is maintained at 22±3℃					
Specimen	1	2	3	4	5
Thickness (cm)	0.055	0.055	0.055	0.055	0.055
T_1 (℃)	61.1	61.5	59.1	59.3	57.9
T_2 (℃)	57.7	58.2	55.7	56.2	54.8
T_3 (℃)	45.0	45.7	43.4	44.6	43.5
T_4 (℃)	41.4	42.1	39.8	41.2	40.1
Specimen temp. (℃)	51.4	52.0	49.6	50.4	49.2
Thermal impedance (℃ − cm^2/W)	3.036	3.029	2.893	2.962	2.846

Table A-37 Representative experimental result showing the thermal impedance values of TIM#976 at 61±2℃.

Thickness under no pressure=0.1 cm Thickness under 50psi=0.055 cm Specimen temperature is controlled at 61±2℃ T_w=10℃ Contact pressure=50 psi Ambient temperature is maintained at 22±3℃					
Specimen	1	2	3	4	5
Thickness (cm)	0.055	0.055	0.055	0.055	0.055
T_1 (℃)	75.0	75.9	74.5	75.5	74.7
T_2 (℃)	70.5	71.4	70.1	70.8	69.8
T_3 (℃)	53.6	54.4	53.8	53.6	52.6
T_4 (℃)	48.8	49.7	49.2	48.9	47.9
Specimen temp. (℃)	62.1	62.4	62.0	62.2	61.2
Thermal impedance ($℃-cm^2/W$)	3.043	3.120	3.028	3.074	2.979

Table A-38 Representative experimental result showing the thermal impedance values of TIM#A580 at 18±1℃.

Thickness under no pressure=0.05 cm Thickness under 50psi=0.035 cm Specimen temperature is controlled at 18±1℃ T_w=10℃ Contact pressure=50 psi Ambient temperature is maintained at 22±3℃					
Specimen	1	2	3	4	5
Thickness (cm)	0.035	0.035	0.035	0.035	0.035
T_1 (℃)	18.8	18.3	20.3	19.8	19.0
T_2 (℃)	18.2	17.8	19.8	19.5	18.3
T_3 (℃)	16.5	16.3	18.1	17.8	16.4
T_4 (℃)	16.1	15.9	17.6	17.1	16.0
Specimen temp. (℃)	17.4	17.1	19.0	18.7	17.4
Thermal impedance ($℃-cm^2/W$)	2.750	2.667	2.750	2.750	2.818

Table A-39 Representative experimental result showing the thermal impedance values of TIM#A580 at 50±2℃.

Thickness under no pressure=0.05 cm Thickness under 50psi=0.035 cm Specimen temperature is controlled at 50±2℃ T_w=10℃ Contact pressure=50 psi Ambient temperature is maintained at 22±3℃					
Specimen	1	2	3	4	5
Thickness (cm)	0.035	0.035	0.035	0.035	0.035
T_1 (℃)	54.5	55.3	56.0	59.7	60.1
T_2 (℃)	52.6	53.0	53.9	56.7	56.9
T_3 (℃)	44.0	44.3	45.3	43.3	43.6
T_4 (℃)	40.9	41.3	42.3	38.4	38.8
Specimen temp. (℃)	48.3	48.7	49.6	50.0	50.3
Thermal impedance ($℃-cm^2/W$)	2.800	2.604	2.716	2.741	2.656

Table A-40 Representative experimental result showing the thermal impedance values of TIM#A580 at 61±2℃.

Thickness under no pressure=0.05 cm Thickness under 50psi=0.035 cm Specimen temperature is controlled at 61±2℃ T_w=10℃ Contact pressure=50 psi Ambient temperature is maintained at 22±3℃					
Specimen	1	2	3	4	5
Thickness (cm)	0.035	0.035	0.035	0.035	0.035
T_1 (℃)	72.4	74.5	72.3	72.7	70.0
T_2 (℃)	69.1	70.6	68.4	68.9	66.6
T_3 (℃)	51.6	52.5	50.6	51.7	50.0
T_4 (℃)	44.8	45.7	43.8	45.1	43.6
Specimen temp. (℃)	60.4	61.6	59.5	60.3	60.3
Thermal impedance ($℃-cm^2/W$)	2.832	2.729	2.659	2.635	2.735

Table A-41 Representative experimental result showing the thermal impedance values of designed TIM 1 at 18±1℃.

Thickness under no pressure=0.0025 cm Thickness under 50psi=0.0025 cm Specimen temperature is controlled at 18±1℃ T_w=10℃ Contact pressure=50 psi Ambient temperature is maintained at 22±3℃					
Specimen	1	2	3	4	5
Thickness (cm)	0.0025	0.0025	0.0025	0.0025	0.0025
T_1 (℃)	19.0	19.4	19.7	19.3	20.1
T_2 (℃)	18.0	18.3	18.6	18.3	19.0
T_3 (℃)	16.4	16.5	16.8	16.7	17.3
T_4 (℃)	15.7	15.7	16.0	16.0	16.6
Specimen temp. (℃)	17.2	17.4	17.7	17.5	18.2
Thermal impedance ($℃-cm^2/W$)	0.853	0.868	0.868	0.853	0.861

Table A-42 Representative experimental result showing the thermal impedance values of designed TIM 1 at 50±2℃.

Thickness under no pressure=0.0025 cm Thickness under 50psi=0.0025 cm Specimen temperature is controlled at 50±2℃ T_w=10℃ Contact pressure=50 psi Ambient temperature is maintained at 22±3℃					
Specimen	1	2	3	4	5
Thickness (cm)	0.0025	0.0025	0.0025	0.0025	0.0025
T_1 (℃)	58.0	59.4	56.3	58.4	58.6
T_2 (℃)	53.5	54.9	52.6	54.5	54.0
T_3 (℃)	46.2	47.5	46.0	48.0	46.5
T_4 (℃)	42.8	44.2	42.9	44.9	43.2
Specimen temp. (℃)	49.9	51.2	49.3	51.3	50.3
Thermal impedance ($℃-cm^2/W$)	0.810	0.872	0.926	0.821	0.873

Table A-43 Representative experimental result showing the thermal impedance values of designed TIM 1 at 61±2℃.

Thickness under no pressure=0.0025 cm Thickness under 50psi=0.0025 cm Specimen temperature is controlled at 61±2℃ T_w=10℃ Contact pressure=50 psi Ambient temperature is maintained at 22±3℃					
Specimen	1	2	3	4	5
Thickness (cm)	0.0025	0.0025	0.0025	0.0025	0.0025
T_1 (℃)	69.2	70.7	68.3	66.1	68.2
T_2 (℃)	64.6	66.0	63.9	62.7	64.8
T_3 (℃)	57.1	58.3	55.8	56.6	58.7
T_4 (℃)	53.7	54.9	51.4	53.5	55.7
Specimen temp. (℃)	60.9	62.2	59.9	59.7	61.8
Thermal impedance ($℃-cm^2/W$)	0.844	0.877	0.801	0.846	0.883

Table A-44 Representative experimental result showing the thermal impedance values of designed TIM 2 at 18±1℃.

Thickness under 50psi=0.0035 cm Specimen temperature is controlled at 18±1℃ T_w=10℃ Contact pressure=50 psi Ambient temperature is maintained at 22±3℃					
Specimen	1	2	3	4	5
Thickness (cm)	0.0035	0.0035	0.0035	0.0035	0.0035
T_1 (℃)	19.2	18.4	20.1	19.3	19.5
T_2 (℃)	18.6	18.1	19.5	18.9	18.7
T_3 (℃)	17.4	17.1	18.2	17.7	17.3
T_4 (℃)	16.3	16.0	17.0	16.4	16.1
Specimen temp. (℃)	18.0	17.6	18.9	19.3	18.0
Thermal impedance ($℃-cm^2/W$)	0.265	0.286	0.306	0.265	0.250

Table A-45 Representative experimental result showing the thermal impedance values of designed TIM 2 at 50±2℃.

Thickness under 50psi=0.0035 cm Specimen temperature is controlled at 50±2℃ T_w=10℃ Contact pressure=50 psi Ambient temperature is maintained at 22±3℃					
Specimen	1	2	3	4	5
Thickness (cm)	0.0035	0.0035	0.0035	0.0035	0.0035
T_1 (℃)	57.1	58.6	60.5	58.1	56.9
T_2 (℃)	52.3	53.6	55.5	53.2	52.1
T_3 (℃)	44.9	46.0	47.9	45.7	44.8
T_4 (℃)	39.3	40.2	42.2	40.1	39.2
Specimen temp. (℃)	48.6	49.8	51.7	49.5	48.5
Thermal impedance ($℃-cm^2/W$)	0.279	0.259	0.276	0.286	0.255

Table A-46 Representative experimental result showing the thermal impedance values of designed TIM 2 at 61±2℃.

Thickness under 50psi=0.0035 cm Specimen temperature is controlled at 61±2℃ T_w=10℃ Contact pressure=50 psi Ambient temperature is maintained at 22±3℃					
Specimen	1	2	3	4	5
Thickness (cm)	0.0035	0.0035	0.0035	0.0035	0.0035
T_1 (℃)	73.3	74.3	72.8	71.0	71.5
T_2 (℃)	66.8	67.6	66.1	64.6	64.9
T_3 (℃)	57.3	58.0	56.4	55.4	55.6
T_4 (℃)	50.5	51.2	49.5	48.8	49.3
Specimen temp. (℃)	62.1	62.8	61.3	60.0	60.3
Thermal impedance ($℃-cm^2/W$)	0.286	0.278	0.283	0.269	0.302

7. Experimental data of thermal impedance values of TIMs tested with meter bars with different surface roughness

Table A-47 Representative experimental result showing the thermal impedance values of TIM#976 under meter-bar surface roughness 0.4 μm.

Thickness under no pressure=0.1 cm Thickness under 50psi=0.055 cm Meter bar surface roughness=0.4μm Specimen temperature is controlled at 50±2℃ T_w=10℃ Contact pressure=50 psi Ambient temperature is maintained at 22±3℃					
Specimen	1	2	3	4	5
Roughness (μm)	0.4	0.4	0.4	0.4	0.4
T_1 (℃)	61.1	61.5	59.1	59.3	57.9
T_2 (℃)	57.7	58.2	55.7	56.2	54.8
T_3 (℃)	45.0	45.7	43.4	44.6	43.5
T_4 (℃)	41.4	42.1	39.8	41.2	40.1
Specimen temp. (℃)	51.4	52.0	49.6	50.4	49.2
Thermal impedance ($℃-cm^2/W$)	3.036	3.029	2.893	2.962	2.846

Table A-48 Representative experimental result showing the thermal impedance values of TIM#976 under meter-bar surface roughness 25 μm.

Thickness under no pressure=0.1 cm Thickness under 50psi=0.055 cm Meter bar surface roughness=25 μm Specimen temperature is controlled at 50±2℃ T_w=10℃ Contact pressure=50 psi Ambient temperature is maintained at 22±3℃					
Specimen	1	2	3	4	5
Roughness (μm)	25	25	25	25	25
T_1 (℃)	57.6	55.6	54.1	55.4	55.8
T_2 (℃)	55.2	53.8	52.0	53.1	53.5
T_3 (℃)	46.4	47.8	44.6	44.6	44.9
T_4 (℃)	44.0	46.3	42.5	42.1	42.5
Specimen temp. (℃)	50.8	50.8	48.3	48.9	49.2
Thermal impedance ($℃-cm^2/W$)	3.083	3.045	2.905	2.927	3.074

Table A-49 Representative experimental result showing the thermal impedance values of TIM#A580 under meter-bar surface roughness 0.4 μm.

Thickness under no pressure=0.05 cm Thickness under 50psi=0.035 cm Meter bar surface roughness=0.4μm Specimen temperature is controlled at 50±2℃ T_w=10℃ Contact pressure=50 psi Ambient temperature is maintained at 22±3℃					
Specimen	1	2	3	4	5
Roughness (μm)	0.4	0.4	0.4	0.4	0.4
T_1 (℃)	54.5	55.3	56.0	59.7	60.1
T_2 (℃)	52.6	53.0	53.9	56.7	56.9
T_3 (℃)	44.0	44.3	45.3	43.3	43.6
T_4 (℃)	40.9	41.3	42.3	38.4	38.8
Specimen temp. (℃)	48.3	48.7	49.6	50.0	50.3
Thermal impedance ($℃-cm^2/W$)	2.800	2.604	2.716	2.741	2.656

Table A-50 Representative experimental result showing the thermal impedance values of TIM#A580 under meter-bar surface roughness 25 μm.

Thickness under no pressure=0.05 cm Thickness under 50psi=0.035 cm Meter bar surface roughness=25 μm Specimen temperature is controlled at 50±2℃ T_w=10℃ Contact pressure=50 psi Ambient temperature is maintained at 22±3℃					
Specimen	1	2	3	4	5
Roughness (μm)	25	25	25	25	25
T_1 (℃)	65.1	64.1	61.1	62.3	63.2
T_2 (℃)	60.0	59.1	56.7	57.8	58.5
T_3 (℃)	43.9	43.3	41.8	42.7	43.0
T_4 (℃)	39.7	39.1	37.7	38.5	38.8
Specimen temp. (℃)	52.0	51.2	49.3	50.3	50.8
Thermal impedance ($℃-cm^2/W$)	2.828	2.793	2.882	2.839	2.854

Table A-51 Representative experimental result showing the thermal impedance values of designed TIM 1 under meter-bar surface roughness 0.4 μm.

Thickness under 50psi=0.0025 cm Meter bar surface roughness=0.4μm Specimen temperature is controlled at 50±2℃ T_w=10℃ Contact pressure=50 psi Ambient temperature is maintained at 22±3℃					
Specimen	1	2	3	4	5
Roughness (μm)	0.4	0.4	0.4	0.4	0.4
T_1 (℃)	58.0	59.4	56.3	58.4	58.6
T_2 (℃)	53.5	54.9	52.6	54.5	54.0
T_3 (℃)	46.2	47.5	46.0	48.0	46.5
T_4 (℃)	42.8	44.2	42.9	44.9	43.2
Specimen temp. (℃)	49.9	51.2	49.3	51.3	50.3
Thermal impedance ($℃-cm^2/W$)	0.810	0.872	0.926	0.821	0.873

Table A-52 Representative experimental result showing the thermal impedance values of designed TIM 1 under meter-bar surface roughness 25 μm.

Thickness under 50psi=0.0025 cm Meter bar surface roughness=25 μm Specimen temperature is controlled at 50±2℃ T_w=10℃ Contact pressure=50 psi Ambient temperature is maintained at 22±3℃					
Specimen	1	2	3	4	5
Roughness (μm)	25	25	25	25	25
T_1 (℃)	65.9	60.3	62.8	58.8	65.4
T_2 (℃)	58.2	55.5	57.0	53.6	58.7
T_3 (℃)	43.9	46.2	46.7	43.8	44.7
T_4 (℃)	36.8	41.2	41.6	38.8	36.8
Specimen temp. (℃)	51.4	50.9	51.9	48.7	51.7
Thermal impedance ($℃-cm^2/W$)	0.916	0.872	0.862	0.902	0.897

Table A-53 Representative experimental result showing the thermal impedance values of designed TIM 2 under meter-bar surface roughness 0.4 μm.

Thickness under 50psi=0.0035 cm Meter bar surface roughness=0.4μm Specimen temperature is controlled at 50±2℃ T_w=10℃ Contact pressure=50 psi Ambient temperature is maintained at 22±3℃					
Specimen	1	2	3	4	5
Roughness (μm)	0.4	0.4	0.4	0.4	0.4
T_1 (℃)	57.1	58.6	60.5	58.1	56.9
T_2 (℃)	52.3	53.6	55.5	53.2	52.1
T_3 (℃)	44.9	46.0	47.9	45.7	44.8
T_4 (℃)	39.3	40.2	42.2	40.1	39.2
Specimen temp. (℃)	48.6	49.8	51.7	49.5	48.5
Thermal impedance ($℃-cm^2/W$)	0.279	0.259	0.276	0.286	0.255

Table A-54 Representative experimental result showing the thermal impedance values of designed TIM 2 under meter-bar surface roughness 25 μm.

Thickness under 50psi=0.0035 cm Meter bar surface roughness=25 μm Specimen temperature is controlled at 50±2℃ T_w=10℃ Contact pressure=50 psi Ambient temperature is maintained at 22±3℃					
Specimen	1	2	3	4	5
Roughness (μm)	25	25	25	25	25
T_1 (℃)	63.4	62.0	58.0	60.9	59.2
T_2 (℃)	56.4	54.2	52.0	53.4	53.2
T_3 (℃)	47.1	44.5	44.7	44.6	45.9
T_4 (℃)	41.4	38.9	40.8	40.0	41.9
Specimen temp. (℃)	51.8	49.4	48.4	49.0	49.6
Thermal impedance ($℃-cm^2/W$)	0.331	0.310	0.343	0.318	0.325

8. Experimental data of thermal impedance values of designed TIM 1 at different specimen thicknesses for the determination of thermal conductivity

Table A-55 Representative experimental result showing the thermal impedance values of designed TIM 1 at 25 μm.

Thickness under 50psi=0.0025 cm Specimen temperature is controlled at 50±2℃ T_w=10℃ Contact pressure=50 psi Ambient temperature is maintained at 22±3℃					
Specimen	1	2	3	4	5
Specimen thickness (μm)	25	25	25	25	25
T_1 (℃)	58.3	62.6	58.1	57.2	57.9
T_2 (℃)	53.4	56.0	53.2	52.6	53.6
T_3 (℃)	46.4	46.2	45.7	45.1	46.3
T_4 (℃)	43.8	42.4	42.7	41.7	42.9
Specimen temp. (℃)	49.9	51.1	49.5	48.9	50.0
Thermal impedance ($℃-cm^2/W$)	0.833	0.856	0.873	0.843	0.870

Table A-56 Representative experimental result showing the thermal impedance values of designed TIM 1 at 40 μm.

Thickness under 50psi=0.0040 cm Specimen temperature is controlled at 50±2℃ T_w=10℃ Contact pressure=50 psi Ambient temperature is maintained at 22±3℃					
Specimen	1	2	3	4	5
Specimen thickness (μm)	40	40	40	40	40
T_1 (℃)	59.4	61.8	62.5	60.7	63.1
T_2 (℃)	54.2	56.6	56.7	54.7	57.1
T_3 (℃)	44.2	46.5	45.3	42.8	45.1
T_4 (℃)	40.3	42.7	41.1	38.2	40.2
Specimen temp. (℃)	49.2	51.6	51.0	48.8	51.1
Thermal impedance ($℃-cm^2/W$)	1.247	1.306	1.350	1.307	1.252

Table A-57 Representative experimental result showing the thermal impedance values of designed TIM 1 at 60 μm.

Thickness under 50psi=0.0060 cm Specimen temperature is controlled at 50±2℃ T_w=10℃ Contact pressure=50 psi Ambient temperature is maintained at 22±3℃					
Specimen	1	2	3	4	5
Specimen thickness (μm)	60	60	60	60	60
T_1 (℃)	60.1	60.7	55.8	56.3	57.2
T_2 (℃)	56.1	56.3	53.0	53.3	53.5
T_3 (℃)	45.7	46.0	45.4	45.7	44.0
T_4 (℃)	42.1	42.5	42.7	43.1	40.6
Specimen temp. (℃)	50.9	51.2	49.2	49.5	48.8
Thermal impedance ($℃-cm^2/W$)	1.921	2.010	1.955	1.893	1.845

9. Experimental data of thermal impedance values of designed TIM 2 at different specimen thicknesses for the determination of thermal conductivity

Table A-58 Representative experimental result showing the thermal impedance values of designed TIM 2 at 35 μm.

Thickness under 50psi=0.0035 cm Specimen temperature is controlled at 50±2℃ T_w=10℃ Contact pressure=50 psi Ambient temperature is maintained at 22±3℃					
Specimen	1	2	3	4	5
Specimen thickness (μm)	35	35	35	35	35
T_1 (℃)	63.9	62.7	61.8	64.6	62.6
T_2 (℃)	56.0	55.8	53.9	56.9	55.2
T_3 (℃)	46.4	47.1	44.6	47.0	45.7
T_4 (℃)	40.9	41.9	39.4	40.8	39.7
Specimen temp. (℃)	51.2	51.5	49.3	52.0	50.5
Thermal impedance ($℃-cm^2/W$)	0.291	0.298	0.275	0.281	0.272

Table A-59 Representative experimental result showing the thermal impedance values of designed TIM 2 at 50 μm.

Thickness under 50psi=0.0050 cm Specimen temperature is controlled at 50±2℃ T_w=10℃ Contact pressure=50 psi Ambient temperature is maintained at 22±3℃					
Specimen	1	2	3	4	5
Specimen thickness (μm)	50	50	50	50	50
T_1 (℃)	62.7	60.0	60.4	60.9	58.6
T_2 (℃)	55.9	54.0	54.8	55.1	54.1
T_3 (℃)	47.0	46.6	47.3	47.6	47.5
T_4 (℃)	42.1	42.9	43.0	43.4	43.3
Specimen temp. (℃)	51.5	50.3	51.1	51.4	50.8
Thermal impedance ($℃-cm^2/W$)	0.402	0.407	0.394	0.375	0.397

Table A-60 Representative experimental result showing the thermal impedance values of designed TIM 2 at 70 μm.

Thickness under 50psi=0.0070 cm Specimen temperature is controlled at 50±2℃ T_w=10℃ Contact pressure=50 psi Ambient temperature is maintained at 22±3℃					
Specimen	1	2	3	4	5
Specimen thickness (μm)	70	70	70	70	70
T_1 (℃)	60.5	61.6	60.3	60.1	61.0
T_2 (℃)	55.0	56.2	54.3	54.3	55.9
T_3 (℃)	46.2	47.6	45.1	44.9	47.6
T_4 (℃)	40.9	42.4	39.9	39.2	42.6
Specimen temp. (℃)	50.6	51.9	49.7	49.6	51.8
Thermal impedance ($℃-cm^2/W$)	0.537	0.528	0.554	0.543	0.554

Table A-61 Representative experimental result showing the thermal impedance values of thermal grease T670.

Published thermal impedance value= 0.07℃ − cm^2/W T_w=10℃ Contact pressure=50 psi Ambient temperature is maintained between 22±3℃					
Specimen	1	2	3	4	5
T_1 (℃)	60.0	60.8	63.1	58.8	59.4
T_2 (℃)	53.8	54.5	56.5	52.9	53.3
T_3 (℃)	44.1	44.7	46.0	43.5	43.9
T_4 (℃)	37.6	38.1	38.9	37.2	37.6
Specimen temp. (℃)	49.0	49.6	51.3	48.2	48.6
Thermal impedance (℃ − cm^2/W)	0.409	0.399	0.416	0.426	0.395

Table A-62 Arithmetic means and standard deviations of TIMs at specified specimen thicknesses (25, 40, and 60μm).

TIM	$\bar{X}_{0,25\mu m}$ (℃ − cm^2/W)	$S_{1,25\mu m}$	$\bar{X}_{0,40\mu m}$ (℃ − cm^2/W)	$S_{2,40\mu m}$	$\bar{X}_{0,60\mu m}$ (℃ − cm^2/W)	$S_{3,60\mu m}$
976[1,2]	2.254	0.1536	2.277	0.1536	2.309	0.1536
A580[1,2]	1.723	0.2917	1.771	0.2917	1.835	0.2917
Designed TIM 1	0.850	0.0467	1.261	0.0540	1.905	0.0734
Designed TIM 2[1,2]	0.200	0.0157	0.316	0.0157	0.471	0.0157

[1] For TIM#976, A580, and designed TIM 2, the sample average thermal impedance values at thicknesses=25, 40, 60 μm were derived by extending the linear regression equations and substituting the thicknesses with 25, 40, 60 μm. These values were assumed to be the sample average thermal impedances for TIM#976, A580, and designed TIM 2 at the specified specimen thicknesses.
[2] For TIM#976, A580, and designed TIM 2, the sample standard deviation values at thicknesses=25, 40, 60 μm were obtained by calculating the average of standard deviation values of those derived from experimental results. The standard deviation of TIM#976, A580, and designed TIM 2 at thicknesses=25, 40, 60 μm was assumed to be the same.

Table A-63 Pair-wise comparisons of thermal impedance values of TIMs with the same specimen thickness 25μm based on the post-hoc test (Tukey's procedure).

Multiple Comparisons

Dependent Variable: Thermal impedance (C-cm^2/W)
Tukey HSD

(I) TIM types	(J) TIM types	Mean Difference (I-J)	Std. Error	Sig.	95% Confidence Interval	
					Lower Bound	Upper Bound
976	A580	.47121*	.05057	.000	.3390	.6034
	TIM 1	1.38256*	.05057	.000	1.2503	1.5148
	TIM 2	2.03101*	.05057	.000	1.8988	2.1632
A580	976	-.47121*	.05057	.000	-.6034	-.3390
	TIM 1	.91134*	.05057	.000	.7791	1.0436
	TIM 2	1.55980*	.05057	.000	1.4276	1.6920
TIM 1	976	-1.38256*	.05057	.000	-1.5148	-1.2503
	A580	-.91134*	.05057	.000	-1.0436	-.7791
	TIM 2	.64846*	.05057	.000	.5162	.7807
TIM 2	976	-2.03101*	.05057	.000	-2.1632	-1.8988
	A580	-1.55980*	.05057	.000	-1.6920	-1.4276
	TIM 1	-.64846*	.05057	.000	-.7807	-.5162

*. The mean difference is significant at the .05 level.

Table A-64 Pair-wise comparisons of thermal impedance values of TIMs with the same specimen thickness 40µm based on the post-hoc test (Tukey's procedure).

Multiple Comparisons

Dependent Variable: Thermal impedance (C-cm^2/W)
Tukey HSD

(I) TIM types	(J) TIM types	Mean Difference (I-J)	Std. Error	Sig.	95% Confidence Interval	
					Lower Bound	Upper Bound
976	A580	.51586*	.04717	.000	.3925	.6392
	TIM 1	1.05792*	.04717	.000	.9346	1.1813
	TIM 2	1.99883*	.04717	.000	1.8755	2.1222
A580	976	-.51586*	.04717	.000	-.6392	-.3925
	TIM 1	.54206*	.04717	.000	.4187	.6654
	TIM 2	1.48298*	.04717	.000	1.3596	1.6063
TIM 1	976	-1.05792*	.04717	.000	-1.1813	-.9346
	A580	-.54206*	.04717	.000	-.6654	-.4187
	TIM 2	.94091*	.04717	.000	.8176	1.0642
TIM 2	976	-1.99883*	.04717	.000	-2.1222	-1.8755
	A580	-1.48298*	.04717	.000	-1.6063	-1.3596
	TIM 1	-.94091*	.04717	.000	-1.0642	-.8176

*. The mean difference is significant at the .05 level.

Table A-65 Pair-wise comparisons of thermal impedance values of TIMs with the same specimen thickness 60µm based on the post-hoc test (Tukey's procedure).

Multiple Comparisons

Dependent Variable: Thermal impedance (C-cm^2/W)
Tukey HSD

(I) TIM types	(J) TIM types	Mean Difference (I-J)	Std. Error	Sig.	95% Confidence Interval	
					Lower Bound	Upper Bound
976	A580	.51663*	.04777	.000	.3917	.6415
	TIM 1	.40719*	.04777	.000	.2823	.5321
	TIM 2	1.84068*	.04777	.000	1.7158	1.9656
A580	976	-.51663*	.04777	.000	-.6415	-.3917
	TIM 1	-.10944	.04777	.107	-.2344	.0155
	TIM 2	1.32405*	.04777	.000	1.1991	1.4490
TIM 1	976	-.40719*	.04777	.000	-.5321	-.2823
	A580	.10944	.04777	.107	-.0155	.2344
	TIM 2	1.43349*	.04777	.000	1.3086	1.5584
TIM 2	976	-1.84068*	.04777	.000	-1.9656	-1.7158
	A580	-1.32405*	.04777	.000	-1.4490	-1.1991
	TIM 1	-1.43349*	.04777	.000	-1.5584	-1.3086

*. The mean difference is significant at the .05 level.

VITA

Name: Juei-Chun Chiang

Address: 2F, NO.8, LN.28, Dongyuan St., Wanhua District, Taipei, Taiwan

Email Address: dimlaughter@hotmail.com

Education: B.S., Bioenvironmental Systems Engineering, National Taiwan University, 2004

M.S., Mechanical Engineering, Texas A&M University, 2008